Harmonizing and Optimizing CT Perfusion Stroke Imaging

Daan Peerlings

Harmonizing and Optimizing CT Perfusion Stroke Imaging

Daan Peerlings

PhD thesis, Utrecht University, the Netherlands

ISBN 978-94-93391-13-0

This thesis was printed by Proefschriftspecialist (which I recommend). Financial support from the Dutch Heart Foundation for printing this thesis is gratefully acknowledged.

Harmonizing and Optimizing CT Perfusion Stroke Imaging

Het Harmoniseren en Optimaliseren van CT-perfusie Beroertebeeldvorming
(met een samenvatting in het Nederlands)

Proefschrift

ter verkrijging van de graad van doctor aan de Universiteit Utrecht
op gezag van de rector magnificus, prof. dr. H.R.B.M. Kummeling,
ingevolge het besluit van het College voor Promoties in het openbaar te verdedigen
op dinsdag 27 augustus 2024 des ochtends te 10.15 uur

door

Daan Peerlings
geboren op 14 juli 1995 te Middelburg

Promotoren

Prof. dr. H.W.A.M. de Jong

Prof. dr. H.A. Marquering

Copromotoren

Dr. H.E. Bennink

Dr. J.W. Dankbaar

Beoordelingscommissie

Prof. dr. E.T. van Bavel

Prof. dr. R.M. Dijkhuizen

Prof. dr. J. Hendrikse

Prof. dr. L.J. Kappelle

Prof. dr. W.H. van Zwam

The research in this thesis was funded by the Leading the Change (LtC) program (grant number 80-85009-98-2015). Leading the Change is financed by Zorgverzekeraars Nederland and supports various healthcare evaluations in the Netherlands as part of the Zorgevaluatie Nederland and the Zorgevaluatie & Gepast Gebruik (ZE&GG) program.

Contents

Chapter 1

General introduction

On ischemic stroke, stroke imaging, CT perfusion imaging as patient selection tool for thrombectomy, the CLEOPATRA healthcare evaluation, the CT perfusion imaging acquisition protocol, and the CT perfusion imaging processing protocol.

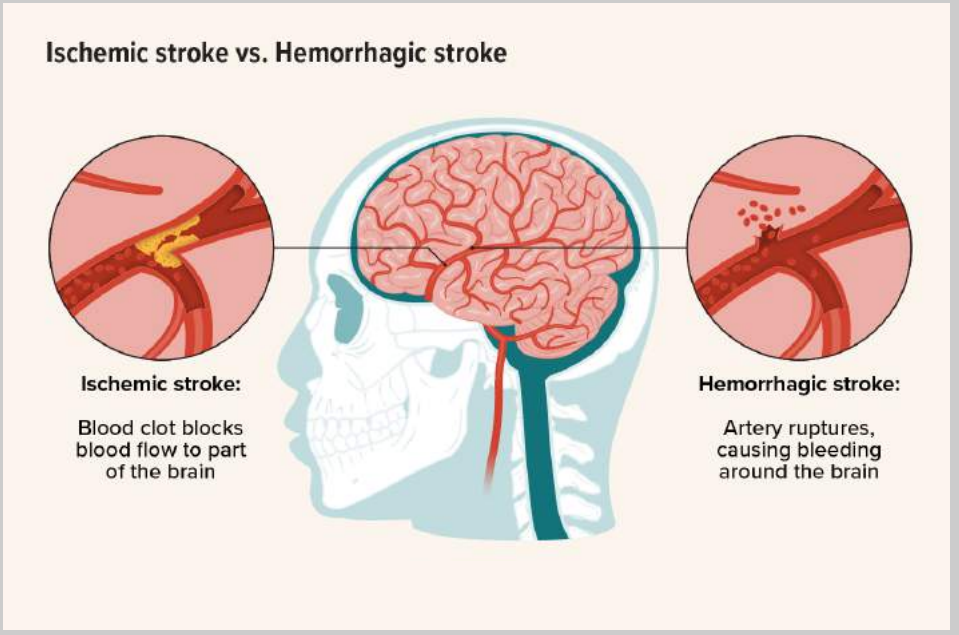

Figure 1

Ischemic and hemorrhagic stroke. In an ischemic stroke, a blood clot restricts the blood flow to downstream vessels and brain regions. In a hemorrhagic stroke, a blood vessel ruptures, causing bleeding around the brain. Reprinted with permission from healthline.com

Ischemic stroke

Ischemic stroke is a medical condition that arises from the occlusion of a vessel that supplies blood to the brain (Figure 1). The vessel occlusion causes ischemia, which is a restriction of blood supply that disrupts the cellular metabolism. Besides from a vessel occlusion, stroke can also arise from the rupture of a vessel leading to a hemorrhage, bleeding, in the brain. Hemorrhagic stroke is ten times less frequent in western countries than ischemic stroke [1]. In case of an ischemic stroke, the brain cells in the ischemic region rapidly perish as they are deprived of oxygen and nutrients. The resulting infarction, which is tissue death due to ischemia, can cause serious and lasting damage to the patient.

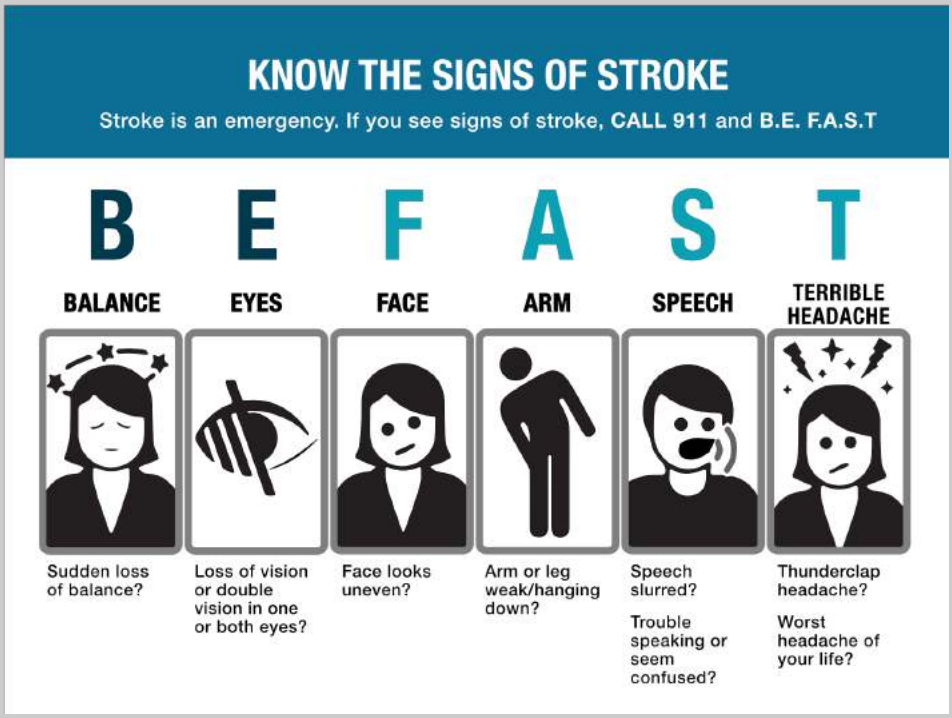

Figure 2

Stroke symptoms. Stroke symptoms include problems with balance and vision, a drooping face, weakness in the arm, difficulty with speech, and headache. Acting fast is important to reduce the risk of early complications and long-term disability. Reprinted with permission from befast.org

Key symptoms of a stroke include sudden weakness or numbness on one side of the body, difficulty speaking or understanding speech, problems with vision, and a lack of coordination (Figure 2). To emphasize the relevance of this condition, an ischemic stroke occurs every four seconds worldwide, with two out of five resulting in fatality and three out of five resulting in long-term disability more likely than not [2]. These statistics contribute to making stroke the third-leading medical cause of death and disability, with an annual global cost of 650 billion euros, equivalent to 0.66% of the global gross domestic product [3]. Timely treatment of ischemic stroke is crucial in order to minimize the risk of death and disability.

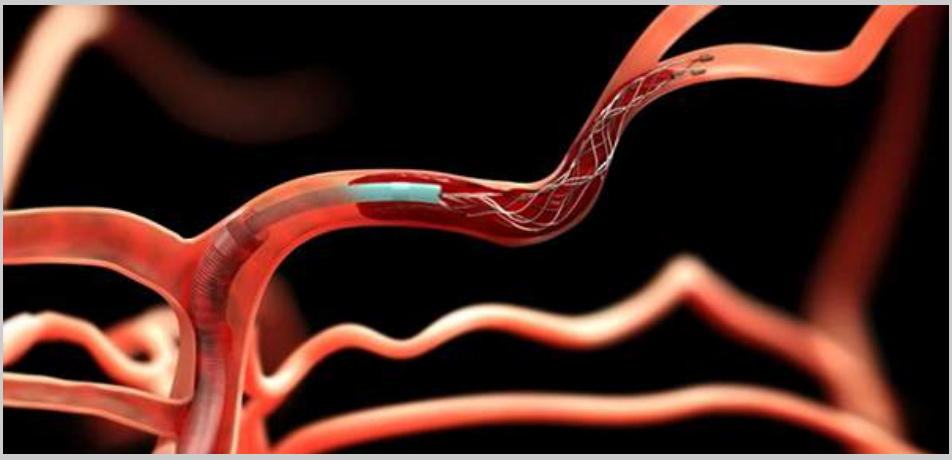

Figure 3

Mechanical thrombectomy. A recently validated medical procedure, called thrombectomy, mechanically removes the blood clot (thrombus) from a blood vessel. During the procedure, a specialized catheter is guided through the blood vessels to the site of the clot. Once in position, a device is employed to break up or extract the clot, restoring blood flow and preventing further damage. Reprinted with permission from medtronic.com

The choice of treatment for ischemic stroke depends on multiple factors, such as the location of the vessel occlusion, the extent of the ischemia, the time since the stroke onset, and the patient's age and overall health. One common treatment for ischemic stroke is thrombolysis, where clot-dissolving drugs are administered in an attempt to recanalize the vessel and restore the blood flow to the ischemic regions. These drugs work best when administered within the first few hours after the onset of the stroke symptoms and require careful monitoring in order to avoid the risk of bleeding or other complications. A different and more recent treatment option, called thrombectomy, involves the use of specialized tools to mechanically remove the clot from the occluded vessel (Figure 3). Either or both treatment options can be applied. In general, thrombectomy is more effective than thrombolysis for the treatment of large, proximal clots in the brain. However, it is also more invasive and time-consuming than thrombolysis and may carry a higher risk of complications by damaging the arterial wall [4]. Hence, the available treatment options require an accurate patient selection for treatment.

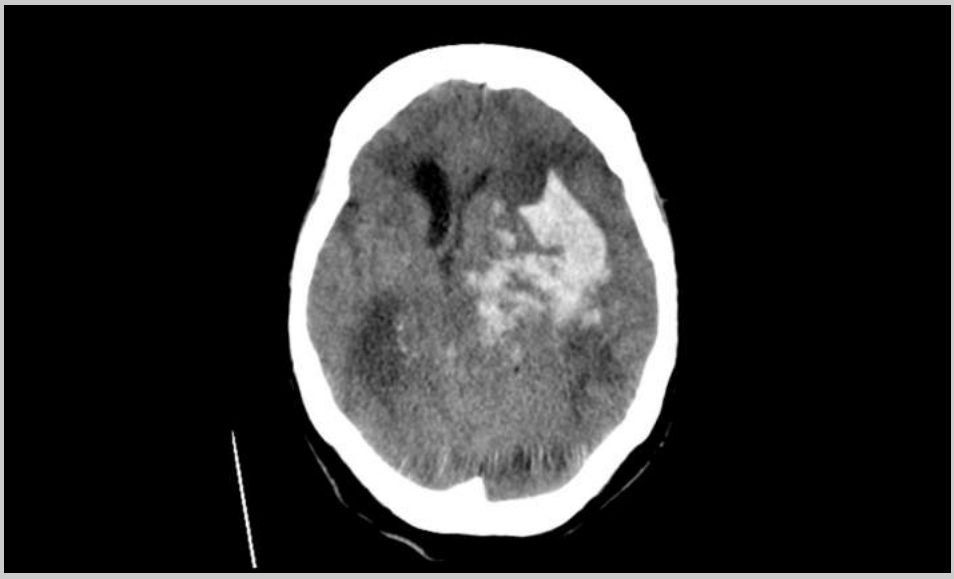

Figure 4

Non-contrast CT scan of a hemorrhagic stroke patient. The hyperintense region on the right side of the image indicates a hyperdense region due to bleeding. Case courtesy of David Cuete [5].

Stroke imaging

To help physicians tailor their approach to each patient's circumstances, they are assisted by multimodal imaging techniques. These techniques can provide critical information about the severity of the ischemic stroke [6]. First, a hemorrhagic stroke needs to be ruled out with a non-contrast CT scan, which can reveal a hemorrhage as a hyperintense region (Figure 4). After the non-contrast CT scan, the ischemic stroke patient will move on to a contrast-enhanced phase of CT scanning. Contrast-enhanced CT scanning involves the injection of a contrast agent when the patient is scanned. The contrast agent contains iodine, which illuminates on a CT scan. Whether or not certain vessels and tissue illuminate, helps to establish the location and extent of the vessel occlusion, ischemia, and infarction.

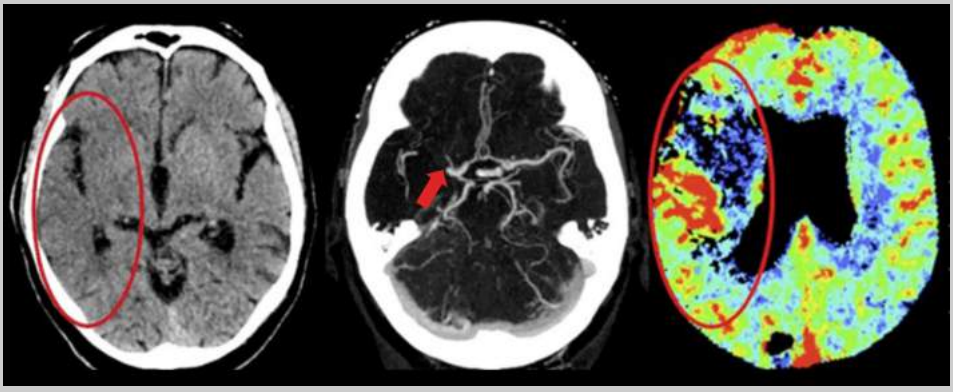

Figure 5

Multimodal imaging of an ischemic stroke patient. From left to right: a non-contrast CT scan which rules out hemorrhagic stroke, a CT angiography scan which shows the blood vessels and the location of the vessel occlusion on the left side of the image, and a CT perfusion scan which shows an ischemic region. The red oval roughly indicates the total ischemic region, in which a severely ischemic region with a low cerebral blood volume can be recognized. The slice that is shown for the CT perfusion scan is different from the slice that is shown for the other scans. Case courtesy of Frans Kauw [7].

The contrast-enhanced phase of CT scanning consists of CT angiography (CTA) imaging and CT perfusion (CTP) imaging (Figure 5). CTA imaging aims to visualize the vessels in order to establish the location and extent of the vessel occlusion. CTP imaging aims to visualize the blood flow to the brain tissue in order to establish the location and extent of the ischemia and infarction. The location of a vessel occlusion, the degree of alternate circulation around an occluded vessel, and the extent to which ischemic tissue has infarcted can each affect the clinical outcome and treatment options for ischemic stroke patients [8–10]. Both CTA and CTP imaging can thus provide information to evaluate and manage ischemic stroke.

Instead of CT, MR is sometimes used to image stroke patients in the acute setting. MR imaging can provide detailed images of the brain through the diffusion of water molecules and is more sensitive to infarction, making it better at detecting small and early infarcts. In the acute setting though, CT imaging has the advantages of being faster, more easily and widely available, and having less contraindications. It is also better at ruling out hemorrhagic stroke and providing quantitative data on the perfusion of the brain. Because of its practicality, CT imaging has remained preferred in acute ischemic stroke care, whereas MR imaging is still used to provide accurate follow-up imaging of ischemic stroke patients.

CT perfusion imaging as patient selection tool for thrombectomy

Since the publication of the MR CLEAN trial in 2015, thrombectomy has radically improved the outlook for stroke patients with a large vessel occlusion [11]. However, this initial trial only covered those who received treatment within 6 hours of symptom onset, making thrombectomy the standard of care for early large vessel occlusion patients but not for later arrivals or for patients with smaller vessel occlusions. With the publication of the DAWN and DEFUSE 3 trials in 2018, CTP imaging emerged as a tool to select ischemic stroke patients for thrombectomy [12, 13]. The rationale is that patients with a smaller infarcted region, which can be measured both in absolute terms and in terms relative to the total ischemic region, stand to benefit more from thrombectomy.

CLEOPATRA healthcare evaluation

The CLEOPATRA (cost-effectiveness of CT perfusion for patients suffering from acute ischemic stroke) healthcare evaluation was launched to investigate the cost-effectiveness of selecting ischemic stroke patients for thrombectomy with CTP imaging [14]. With around 3600 large vessel occlusion stroke patients annually in the Netherlands, both ineffective and withheld treatments not only pose risks to the patient but to society at large. Long-term care costs are steep, exceeding 50,000 euros per patient per year, and the overall success of thrombectomy strains healthcare resources in the acute setting [15–18]. To help elicit the use of CTP imaging as a patient selection tool for thrombectomy, seventeen stroke centers in the Netherlands participated in the CLEOPATRA healthcare evaluation and contributed both retrospective and prospective data.

Figure 6

Acquisition of a contrast-enhanced CT scan. The injection protocol is set on the injector. The scan protocol is selected on the computer by the radiologic technologist behind the radiation shielding window. Reprinted with permission from mayoclinic.org

The CLEOPATRA healthcare evaluation comprised a technical, clinical, and economic component. This thesis is dedicated to the technical component, which focused on harmonizing and optimizing the CTP imaging acquisition and processing protocol. The practicality of CTP imaging has been questioned at times because of a lack of standardized protocols for acquisition and processing. The CT market is very mature, featuring several major players offering multiple scanner models and utilizing proprietary software. These tools not only differ in interface, but also in the underlying algorithms that are employed to transform the scans into perfusion data. The lack of consensus on the CTP imaging acquisition and processing protocol has hindered the widespread adoption of image-based criteria for stroke diagnosis and treatment planning [19–21]. A thorough examination of these technical aspects is necessary to assess the clinical use of CTP imaging in a multicenter setting.

CT perfusion imaging acquisition protocol

The acquisition of a CTP scan requires both an injection and a scan protocol (Figure 6). The injection protocol dictates the passing of the iodinated contrast agent through the brain vasculature. In the span of roughly a minute, CT scans are taken every few seconds as determined by the scan protocol. These CTP frames collectively depict the dynamic contrast enhancement in the brain to provide insight into the perfusion of the brain when analyzed with dedicated software (Figure 7).

Injection protocol

The injection protocol controls the signal to be measured with the CT scanner. The injection protocol is specified by choosing a contrast agent of a certain concentration (mg I/mL), an injection volume (mL), and an injection rate (mL/s). The injection of the contrast bolus is followed by a saline flush, which ensures that no contrast material is left in the syringe. The injection normally occurs in a vein in the upper arm, meaning that most of the contrast bolus does not reach the brain. A typical injection protocol consists of injecting a contrast bolus with a volume of 40 to 50 mL and a concentration of 300 mg I/mL at a rate of 6 mL/s, followed by injecting a saline flush of the same volume at the same rate. The injection protocol parameters should ensure a signal that can be measured accurately with a CT scanner and that is sufficient to distinguish ischemic tissue from healthy tissue.

Scan protocol

The scan protocol controls the measurement of the signal. The scan protocol may be specified by the strength of the X-ray beam (mA), the energy of the X-ray beam (kV), and the timing of the CTP frames. Together, the mA and kV determine the visibility of the iodinated contrast agent on a CT scan. A higher mA decreases noise, which makes the signal easier to measure. A higher kV also decreases noise, but at the same time reduces the relative contrast enhancement of the iodine, which makes the signal harder to measure. The timing of the CTP frames should be such that the signal is sampled sufficiently. Important data for the perfusion analysis may be missed if the signal is not sampled frequently, early, or late enough.

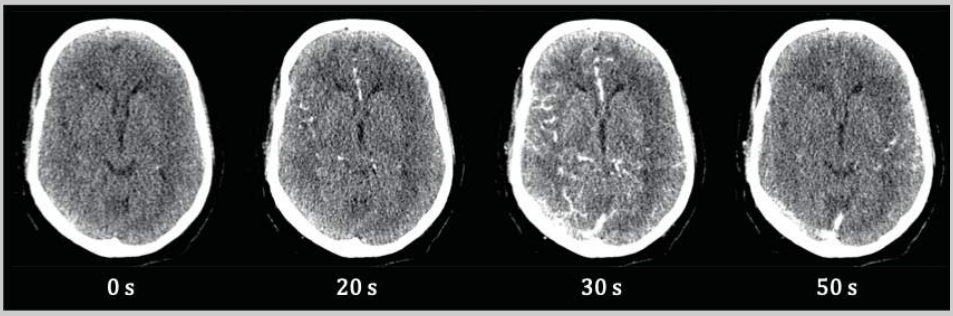

Figure 7

Frames of a CT perfusion scan. The CT frames depict the dynamic contrast enhancement in the brain. The frame at 0 seconds does not show any contrast enhancement. The frame at 20 seconds shows contrast enhancement in large arteries. The frame at 30 seconds shows contrast enhancement throughout the brain. The frame at 50 seconds shows contrast enhancement mostly in the veins. Case courtesy of Edwin Bennink [22].

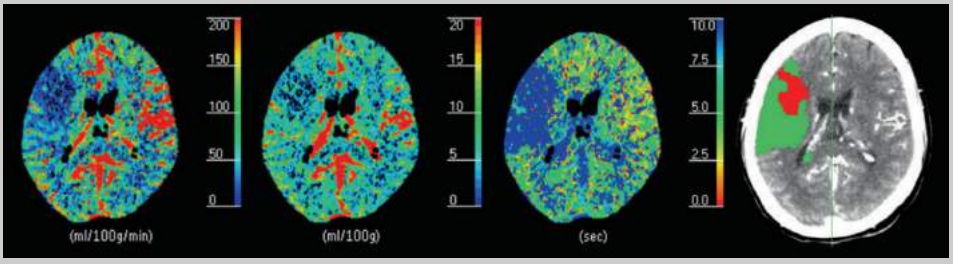

Figure 8

Analysis of a CT perfusion scan. Dedicated perfusion software translates the dynamic contrast-enhanced CT frames (Figure 7) to perfusion parameter maps that provide insight into the brain's perfusion. From left to right, we see the cerebral blood flow, the cerebral blood volume, the mean transit time, and a so-called summary map. The summary map is derived from the perfusion parameter maps and shows an estimation of the infarcted brain region in red and an estimation of a brain region that will still infarct if the vessel occlusion persists in green. Screenshots from Philips Extended Brilliance Workspace 4.0. Case courtesy of Edwin Bennink [22].

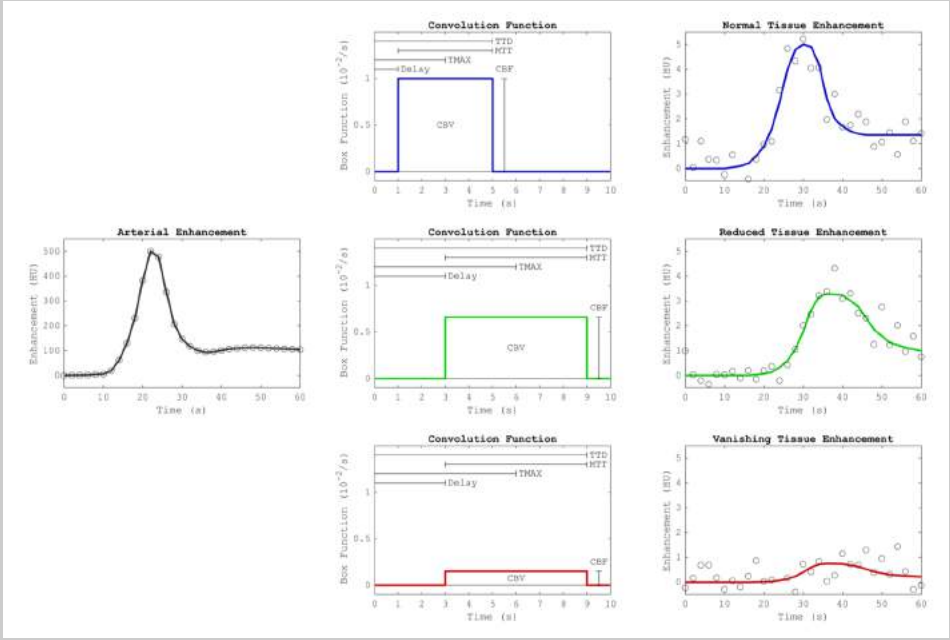

Figure 9

Perfusion analysis by a non-linear regression model [23]. On the left is the arterial input function, which is determined from the CT measurements, shown in the plot as circles. The arterial input function is reshaped by convolving it with a box function. Three different box functions are shown in the middle column. The convolution results in a calculated tissue enhancement curve. Different box functions result in different calculated tissue enhancement curves. These calculated curves are shown in the right column, together with the CT measurements, shown in the plot as circles. The calculated curves should approximate the CT measurements as closely as possible. This fixes the shape of the box function. From the shape of the fixed box function, several perfusion parameters can be derived: the cerebral blood flow (CBF), cerebral blood volume (CBV), mean transit time (MTT), time to maximum (TMAX), time to drain (TTD), and the delay.

In practice, the X-ray beam is specified by setting the mAs and kVp ('p' for 'peak') instead of the mA and kV. The mAs is the X-ray tube exposure time product. This parameter indicates the radiation dose more directly than the strength of the X-ray beam, as it is multiplied by the duration of the exposure, the fixed rotation time of the X-ray tube. Setting the kVp results in a distribution of energies for the X-ray beam that cannot be higher than the specified kVp and that is considerably lower on average. A typical scan protocol consists of thirty CTP frames, scanned with an interval of 2 seconds, at 80 kVp, and at 100 to 150 mAs. The scan protocol parameters determine the quality of the images on which to perform the perfusion analysis.

CT perfusion imaging processing protocol

The dynamic contrast-enhanced CTP frames can be analyzed with dedicated perfusion software. The CTP frames are first corrected for motion, which is called registration, and noise, which is called filtering. Then, an arterial input function, which is a curve of the contrast enhancement in a large artery, is determined. As the contrast agent travels from the large artery through the arterioles and capillaries, the contrast enhancement curve changes due to several physiological factors such as the local microvascular structure, capillary flow dynamics, dispersion, collateral circulation, and ischemia. This results in varying tissue enhancement curves, which each corresponds to a so-called voxel, which is typically of size 0.5 mm x 0.5 mm x 5.0 mm. The tissue enhancement curve of each voxel is compared with the arterial input function to produce several perfusion parameters for each voxel. Taken together, the voxels make up a perfusion map for each perfusion parameter (Figure 8).

Perfusion parameters

To understand how to generate the perfusion parameters, we consider a non-linear regression model [23]. This model-based perfusion algorithm reshapes the arterial input function, by convolving it with a box function, into a calculated tissue enhancement curve (Figure 9). This calculated curve should approximate the measured tissue enhancement as closely as possible. The shape of the calculated curve follows from the shape of the box function. From the shape of the box function, we can derive several perfusion parameters. Typically, four perfusion parameters are calculated: the cerebral blood flow (CBF), the cerebral blood volume (CBV), the mean transit time (MTT), and the time to maximum (TMAX). Other perfusion parameters, such as the delay, the time to drain (TTD), and the time to peak (TTP), are sometimes also calculated (Figure 9). We note that CBF = CBV / MTT and TMAX = delay + MTT/2. The TTP is the time at which the tissue enhancement curve, so not the convolution function, is at its maximum.

Table 1

The default thresholds to estimate the ischemic regions for different vendor software. CBF is cerebral blood flow, CBV is cerebral blood volume, MTT is mean transit time, and TMAX is time to maximum. Values relative to the opposite hemisphere are indicated by an 'r'. The units of the CBF and CBV are given per 100 g of (hypothetical) brain tissue.

Software vendor	Infarct core	Total ischemic region
Philips Healthcare (ISP)	CBV < 2.0 mL/100g & rMTT > 150%	rMTT > 150%
Siemens Healthineers	CBV < 1.2 mL/100g	CBF < 27.0 mL/100g/min
Canon Medical Systems	rCBV < 38% & TMAX > 2.30 s	TMAX > 2.30 s
iSchemaView (RAPID)	rCBF < 30%	TMAX > 6 s

Ischemic regions

The perfusion parameters describe different aspects of the perfusion, which enables the identification of different ischemic regions (Figure 8). The total ischemic region is characterized by an increased delay and MTT, so also an increased TMAX. The total ischemic region can contain both a region with a sustained CBV and a region with a decreased CBV. Where the CBV is sustained, the CBF is slightly decreased, in accordance with the increased MTT. As the CBV decreases, the CBF further decreases with it (Figure 9).

The ischemic brain region with a decreased CBV is typically called the infarct core. The rest of the total ischemic region is typically called the penumbra. Clinical threshold values used to estimate the infarct core and penumbra are found in Table 1. Applying these threshold values to the perfusion maps results in a so-called summary map (Figure 8). The summary map indicates two scenarios. In the first scenario of a persistent vessel occlusion, both the infarct core and penumbra are assumed to infarct. In the second scenario of a complete and immediate recanalization of the occluded vessel, only the infarct core is assumed to infarct. The smaller the infarct core and the larger the penumbra, the more a patient might benefit from a successful treatment. As such, the infarct core and penumbra may provide image-based criteria for the treatment decision in ischemic stroke.

Thesis outline

This thesis is concerned with harmonizing and optimizing the CTP imaging acquisition and processing protocol. Chapters 2 and 3 examine the acquisition protocol. Chapter 2 examines the effect of the injection protocol on the perfusion maps and on the summary map. Chapter 3 examines the effect of the scan protocol on the perfusion maps and on the summary map. Both chapters are studies that were performed with an anthropomorphic digital CTP phantom. Chapter 4 describes our efforts to construct a physical CTP phantom, based on the digital phantom used in chapters 2 and 3. Chapters 5 and 6, both patient studies, consider the processing protocol. Chapter 5 introduces a method to standardize the estimation of ischemic regions. This standardized method is also applied in chapter 3 (written more recently than chapter 5), which includes a comparison of processing protocols in addition to a comparison of scan protocols. Chapter 6 compares the segmentations from four methods to estimate ischemic regions: the clinical default segmentations, segmentations from the standardized method, manual segmentations of perfusion maps, and segmentations from acute MR imaging. Chapter 7 provides a perspective into a novel use of CTP imaging as a tool to locate the vessel occlusion. Chapter 8 discusses the previous chapters.

References

1 Andersen KK, Olsen TS, Dehlendorff C, Kammersgaard LP (2009) Hemorrhagic and ischemic strokes compared: Stroke severity, mortality, and risk factors. Stroke 40:2068–2072. https://doi.org/10.1161/STROKEAHA.108.540112

2 Pu L, Wang L, Zhang R, et al (2023) Projected Global Trends in Ischemic Stroke Incidence, Deaths and Disability-Adjusted Life Years From 2020 to 2030. Stroke 54:1330–1339. https://doi.org/10.1161/STROKEAHA.122.040073

3 Feigin VL, Brainin M, Norrving B, et al (2022) World Stroke Organization (WSO): Global Stroke Fact Sheet 2022. International Journal of Stroke 17:18–29

4 Bourcier R, Saleme S, Labreuche J, et al (2019) More than three passes of stent retriever is an independent predictor of parenchymal hematoma in acute ischemic stroke. J Neurointerv Surg 11:625–629. https://doi.org/10.1136/neurintsurg-2018-014380

5 Sheikh Y, Cuete D (2013) Intracerebral haemorrhage. In: Radiopaedia.org. Radiopaedia.org

6 Powers WJ, Rabinstein AA, Ackerson T, et al (2019) Guidelines for the early management of patients with acute ischemic stroke: 2019 update to the 2018 guidelines for the early management of acute ischemic stroke a guideline for healthcare professionals from the American Heart Association/American Stroke Association. Stroke 50:E344–E418

7 Kauw F, Dankbaar JW, Habets J, et al (2018) A change of heart: Yield of cardiac imaging in acute stroke workup. Case Rep Neurol 10:118–123. https://doi.org/10.1159/000489254

8 Menon BK, Smith EE, Modi J, et al (2011) Regional leptomeningeal score on CT angiography predicts clinical and imaging outcomes in patients with acute anterior circulation occlusions. American Journal of Neuroradiology 32:1640–1645. https://doi.org/10.3174/ajnr.A2564

9 Ernst M, Boers AMM, Aigner A, et al (2017) Association of Computed Tomography Ischemic Lesion Location with Functional Outcome in Acute Large Vessel Occlusion Ischemic Stroke. Stroke 48:2426–2433. https://doi.org/10.1161/STROKEAHA.117.017513

10 Tian H, Parsons MW, Levi CR, et al (2019) Influence of occlusion site and baseline ischemic core on outcome in patients with ischemic stroke. Neurology 92:E2626–E2643. https://doi.org/10.1212/WNL.0000000000007553

11 Berkhemer OA, Fransen PSS, Beumer D, et al (2015) A Randomized Trial of Intraarterial Treatment for Acute Ischemic Stroke. New England Journal of Medicine 372:11–20. https://doi.org/10.1056/nejmoa1411587

12 Albers GW, Marks MP, Kemp S, et al (2018) Thrombectomy for stroke at 6 to 16 hours with selection by perfusion imaging. New England Journal of Medicine 378:708–718. https://doi.org/10.1056/NEJMoa1713973

13 Nogueira RG, Jadhav AP, Haussen DC, et al (2018) Thrombectomy 6 to 24 hours after stroke with a mismatch between deficit and infarct. New England Journal of Medicine 378:11–21. https://doi.org/10.1056/NEJMoa1706442

14 Koopman MS, Hoving JW, van Voorst H, et al (2022) Cost-effectiveness of CT perfusion for patients with acute ischemic stroke (CLEOPATRA)-Study protocol for a healthcare evaluation study. Eur Stroke J. https://doi.org/10.1177/23969873221092535

15 Jansen IGH, Mulder MJHL, Goldhoorn RJB (2018) Endovascular treatment for acute ischaemic stroke in routine clinical practice: Prospective, observational cohort study (MR CLEAN Registry). BMJ (Online) 360:. https://doi.org/10.1136/bmj.k949

16 Williams MM, Wilson TA, Leslie-Mazwi T, et al (2018) The burden of neurothrombectomy call: A multicenter prospective study. J Neurointerv Surg 10:. https://doi.org/10.1136/neurintsurg-2018-013772

17 Desai SM, Rocha M, Molyneaux BJ, et al (2018) Thrombectomy 6-24 hours after stroke in trial ineligible patients. J Neurointerv Surg 10:1033–1038. https://doi.org/10.1136/neurintsurg-2018-013915

18 Campbell BCV, Mitchell PJ, Churilov L, et al (2017) Endovascular thrombectomy for ischemic stroke increases disability-free survival, quality of life, and life expectancy and reduces cost. Front Neurol 8:. https://doi.org/10.3389/fneur.2017.00657

19 Konstas AA, Goldmakher G V., Lee TY, Lev MH (2009) Theoretic basis and technical implementations of CT perfusion in acute ischemic stroke, Part 2: Technical implementations. American Journal of Neuroradiology 30:885–892. https://doi.org/10.3174/ajnr.A1492

20 Konstas AA, Lev MH (2010) CT perfusion imaging of acute stroke: The need for arrival time, delay insensitive, and standardized postprocessing algorithms? Radiology 254:22–25. https://doi.org/10.1148/radiol.09091610

21 Shankar JJS (2021) Variation in CT perfusion protocol has implications on defining irreversibly damaged ischemic brain parenchyma. Eur Radiol 31:8315–8316. https://doi.org/10.1007/s00330-021-08209-w

22 Bennink E (2016) Quantitative CT Perfusion Analysis in Ischemic Stroke. Utrecht University

23 Bennink E, Oosterbroek J, Kudo K, et al (2016) Fast nonlinear regression method for CT brain perfusion analysis. Journal of Medical Imaging 3:026003. https://doi.org/10.1117/1.jmi.3.2.026003

Supplementary Table 1

List of the abbreviations that appear in this thesis.

Abbreviation	Full phrase
AIF	Arterial Input Function
ASPECTS	Alberta Stroke Program Early CT Score
AUC	Area Under the Curve
BAT	Bolus Arrival Time
bSVD	block-circulant Singular Value Decomposition
CBF	Cerebral Blood Flow
CBV	Cerebral Blood Volume
CLEOPATRA	Cost-effectiveness of CT perfusion for patients with acute ischemic stroke (healthcare evaluation)
CONTRAST	Collaboration for New Treatments of Acute Stroke (consortium)
CSF	Cerebrospinal Fluid
CT	Computed Tomography (imaging)
CTP	CT Perfusion
CTA	CT Angiography
DSA	Digital Subtraction Angiography
DSC	Dice Similarity Coefficient
DUST	Dutch acute Stroke (study)
ISLES	Ischemic Stroke Lesion Segmentation (challenge)
ISP	IntelliSpace Portal
mAOL	modified Arterial Occlusive Lesion (grade)
MR	Magnetic Resonance (imaging)
MRCLEAN	Multicenter Randomized Clinical trial of Endovascular treatment for Acute ischemic stroke in the Netherlands
mRS	modified Rankin Scale
MTT	Mean Transit Time

Continued	
NCCT	Non-Contrast CT
NIHSS	National Institutes of Health Stroke Scale
PMMA	Polymethyl Methacrylate
ROC	Receiver Operating Characteristic (curve)
TMAX	Time to Maximum
TTP	Time To Peak
VOF	Venous Output Function

Chapter 2

We aimed to report the variation in computed tomography perfusion (CTP) arterial input function (AIF) in a multicenter stroke study and to assess the impact this has on CTP results.

CTP data sets from 14 different centers were included from the Dutch acute Stroke (DUST) study. The AIF was taken as a direct measure to characterize contrast bolus injection. Statistical analysis was applied to evaluate differences in amplitude, area under the curve (AUC), bolus arrival time (BAT) and time to peak (TTP). To assess the clinical relevance of differences in AIF, CTP acquisitions were simulated with a realistic anthropomorphic digital phantom. Perfusion parameters were extracted by CTP analysis using commercial software (IntelliSpace Portal (ISP), version 10.1) as well as an in-house method based on block-circulant singular value decomposition (bSVD).

A total of 1422 CTP data sets were included, ranging from 6 to 322 included patients per center. The measured values of the parameters used to characterize the AIF differed significantly with approximate interquartile ranges of 200-750 HU for the amplitude, 2,500-10,000 HU*s for the AUC, 0-17 s for the BAT and 10-26 s for the TTP. Mean infarct volumes of the phantom were significantly different between centers for both methods of perfusion analysis.

Although guidelines for the acquisition protocol are often provided for centers participating in a multicenter study, contrast medium injection protocols still vary. The resulting volumetric differences in infarct core and penumbra may impact clinical decision making in stroke diagnosis.

Comparing injection protocols

Published as 'Daan Peerlings, Edwin Bennink, Jan W Dankbaar, Birgitta K Velthuis, Hugo WAM de Jong. Variation in arterial input function in a large multicenter computed tomography perfusion study. *European Radiology* 31.11 (2021): 8317-8325.'

Introduction

The computed tomography perfusion (CTP) protocol is central to a large number of multicenter stroke studies. These studies often focus on the impact of endovascular or intra-arterial therapies on stroke outcome and use CTP as a selection modality [1–3]. A premise in these studies is that the CTP data from the contributing centers is uniform in diagnostic quality and quantitative results (e.g. infarct core volume), and can be pooled to form a homogeneous database.

However, the CTP protocol involves a number of technical acquisition and processing steps that may violate this assumption of uniformity [4, 5]. This heterogeneity may lead to significantly different (quantitative) results, necessitating harmonization of the acquisition and processing steps.

Studies have already shown that variation in the injection protocol can influence CTP results. The effect of contrast medium factors and patient factors on the time attenuation curve has been studied with a physiologically based pharmacokinetic model [6]. Also in a patient study, some of these contrast medium and patient factors were found to affect the time attenuation curve [7]. Furthermore, it was shown that a higher iodine contrast concentration can improve the quality of patient perfusion data [8]. Although several aspects of the injection protocol have been deliberated, the clinical variation between centers participating in a harmonized multicenter study and the effect this variation can have on the perfusion analysis have not been studied.

This paper explores the variation in contrast injection protocol, as characterized by the arterial input function (AIF), for centers participating in a multicenter CTP study to test the hypothesis that substantial differences in CTP results arise.

Methods

The methods of our study follow the steps visualized in Figure 1.

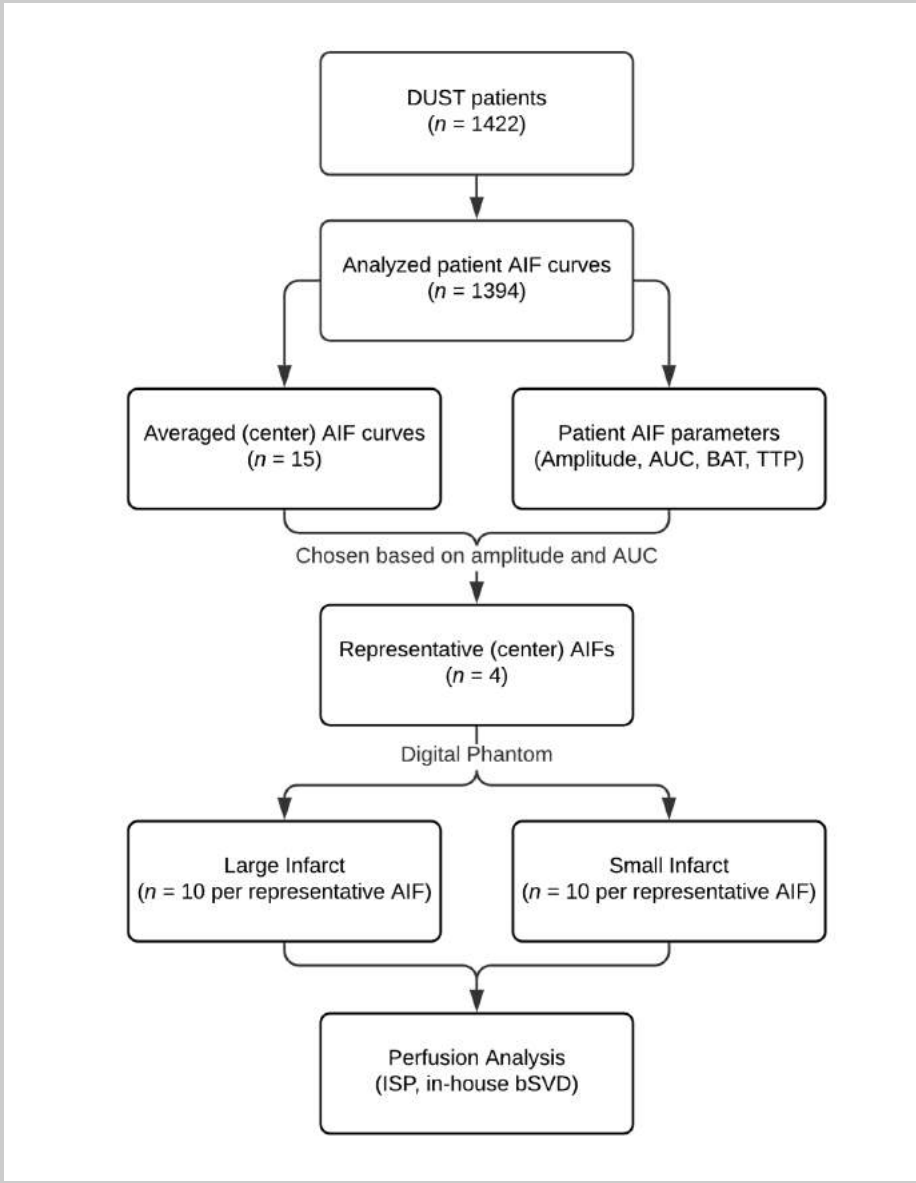

Figure 1

Flow chart of our study. AIF stands for arterial input function, AUC stands for area under the curve, BAT stands for bolus arrival time, and TTP stands for time to peak.

Acquisition of imaging data

Imaging data was acquired from fourteen stroke centers (labelled center A-M) that participated in the Dutch acute stroke (DUST) study [9]. Patients with a clinical diagnosis of acute ischemic stroke were included if they were older than eighteen years, if they had an acute neurological deficit of less than nine hours, and if the National Institutes of Health Stroke Scale was at least two or, if an indication for intravenous recombinant tissue plasminogen activator was present, was equal to one.

The DUST study protocol design describes acquisition at 80 kVp and 150 mAs on 40- to 320-detector CT scanners (GE Healthcare, Philips, Siemens, Toshiba) with a two-second interval for a duration of 50 seconds and reconstructed to a slice thickness of 5 mm. The advised injection protocol was a 40 mL contrast bolus injected at a rate of 6 mL/s followed by a saline flush of 40 mL injected at a rate of 6 mL/s.

Determination of acquisition protocols

Although a general CTP acquisition protocol was formulated for the centers participating in the DUST study, the acquisition protocols still varied between centers. Since these protocols were not inventoried at the time of the DUST study and we were unable to retrieve them retrospectively, the acquisition protocols were reconstructed from the imaging data.

Whereas the scan protocols could be reproduced from the DICOM metadata of the CTP scans, information about the injection protocol was not stored in the DICOM dataset. In order to still study the injection protocol, we looked at the variation in AIF, which reflects all important aspects of the injection protocol.

Determination of patient AIFs

All CTP data were processed centrally in a uniform manner. Prior to analysis, the scans were corrected for motion by three-dimensional registration on the skull using the registration software package Elastix [10]. For each scan, the AIF was determined from the registered image employing in-house software by averaging all attenuation curves in an automatically segmented part of the arterial tree of at least a hundred voxels. The AIF was then rescaled, such that the area under the curve (AUC) of the AIF equaled the AUC of the automatically segmented venous output function (VOF), to correct for partial volume effects. Contrary to clinical practice, the automatically determined AIF was never manually rectified.

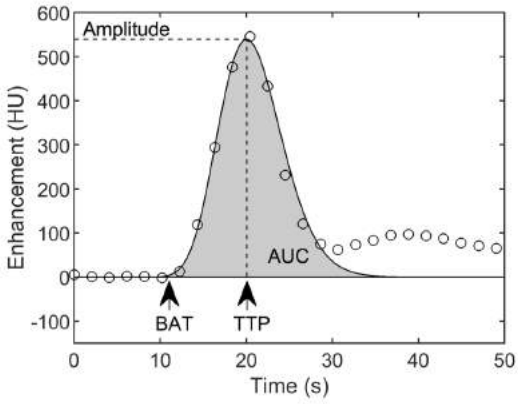

Figure 2

The considered parameters of the arterial input function: amplitude, area under the curve (AUC), bolus arrival time (BAT) and time to peak (TTP). The BAT is defined as the left 0.05% percentile of the maximum of the gamma distribution curve.

Processing of patient AIFs

For each AIF, the amplitude, AUC, bolus arrival time (BAT) and time to peak (TTP) were automatically determined from a gamma distribution fitted to the AIF (Figure 2). A boxplot was made for each parameter to show the variation within and between centers.

To test for significant differences between centers, a one-way analysis of variance (ANOVA) was performed for each parameter of the AIF. Additionally, the average amplitude, AUC, BAT and TTP with 95% confidence intervals were compared between centers, where non-overlapping confidence intervals imply a statistically significant difference. Significant differences between groups of scanner manufacturers were also tested for with a one-way ANOVA for each parameter of the AIF. In these statistical calculations, AIFs with outliers in any of its parameters were excluded, where an outlier was defined as a data point more than 1.5 times the interquartile range below the first quartile or above the third quartile.

To indicate the variation of the AIF further, the proportion of explained variance, i.e. the sum of squares between groups divided by the sum of squares total, was determined for each parameter of the AIF. These proportions indicate how much of the variation is due to the center of admission and were compared to see which parameters would benefit the most

from harmonization. Four centers were chosen as representative of the variation in AIF that results from the admission center. Although we were unable to retrieve all injection protocols retrospectively, these four centers were able to provide us with the injection protocols at the time of the DUST study.

Design of simulation study

To assess the clinical impact of the variation in AIF between centers, a simulation study was performed demonstrating the effect on the estimated infarct core and penumbra volumes. The average AIF curve of each chosen center served as input for an updated version of an anthropomorphic digital phantom [11]. These center specific average AIFs were constructed by aligning the peak of each individual patient curve before averaging these curves. If necessary, padding was performed by repeating the endpoints of the aligned AIFs.

We simulated a standard scanning protocol for the phantoms, consisting of 25 acquisitions at 80 kVp and 150 mAs for a total duration of 48 seconds with a two-second interval between acquisitions and a slice thickness of 5 mm. In the first series of phantoms a small infarct core with penumbra (8 mL core and 48 mL penumbra) was included in the right hemisphere, and in a second series a large infarct core with penumbra (26 mL core and 243 mL penumbra) was included in the right hemisphere. In both series, ten identical phantoms were generated for each of the four AIFs but with different randomly generated noise realizations, so we could take into account the influence of noise on the parameters [11].

CTP analysis of digital phantoms

Because the AIF might affect infarct quantification differently depending on the perfusion software, the images were analyzed both with a commercial method ('Arrival Time Sensitive') in IntelliSpace Portal (ISP; Brain Perfusion, IntelliSpace Portal 10.1, Philips Healthcare) and with in-house developed software based on a bSVD method, currently considered the clinical state-of-the-art to perform deconvolution on CTP data [4].

In ISP, the phantoms were automatically processed (filtering and automatic AIF/VOF selection) using proprietary methods. Factory default thresholds were applied to estimate volumes of the infarct core and penumbra, where infarct core is defined as tissue with a relative mean transit time (rMTT) $>$ 150% and cerebral blood volume (CBV) $<$ 2.0 mL/100g, and penumbra as tissue with rMTT $>$ 150% and CBV $>$ 2.0 mL/100g. For each set of ten noise realizations, the estimated core and penumbra volumes were displayed in a boxplot.

The in-house deconvolution software automatically determined the AIF of each phantom from the CTP image before filtering, using the method that was described earlier. After this, a bilateral filter with an isotropic spatial kernel of 3 mm and an intensity kernel of 20 HU was applied to filter the phantom noise realizations. Perfusion analysis was performed following a bSVD deconvolution method [12]. The infarct core was defined as tissue with a relative cerebral blood flow (rCBF) $< 20\%$, and penumbra as tissue with a rCBF between 20% and 45%. These thresholds were found by maximizing the Dice similarity coefficient between the predicted and known regions for the core and penumbra of the digital phantom. The predicted core and penumbra volumes for each center were displayed in a boxplot for each set of the noise realizations.

Statistical analysis of volumes

The mean estimated core and penumbra volumes for each center were compared using ANOVA for both of the processing methods. The mean mismatch, defined as the penumbra volume divided by the sum of the penumbra volume and core volume, was compared in the same way. In case of statistical significance, the volumes and mismatch were tested post-hoc with Tukey's honest significant difference test. The level of significance was defined as a two-tailed $P < 0.05$.

Results

All DUST participants ($n = 1422$) gave informed consent for the use of their clinical and imaging data. Eleven of the acquired scans were excluded due to problems in registration of the data. The scanning protocols, reconstructed from the DICOM metadata of the remaining scans, can be found in the Supplementary Material. Dismissing scans that deviated from the general protocol of their respective centers resulted in another 17 exclusions so that a total of 1394 scans were analyzed. When analyzing the scanning protocols, we found that center F changed their scanning protocol at some point during the study, resulting in two distinct scanning protocols. Therefore we split up this center into centers F1 and F2, corresponding to a scan acquisition with a one second and two second interval respectively.

Analysis of patient AIFs

The boxplots of the amplitude, AUC, BAT and TTP are shown in Figure 3. These show a variation within centers, which can be explained by patient variability [6, 7], as well as between centers. Overall, the amplitude yields approximate interquartile ranges of 200-750 HU, the AUC of 2,500-10,000 HU*s, the BAT of 0-17 seconds and the TTP of 10-26 seconds.

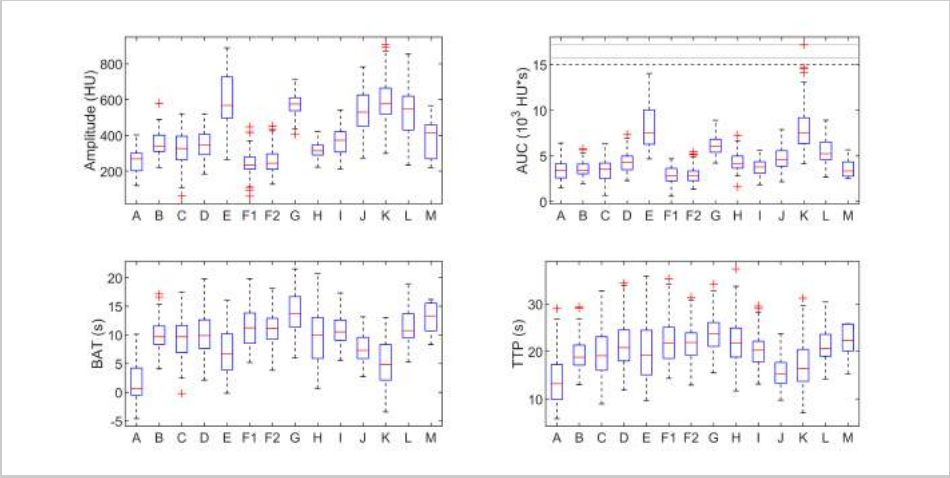

Figure 3

Boxplots of the parameters characterizing the arterial input function per stroke center. Outliers are depicted as red crosses. Extreme values were clipped, retaining the relative order, to avoid compressed boxplots.

The amplitude, AUC, BAT and TTP each differed significantly between centers (all with $P < 0.001$). An indication of which centers differed significantly, can be found in the Supplementary Material. For three groups of scanner manufacturers (i.e. Canon, Philips, and Siemens), no significant differences were found for the amplitude ($P = 0.36$), AUC ($P = 0.20$), BAT ($P = 0.17$) or TTP ($P = 0.25$). A specification of which centers were grouped, according to their scanner manufacturer, can be found in the Supplementary Material.

The proportion of explained variance for the amplitude was 64.6%, for the AUC 63.3%, for the BAT 37.1%, and for the TTP 22.4%. Based on the amplitude and AUC, the centers F2 (light blue in the figures), G (dark blue in the figures), H (light red in the figures) and J (dark red in the figures) were selected for the simulation study, as they represent a large range in AIF. Their average AIF curves can be found in Figure 4. The dark colored curves have a high amplitude and the light colored curves a low amplitude. Blue curves have a comparable width and red curves have a comparable AUC. The injection protocols of these centers are given in Table 1.

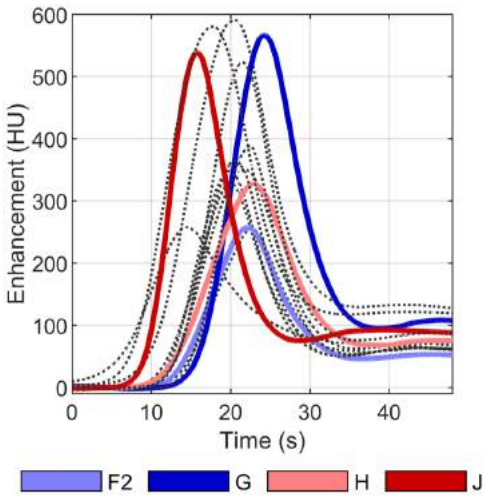

Figure 4

The average arterial input function (AIF) per stroke center. The four colored curves served as input for an anthropomorphic digital phantom. The dotted black curves are the AIFs of the other centers. Red curves have comparable AUCs and blue curves comparable widths. Light curves have a low amplitude and dark curves a high amplitude.

Table 1

Summary of the average parameters characterizing the arterial input functions selected to generate the anthropomorphic digital phantoms.

Center	Solution for injection	Concentration (mg I/mL)	Volume (mL)	Injection rate (mL/s)
F2	Ultravist	300	40	6
G	Xenetix	300	60	5.5
H	Iomeron	300	35	6
J	Iomeron	400	40	6

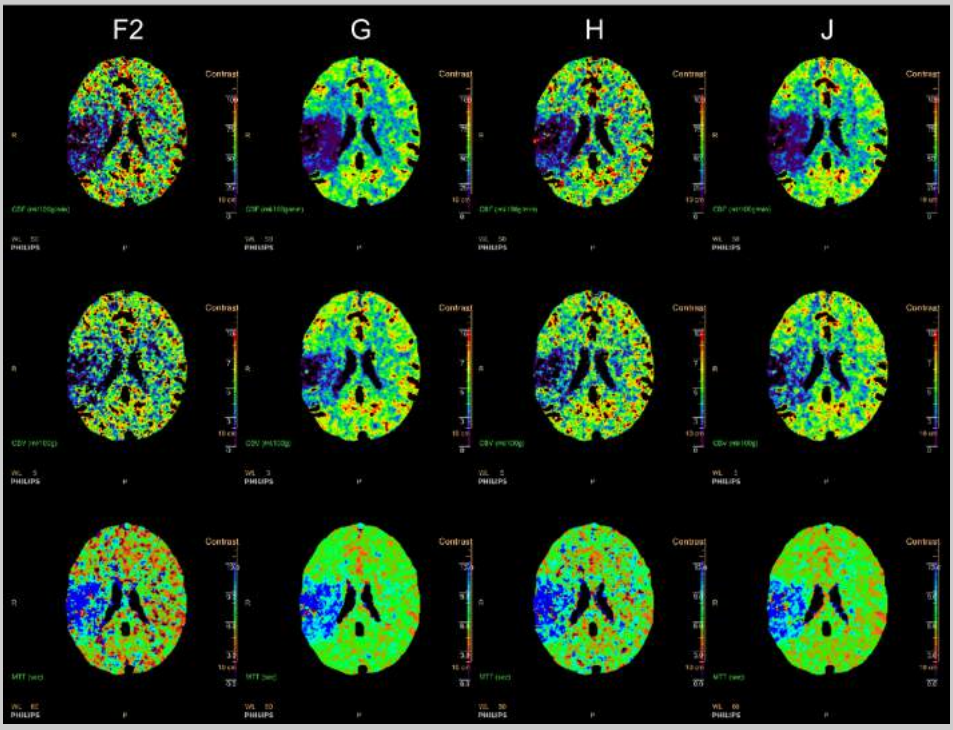

Figure 5

Parameter maps of one of the noise realizations of the anthropomorphic digital phantom with a small infarct for each of the four selected arterial input functions obtained from ISP. The cerebral blood flow (CBF; upper row) is in mL/100g/min, the cerebral blood volume (CBV, middle row) in mL/100g and the mean transit time (MTT; bottom row) in seconds.

CTP analysis of digital phantoms

As an example of the anthropomorphic digital phantom, the parameter maps of ISP for one of the ten noise realizations that include a small infarct are shown in Figure 5. Boxplots of the estimated core and penumbra volumes of the small and large infarct for each of the selected centers are shown in Figure 6. Their median and interquartile range are indicated, along with the mismatch, in Table 2. The median core volume differed between centers from 0.1 to 7.0 mL, the median penumbra volume differed between centers from 0.8 to 34.5 mL, and the median mismatch differed between centers from 0 to 8%.

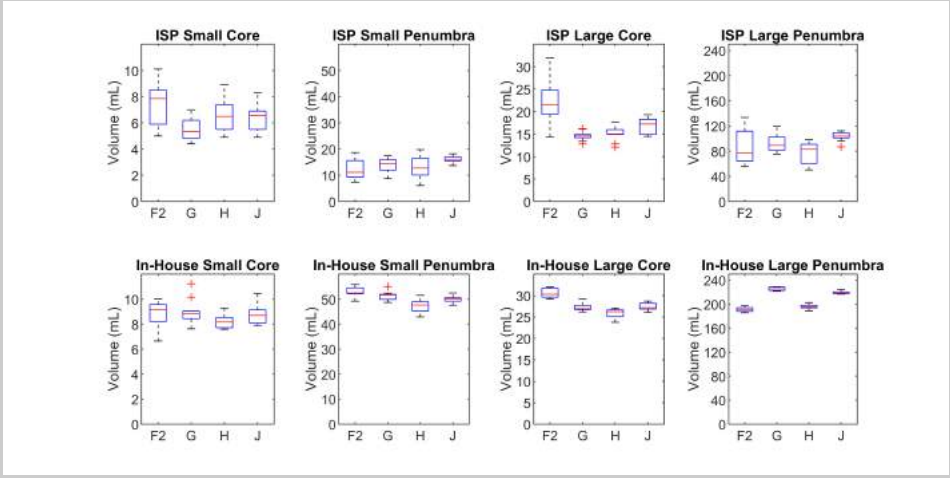

Figure 6

Boxplots of the estimated core and penumbra volumes for a small infarct (8 mL core and 48 mL penumbra) and a large infarct (26 mL core and 243 mL penumbra) obtained from ISP (upper row) and the in-house software (bottom row) for the representative centers. Outliers are depicted as red crosses.

Statistical analysis of volumes

The analysis with ISP yielded significantly different mean infarct core volumes for the small infarct ($P = 0.01$) between center F2 and center G. It also yielded significantly different mean infarct core volumes for the large infarct ($P < 0.001$) between center F2 and the other three centers. Mean penumbra volumes were not significantly different between centers for the small infarct ($P = 0.06$). For the large infarct, mean penumbra volumes differed significantly ($P = 0.03$) between centers H and J. The mean mismatch was significantly different for the small infarct ($P < 0.001$) between center F2 and centers G and J as well as between center H and centers G and J. The mean mismatch was significantly different for the large infarct ($P < 0.001$) for each pair of centers except between centers G and J.

Table 2

Median core volume, penumbra volume, and mismatch with the interquartile range in brackets. The mismatch is defined as the penumbra volume divided by the sum of the penumbra volume and the core volume.

Infarct	Center	Core volume (mL)	Penumbra volume (mL)	Mismatch
Small (ISP)	F2	7.9 (5.9 – 8.5)	11.1 (9.3 – 15.6)	0.63 (0.57 – 0.65)
	G	5.4 (4.8 – 6.2)	14.3 (12.0 – 15.9)	0.70 (0.68 – 0.74)
	H	6.5 (5.5 – 7.4)	12.7 (10.1 – 16.5)	0.67 (0.59 – 0.69)
	J	6.6 (5.5 – 6.9)	16.1 (15.5 – 17.0)	0.71 (0.69 – 0.75)
Large (ISP)	F2	21.6 (19.4 – 24.8)	76.9 (64.1 – 111.8)	0.80 (0.78 – 0.82)
	G	14.6 (14.2 – 14.9)	89.3 (81.5 – 102.6)	0.86 (0.85 – 0.87)
	H	15.0 (14.9 – 16.0)	83.0 (60.4 – 91.0)	0.84 (0.80 – 0.85)
	J	17.3 (14.9 – 18.3)	104.0 (101.0 – 109.4)	0.86 (0.85 – 0.87)
Small (in-house)	F2	9.2 (8.2 – 9.6)	52.5 (52.1 – 54.5)	0.85 (0.84 – 0.86)
	G	8.8 (8.4 – 9.0)	51.7 (49.9 – 51.9)	0.85 (0.85 – 0.86)
	H	8.2 (7.7 – 8.5)	47.7 (45.2 – 49.0)	0.85 (0.85 – 0.86)
	J	8.7 (8.1 – 9.1)	50.1 (49.2 – 50.6)	0.85 (0.84 – 0.86)
Large (in-house)	F2	30.3 (29.6 – 31.7)	191.0 (187.9 – 194.1)	0.86 (0.86 – 0.87)
	G	26.9 (26.7 – 27.7)	225.5 (222.8 – 228.5)	0.89 (0.89 – 0.89)
	H	26.3 (25.1 – 26.6)	195.8 (193.9 – 198.1)	0.88 (0.88 – 0.89)
	J	27.2 (26.9 – 28.2)	218.2 (217.5 – 220.5)	0.89 (0.89 – 0.89)

The analysis with the in-house processing method yielded no significantly different mean core volumes between centers for the small infarct ($P = 0.22$). A significant difference was found for the large infarct ($P < 0.001$) for each pair of centers except between centers G and J. Mean penumbra volumes were significantly different for the small infarct ($P < 0.001$) between center H and the other three centers as well as between center F2 and center J. Mean penumbra volumes were also significantly different for the large infarct ($P < 0.001$) for each pair of centers. The mean mismatch for the small infarct was not significantly different between the centers ($P = 0.80$). For the large infarct, the mean mismatch was significantly different ($P < 0.001$) between center F2 and the other three centers as well as between center G and center H.

Discussion

This study explored the variation in contrast injection protocol between centers, as characterized by their average AIFs, in a large multicenter stroke study. Significant differences in the magnitude and timing of the AIF were found between centers. This variation is important as it influences the variability of CTP analyses in a multicenter study. Harmonization of the injection protocol, as correspondent with the proportions of explained variance, could reduce variation in the amplitude with 64.6%, in the AUC with 63.3%, in the BAT with 37.1%, and in the TTP with 22.4%. Significant differences in infarct quantification were found as a result of the variation in amplitude and AUC between the average AIFs.

In clinical practice, imaging based treatment decisions result from a combination of non-enhanced CT, occlusion site (provided by CT angiography) and CTP. The variation in CTP contrast bolus is relevant for current clinical practice, where treatment decisions may be based on the infarct core volume and the mismatch for patients presenting beyond 6 hours after symptom onset [2, 3] or for patients with wake-up stroke [13, 14]. Although our study considered the variation in CTP contrast bolus, CT angiography also requires a contrast bolus, which is likely to vary between centers.

The influence on the AIF of the injection protocol, e.g. contrast concentration, injection rate and injection volume, as well as some patient characteristics, e.g. patient weight and cardiac output, has already been studied using simulations [6]. For some of these parameters, the effect on the AIF has also been studied within patient groups [7] and, in addition, the effect on the perfusion parameters has been examined for the contrast concentration [8]. Our study reported the variation in AIF between centers in a harmonized multicenter study and showed the clinical impact this variation can have.

In part, this clinical impact depends on the perfusion software. Differences in volumetric prediction between the two methods may be ascribed to different filtering methods, algorithms and definitions of infarct core and penumbra. Harmonization of these image processing steps to reduce the variability of CTP results in a multicenter study presents itself as a major and important challenge. Our study showed that, given the differences in volumetric predictions within each processing method, harmonization of the injection protocol is likewise important.

There were several limitations. One major limitation was that the average AIF had to be used as a surrogate for the injection protocol, while at the same time the AIF was affected by the patient's physiology. We assumed that the AIF of each patient is determined by the combination of the patient's physiology and the contrast injection, which is expected to be constant within each center. Moreover, we assumed that the average physiology of the patients admitted to each center was comparable between the centers. Therefore, the variation between the average AIFs was assumed to be the result of differences in contrast injection. This justifies the average AIF as a proxy for the injection protocol, even though the exact connection between the average AIF and parameters of the injection protocol remains unclear.

Second, we were unable to retrieve the injection protocols of all the centers at the time of patient inclusions. Under the assumption that the average physiology of the patients admitted to each center was comparable between centers, the average AIF served as a surrogate for the injection protocol to check adherence to the advised injection protocol. For the selected representative centers, the injection protocols were made available. These show that the injection protocol of the DUST study, which lacked a restriction on the contrast concentration, was not strictly adhered to with regard to bolus volume and injection rate.

Third, the perfusion maps used to study the clinical impact of the AIF were not generated from patient CTP data but from a digital phantom. This was done in order to keep the pre- and postprocessing constant, so we could isolate the influence of the AIF. Since centers perform their scans on different scanners with different protocols and software, the cause of discrepancies in patient perfusion data is more difficult to establish.

Fourth, our focus with respect to the clinical relevance of varying AIFs has been on the amplitude and AUC of the AIF. Harmonization of the BAT and TTP could also prove to be beneficial as it may allow for more easily implemented modulated scanning protocols [15] and minimization of the risk on truncation of tissue curves [16].

Conclusion

In the present study we have shown that the variation in CTP contrast injection protocol between centers results in significant differences in the magnitude and timing of the AIF. The variation in the magnitude of the AIF between centers was greater than that within centers. This variation results in significant differences in core and penumbra volume estimation, which should be acknowledged in present multicenter studies and is relevant for current clinical practice.

References

1 Borst J, Berkhemer OA, Roos YBWEM, et al (2015) Value of computed tomographic perfusion-based patient selection for intra-arterial acute ischemic stroke treatment. Stroke 46:3375–3382. https://doi.org/10.1161/STROKEAHA.115.010564

2 Nogueira RG, Jadhav AP, Haussen DC, et al (2018) Thrombectomy 6 to 24 hours after stroke with a mismatch between deficit and infarct. New England Journal of Medicine 378:11–21. https://doi.org/10.1056/NEJMoa1706442

3 Albers GW, Marks MP, Kemp S, et al (2018) Thrombectomy for stroke at 6 to 16 hours with selection by perfusion imaging. New England Journal of Medicine 378:708–718. https://doi.org/10.1056/NEJMoa1713973

4 Kudo K, Christensen S, Sasaki M, et al (2013) Accuracy and Reliability Assessment of CT and MR Perfusion Analysis Software Using a Digital Phantom. Radiology 267:201–211. https://doi.org/10.1148/radiol.12112618

5 Dani KA, Thomas RGR, Chappell FM, et al (2011) Computed tomography and magnetic resonance perfusion imaging in ischemic stroke: Definitions and thresholds. Annals of Neurology 70:384–401. https://doi.org/10.1002/ana.22500

6 Bae KT (2010) Intravenous contrast medium administration and scan timing at CT: Considerations and approaches. Radiology 256:32–61. https://doi.org/10.1148/radiol.10090908

7 Awai K, Hiraishi K, Hori S (2004) Effect of Contrast Material Injection Duration and Rate on Aortic Peak Time and Peak Enhancement at Dynamic CT Involving Injection Protocol with Dose Tailored to Patient Weight. Radiology 230:142–150. https://doi.org/10.1148/radiol.2301021008

8 König M, Bültmann E, Bode-Schnurbus L, et al (2007) Image quality in CT perfusion imaging of the brain. European Radiology 17:39–47. https://doi.org/10.1007/s00330-006-0277-3

9 van Seeters T, Biessels GJ, van der Schaaf IC, et al (2014) Prediction of outcome in patients with suspected acute ischaemic stroke with CT perfusion and CT angiography: the Dutch acute stroke trial (DUST) study protocol. BMC Neurol 14:37. https://doi.org/10.1186/1471-2377-14-37

10 Klein S, Staring M, Murphy K, et al (2010) elastix: A Toolbox for Intensity-Based Medical Image Registration. IEEE Trans Med Imaging 29:196–205. https://doi.org/10.1109/TMI.2009.2035616

11 Riordan AJ, Prokop M, Viergever MA, et al (2011) Validation of CT brain perfusion methods using a realistic dynamic head phantom. Med Phys 38:3212–3221. https://doi.org/10.1118/1.3592639

12 Wu O, Østergaard L, Weisskoff RM, et al (2003) Tracer arrival timing-insensitive technique for estimating flow in MR perfusion-weighted imaging using singular value decomposition with a block-circulant deconvolution matrix. Magnetic Resonance in Medicine 50:164–174. https://doi.org/10.1002/mrm.10522

13 Silva GS, Lima FO, Camargo ECS, et al (2010) Wake-Up Stroke: Clinical and Neuroimaging Characteristics. Cerebrovascular Diseases 29:336–342. https://doi.org/10.1159/000278929

14 Campbell BC V, Ma H, Ringleb PA, et al (2019) Extending thrombolysis to 4·5–9 h and wake-up stroke using perfusion imaging: a systematic review and meta-analysis of individual patient data. The Lancet 394:139–147. https://doi.org/10.1016/S0140-6736(19)31053-0

15 Li K, Chen G-H (2016) Noise characteristics of CT perfusion imaging: how does noise propagate from source images to final perfusion maps? In: Kontos D, Flohr TG, Lo JY (eds) American Journal of Gastroenterology. p 978310

16 Copen WA, Deipolyi AR, Schaefer PW, et al (2015) Exposing hidden truncation-related errors in acute stroke perfusion imaging. American Journal of Neuroradiology 36:638–645. https://doi.org/10.3174/ajnr.A4186

Center	Slices	Acquisitions	kVp	mAs	Included	Excluded [based on]
A [C]	8 (4 mm)	25 (2 s)	120	70	35	3 [slices: 4 (8 mm)] 2 [kVp: 80; mAs: 150]
B [P]	12 (5 mm)	25 (2 s)	80	150	76	0
C [S]	6 (4.8 mm) 12 (5 mm)	25 (2 s) 25 (2 s)	80 80	150 140	73 41	0
D [P]	12 (5 mm)	25 (2 s)	80	125	232	3 [slices: 8 (3.5 mm); acquisitions: 40 (1 s); kVp: 90; mAs: 150]
E [C]	32 (5 mm)	19 (variable, see caption)	80	75/100/200	30	5 [slices: 6 (5 mm); acquisitions: 25 (2 s); mAs: 150]
F1 [P]	8/12 (5 mm)	50 (1 s)	80	75	63	1 [acquisitions: 41 (1 s)]
F2 [P]	8/12 (5 mm) 8/12 (5 mm)	25 (2 s) 30 (2 s)	80 80	150 150	226 32	0
G [P]	8 (5 mm)	25 (2 s)	80	200	74	0
H [S]	6 (4.8 mm)	25 (2 s)	80	150	54	0
I [P]	12 (5 mm)	25 (2 s)	80	120/125	124	0
J [S]	18 (4 mm) 15 (5 mm) 19 (4 mm) 25 (3 mm)	32 (1.25 s) 34 (1.5 s) 34 (1.5 s) 34 (1.5 s)	80 80 80 80	250 220 220 220	15 25 7 30	0
K [C]	32 (5 mm)	19 (variable, see caption)	80	100/120/225	189	0
L [C]	8 (5.4 mm)	25 (2.5 s)	80	150	62	1 [acquisitions: 33 (2 s)] 1 [acquisitions: 30 (2.1 s)] 1 [slices: 4 (5.4 mm)]
M [P]	8 (5.3 mm)	25 (2 s)	80	150	6	0

Supplementary Table 1

Overview of the different scanning protocols (by approximation) of the stroke centers. Center J used spiral scanning. Centers E and K used a wide-detector scanner. For the centers with a wide-detector scanner, the protocols are (2 acquisitions (with 4 s interval), 12 acquisitions (2 s), and last 5 acquisitions (5 s)) for center E and (2 acquisitions (3 s), 12 acquisitions (2 s), 5 acquisitions (5 s)) for center K. The scanner manufacturer for each center has been indicated by 'C' for Canon, 'P' for Philips or 'S' for Siemens.

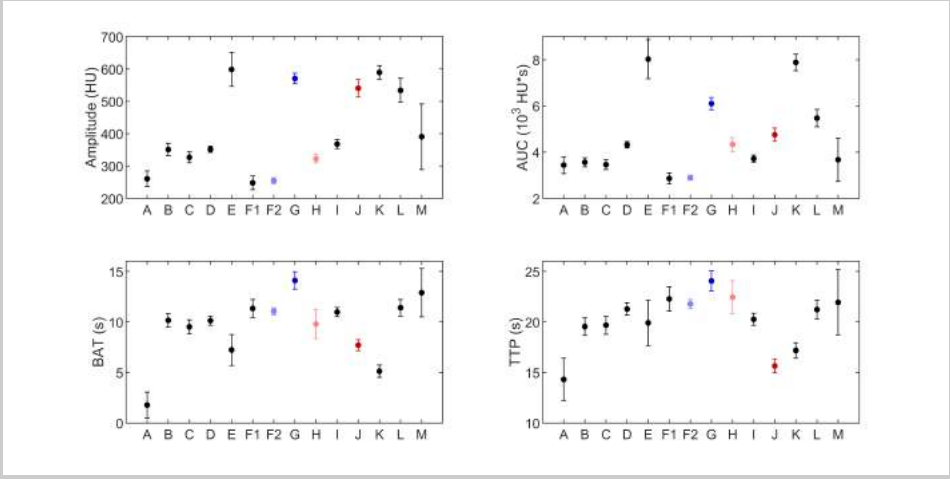

Supplementary Figure 1

Average value and 95% confidence intervals of the parameters characterizing the AIF per stroke center. These show significant differences between stroke centers whenever confidence intervals do not overlap. The AIFs of the four colored centers were used as input for an anthropomorphic digital phantom.

Chapter 3

We aimed to evaluate the real-world variation in CT perfusion (CTP) imaging protocols among stroke centers and to explore the potential for standardizing vendor software to harmonize CTP images.

Stroke centers participating in a nationwide multicenter healthcare evaluation were requested to share their CTP scan and processing protocol. The impact of these protocols on CTP imaging was assessed by analyzing data from an anthropomorphic phantom with center-specific vendor software with default settings from one of three vendors (A-C): IntelliSpace Portal, syngoVIA, and Vitrea. Additionally, standardized infarct maps were obtained using a logistic model.

Eighteen scan protocols were studied, all varying in acquisition settings. Of these protocols, seven, eight, and three were analyzed with center-specific vendor software A, B, and C respectively. The perfusion maps were visually dissimilar between the vendor software but were relatively unaffected by the acquisition settings. The median error [interquartile range] of the infarct core volumes (mL) estimated by the vendor software was -2.5 [6.5] (A)/-18.2 [1.2] (B)/-8.0 [1.4] (C) when compared to the ground truth of the phantom (where a positive error indicates overestimation). Taken together, the median error [interquartile range] of the infarct core volumes (mL) was -8.2 [14.6] before standardization and -3.1 [2.5] after standardization.

CTP imaging protocols varied substantially across different stroke centers, with the perfusion software being the primary source of differences in CTP images. Standardizing the estimation of ischemic regions harmonized these CTP images to a degree.

Comparing scan and processing protocols

Published as 'Daan Peerlings, Edwin Bennink, Jan W Dankbaar, Birgitta K Velthuis, Bart J Emmer, Jan W Hoving, Charles BLM Majoie, Henk A Marquering, Henk van Voorst, Hugo WAM de Jong. Standardizing the estimation of ischemic regions can harmonize CT perfusion stroke imaging. *European Radiology* (2023): 1-11.'

Introduction

Clinical stroke research increasingly relies on multicenter CT perfusion (CTP) imaging [1, 2]. Yet, multicenter CTP imaging is afflicted by a substantial variation in the imaging protocols used across different centers [3]. This variation raises important questions about the consistency of scientific results and the validity of clinical guidelines.

The scan protocol and perfusion software can influence CTP results in numerous ways. Several acquisition settings, such as the tube voltage, exposure, and timing of the frames, have been assessed over the years and have resulted in a multitude of considerations [4–7]. The same holds for different preprocessing steps, such as determining the arterial input function or reducing noise, implemented by the perfusion software [8–10]. Moreover, perfusion algorithms and infarct estimations have been shown to characterize ischemia differently from each other [11–14]. In daily clinical practice, stroke patients are thus evaluated in various ways according to the protocols of their admission center.

To address the daily reality of stroke imaging, this paper presents the first study of real-world variation in CTP imaging protocols among stroke centers. For a large stroke healthcare evaluation, we assess the impact of scan protocols on CTP imaging by analyzing data from an anthropomorphic phantom with center-specific vendor software. Additionally, we explore the potential for standardizing vendor software to harmonize CTP images.

Methods

Phantom data for scan protocols

Stroke centers participating in the CLEOPATRA (cost-effectiveness of CTP for patients with acute ischemic stroke) healthcare evaluation were requested to share their scan protocol [15]. The CLEOPATRA healthcare evaluation combines data from multiple prospective endovascular thrombectomy trials in the Collaboration for New Treatments of Acute Stroke (CONTRAST) consortium [16–18]. In total, 1164 patients were eligible for CLEOPATRA: 228 from the MR CLEAN-NO IV trial, 120 from the MR CLEAN-MED trial, 251 from the MR CLEAN-LATE trial, 419 from the MR CLEAN Registry, and 146 from a local cohort.

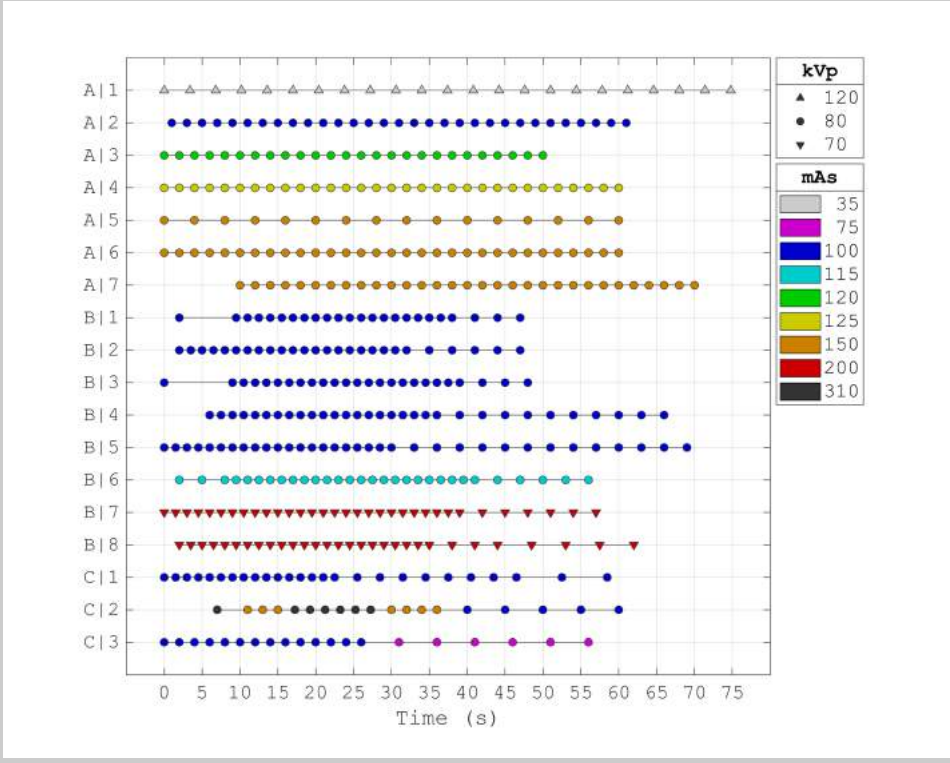

Figure 1

The scan protocols that were all shared upon request. Time is zero at the start of the contrast injection. Each of the eighteen scan protocols is denoted by a letter (A-C) indicating the vendor software and followed by a number, specifying the scan protocol.

The tube voltage (kVp), the exposure (mAs), and the timing of the frames from the CLEOPATRA stroke centers were input to an anthropomorphic digital phantom designed for a realistic CTP simulation of acute ischemic stroke that is entirely digital [19]. These parameters could be implemented in the phantom easily while giving a proper overview of the differences between centers.

Table 1

The default thresholds to estimate the ischemic stroke regions for each vendor software. CBF is cerebral blood flow, CBV is cerebral blood volume, MTT is mean transit time, and TMAX is time to maximum. Values relative to the opposite hemisphere are indicated by an 'r'.

Software	Infarct core	Hypoperfused region	Perfusion algorithm
A	CBV < 2.0 mL/100g & rMTT > 150%	rMTT > 150%	Singular value decomposition
B	CBV < 1.2 mL/100g	CBF < 27.0 mL/100g/min	Singular value decomposition
C	rCBV < 38% & TMAX > 2.30 s	TMAX > 2.30 s	Bayesian

The phantom combined MR brain images with CT imaging parameters. The (nondynamic) MR imaging of a healthy volunteer provided the brain parenchyma and the cerebral vascular system in high resolution (0.34 mm x 0.34 mm x 0.3 mm). On the MR brain images, we manually drew a ground truth infarct core (i.e. irreversibly damaged tissue) of 30 mL and a ground truth penumbra (i.e. salvageable tissue) of 55 mL in the right hemisphere, totaling to 85 mL of hypoperfused tissue.

The CT volumes that were produced from these MR images were of size 512 x 512 x 8 voxels (for each frame) with a voxel size of 0.5 mm x 0.5 mm x 5 mm. We added realistic CT noise to these CT volumes. The noise images were randomly generated with a standard deviation that corresponded to the noise in scans of a physical skull phantom made for a range of CT imaging parameters. (At 500 mAs, the standard deviation of white noise would be 3.7 HU for the digital phantoms used in this study. The actual noise images were adjusted to the reported mAs and were made spatially dependent with a kernel derived from the scans of the physical skull phantom.) For each scan protocol, ten noise realizations of the phantom were generated to take the effect of noise on CTP images into account.

The phantom could not generate noise for a tube voltage of 70 kVp because no scan data of the physical skull phantom was available for 70 kVp. Hence, for acquisitions at 70 kVp, the input parameters for the phantom were adjusted to 80 kVp while halving the mAs, conforming to the rule of thumb that an increase of 15% in tube voltage corresponds to a 50% decrease in tube current for the dose to stay the same [20].

Perfusion analysis by vendor software

For each scan protocol (Figure 1), the ten noise realizations of the phantom were analyzed with center-specific software from one of three vendors (A-C): CT Brain Perfusion (arrival-time-sensitive algorithm) from IntelliSpace Portal version 10.1 (Philips Healthcare), CT Neuro Perfusion from syngoVIA version VB40A-HF02 (Siemens Healthineers), and CT Brain Perfusion 2D (Bayesian algorithm) from Vitrea version 7.14 (Vital Images). For each analysis, we adhered to the default software settings and let the arterial input function be determined automatically. All further data processing and analysis were carried out with MATLAB (MATLAB, R2019b: The Mathworks Inc.).

The three vendor software did not all produce the same set of perfusion parameters. Vendor software A yielded a perfusion map of the cerebral blood flow (CBF), the cerebral blood volume (CBV), the mean transit time (MTT), and the time to peak (TTP). Vendor software B and C generated a time to maximum (TMAX) parameter map instead of a TTP parameter map. The TTP parameter is the time from the start of the scan until maximum enhancement. Loosely speaking, the TMAX parameter is the TTP parameter corrected for the arrival time of the arterial input function. In this paper, we sometimes write 'TMAX or TTP' by which we mean TTP for vendor software A and TMAX for vendor software B and C.

The three vendor software did not all export the perfusion maps in the same way. The perfusion maps from vendor software A and B were exported as DICOM files that contained the actual parameter values. The parameter values from vendor software A were exported as integers whereas the parameter values from vendor software B were not rounded. The perfusion maps from vendor software C were exported as DICOM files that contained grayscale values (i.e. intensities ranging from 0 to 255). These grayscale values were rescaled to obtain the parameter values. The range with which the grayscale DICOM files were exported was 0-150 mL/100g/min for the CBF, 0-10 mL/100g for the CBV, 0-20 seconds for the MTT, and 0-15 seconds for the TMAX. For vendor software A, the exported images were upsampled from 256 x 256 voxels to 512 x 512 voxels (i.e. the original size of the phantom) by repeating each voxel 2 x 2 times.

Ischemic stroke regions estimated by vendor software

The ischemic stroke regions were estimated from the perfusion maps by the vendor software with the default thresholds (Table 1). The volumes of the estimated ischemic stroke regions reported by the vendor software were logged. The segmentations of the estimated ischemic stroke regions could not be exported as DICOM files so we made screenshots of these segmentations instead (for illustrative purposes and to archive the results visually).

Ischemic stroke regions estimated by standardized method

From the perfusion maps that were generated by the vendor software, we estimated the ischemic stroke regions with a standardized method. Our aim was to provide a flexible framework to summarize the perfusion maps into different (ischemic stroke) regions. The model used for this standardization should be robust and generalizable. Little but clear training data should help to provide certainty to evident cases, leaving less certain cases to the predictive ability of the model.

We opted for a logistic model that was multivariable (i.e. more than one input variables) and multivariate (i.e. more than two output variates) [21]. In a multivendor context and from a theoretical perspective, it is preferable to include multiple perfusion parameters because it allows a fairer comparison between perfusion software. Since CTP differentiates between multiple ischemic stroke regions, it is natural to implement multiple outcomes for the tissue fate of a voxel in a single model. So, the logistic model we used to estimate the ischemic stroke regions reads:

$$P_{CORE} = 10^{S_{CORE}} / (1 + 10^{S_{CORE}} + 10^{S_{PENUMBRA}}),$$

$$P_{PENUMBRA} = 10^{S_{PENUMBRA}} / (1 + 10^{S_{CORE}} + 10^{S_{PENUMBRA}}),$$

$$P_{HEALTHY} = 1 - P_{CORE} - P_{PENUMBRA},$$

where

$$S_{CORE} = C_{INT}^{CORE} + C_{CBF}^{CORE} \times CBF + C_{CBV}^{CORE} \times CBV + C_{MTT}^{CORE} \times MTT + C_{TMAX}^{CORE} \times TMAX,$$

and

$$S_{PENUMBRA} = C_{INT}^{PENUMBRA} + C_{CBF}^{PENUMBRA} \times CBF + C_{CBV}^{PENUMBRA} \times CBV + C_{MTT}^{PENUMBRA} \times MTT + C_{TMAX}^{PENUMBRA} \times TMAX.$$

The CBF is in mL/100g/min, the CBV in mL/100g, the MTT in seconds, and the TMAX in seconds. For each vendor software, the regression coefficients C followed from a logistic regression by maximum likelihood estimation. For vendor software A, the algorithm was changed to arrival-time-insensitive (yielding a TMAX parameter map) because variable scanning starting times would otherwise result in a TTP that is not suited as a predicting variable. The arrival-time-insensitive algorithm has no recommended threshold values to estimate the ischemic stroke regions so was otherwise not used in the comparison between vendor software.

To estimate the regression coefficients of the logistic model, training data were obtained from five patient CTP scans included in the DUST (Dutch acute stroke) study [22]. These scans were selected because of an infarct core and a penumbra that were easy to distinguish on the perfusion maps generated by an in-house developed model-based nonlinear regression method [23]. To obtain the ground truth classifications, we drew two regions of ten by ten voxels in what we considered to be 100% infarct core, 100% penumbra, and 100% healthy tissue for each of the five patient scans. Hence, the model was trained on the perfusion parameters of 1000 (= 2 x 10 x 10 x 5) voxels annotated as infarct core, 1000 voxels annotated as penumbra, and 1000 voxels annotated as healthy tissue. We obtained the perfusion maps for the training data by analyzing the patient scans with each vendor software in the same way as the phantoms.

The logistic models were applied to the exported perfusion maps of the phantoms, producing fuzzy segmentations of the ischemic stroke regions. We determined the volumes of the estimated ischemic stroke regions by adding the probabilities in the fuzzy segmentation [24].

Assessment of CTP imaging

We assessed the impact of the scan protocol and the vendor software on both the perfusion parameters and the estimated ischemic stroke regions. For the perfusion parameters, we pooled the ten noise realizations for each scan protocol and depicted the values of the perfusion parameters within the infarct core, the penumbra, healthy white matter, and healthy gray matter with boxplots (given the ground truth regions in the phantom). For the estimated ischemic stroke regions, we depicted the volumes from the scan protocols with boxplots and reported the median, first quartile, and third quartile error of the volumes estimated by the vendor software and after standardization.

Results

Scan protocols and vendor software

All eighteen (A|1-C|3) scan protocols from the CLEOPATRA stroke centers were shared upon request (Figure 1). Seven of the protocols were analyzed with vendor software A, eight with vendor software B, and three with vendor software C. The scan protocols varied considerably between centers in the exposure and timing of the frames.

For scan protocols at 80 kVp, the average exposure was between 100 and 150 mAs, except for scan protocols C|2 and C|3 with an average exposure of 196 mAs and 93 mAs respectively. For lower tube voltages (of 70 kVp in scan protocols B|7 and B|8), the average exposure was 200 mAs. For higher tube voltages (of 120 kVp in scan protocol A|1), the average exposure was 35 mAs.

Scan protocols A|1 and A|5 had a longer interval between frames during contrast enhancement (which was between 10 and 35 seconds): 3.4 seconds and 4.0 seconds for scan protocols A|1 and A|5 respectively compared to at most 2.0 seconds for the other scan protocols. Scan protocol A|7 had a delayed scanning starting time of 10.0 seconds. Also, scan protocol C|2 had only one frame well before contrast arrival (which was around 10 seconds).

Examples of CTP imaging

Figure 2 shows examples of the ischemic stroke regions estimated by the vendor software and after standardization (see Table 2 for the logistic regression coefficients for each vendor software). These estimated ischemic stroke regions were derived from the perfusion maps, shown in Figure 3 for one of the eight slices. Additionally, the CBF parameter map is shown for all eight slices in Figure 4. All eight slices for the CBV, MTT, and TMAX/TTP parameter maps can be found in the Supplementary Material. Between vendor software, both the ischemic stroke regions estimated by the vendor software (Figure 2) and the perfusion maps (Figure 3 and Figure 4) were visually dissimilar.

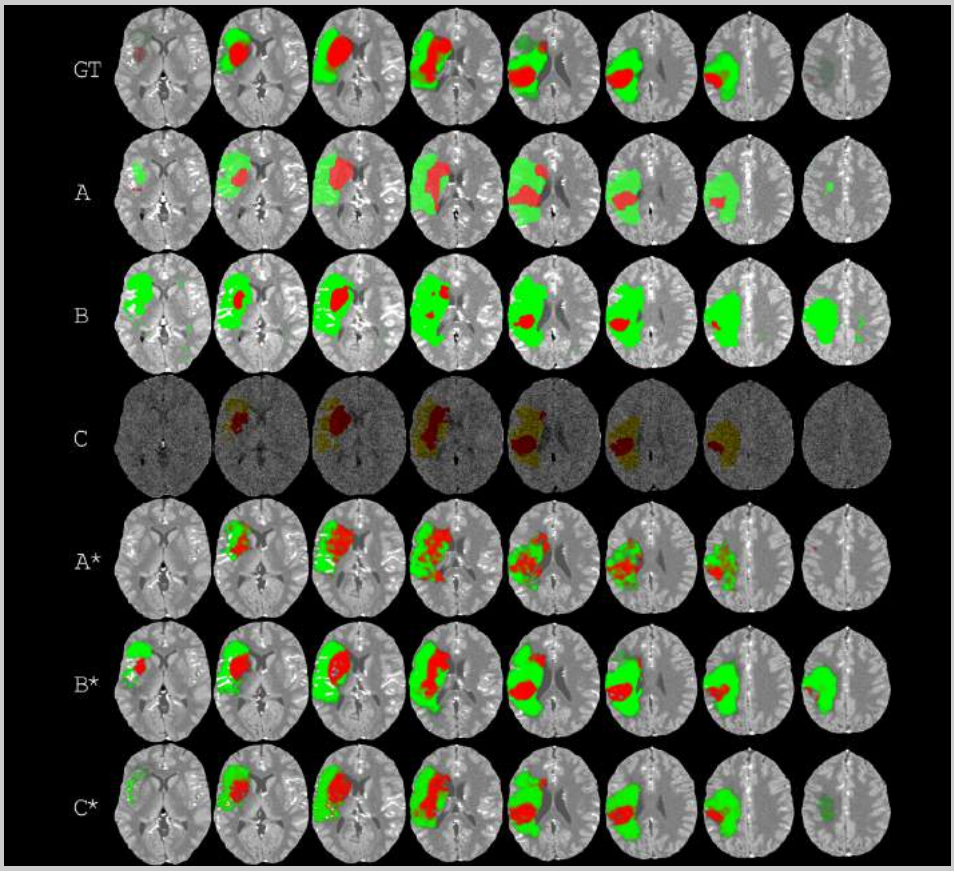

Figure 2

Examples of the ischemic stroke regions estimated by the vendor software and by the standardized method. The infarct core is in red and the penumbra is in green or yellow. Ideally, each column should be the same in all its rows. On the top row, the ground truth segmentations are shown. These segmentations are fuzzy because they were made on thinner MR slices. On the second to fourth row, the ischemic stroke regions estimated by the vendor software (A-C) are shown, obtained from screenshots. The screenshots from vendor software C are darker and noisier because they show the first frame instead of a maximum intensity projection. On the fifth to seventh row, the ischemic stroke regions estimated by the standardized method (A-C*) are shown. The examples are the first noise realization from the representative scan protocols A|4, B|6, and C|1 (see Figure 1).*

Table 2

The logistic regression coefficients for each vendor software. The coefficient for the cerebral blood flow (C_{CBF}) is in $(mL/100g/min)^{-1}$, the coefficient for the cerebral blood volume (C_{CBV}) is in $(mL/100g)^{-1}$, the coefficient for the mean transit time (C_{MTT}) is in $(seconds)^{-1}$, and the coefficient for either the time to maximum or the time to peak (C_{TMAX}) is in $(seconds)^{-1}$.

Software	Ischemic region	C_{INT}	C_{CBF}	C_{CBV}	C_{MTT}	C_{TMAX}
A	Core	-5.0	-0.0391	-4.74	-0.39	2.8
	Penumbra	-18.5	-0.0313	0.73	-0.56	3.2
B	Core	20.7	-0.7049	-8.00	-0.29	2.9
	Penumbra	-13.7	-0.0045	0.54	0.33	2.9
C	Core	-0.2	-0.7486	4.70	-0.41	1.7
	Penumbra	-16.3	-0.1747	3.87	0.48	1.7

It appears from Figure 2 that the estimated ischemic stroke regions were harmonized, to a degree, after standardization. For vendor software B, the estimated penumbra in a slice resembled the ground truth penumbra in that slice and its adjacent slices. In particular, this seemed to result in a reduced estimation of the infarct core by vendor software B as well as an estimated hypoperfused region in the outer slices, where barely any hypoperfusion should exist. Hypoperfusion in the outer slices is also clearly visible on the perfusion maps generated by vendor software B (Figure 4). These results may have been due to the filter size of vendor software B, which was 10 mm i.e. twice the slice thickness. Vendor software A appears to generate the noisiest perfusion parameters.

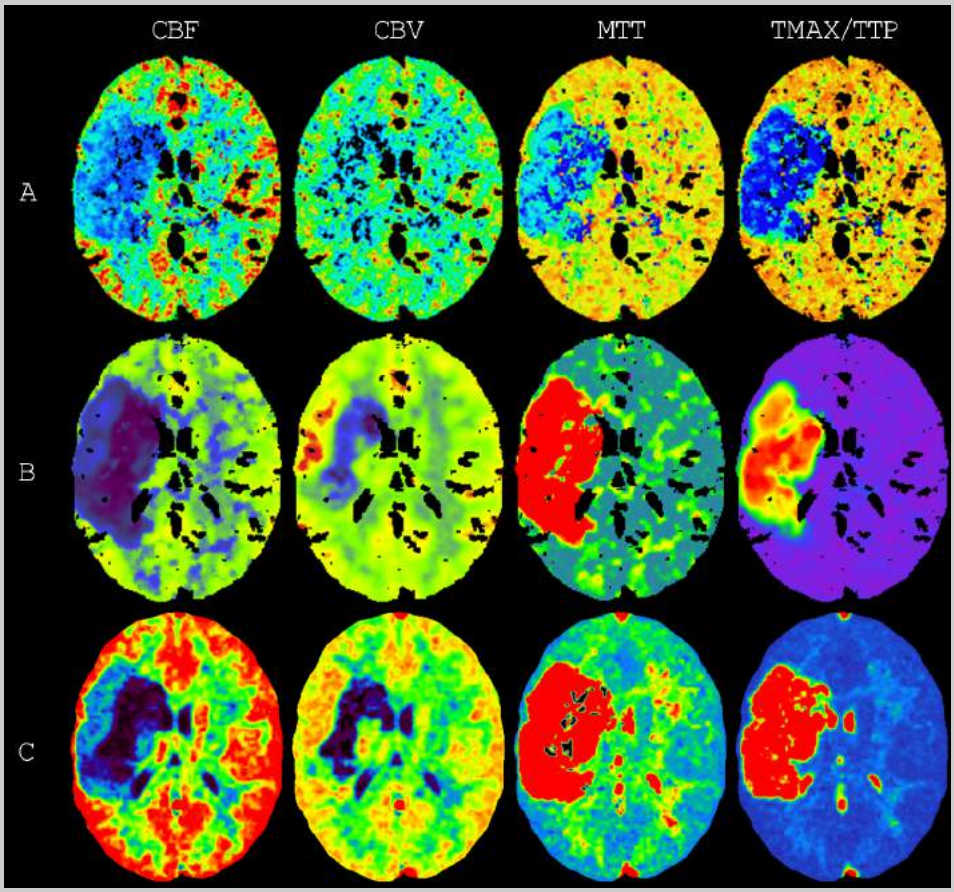

Figure 3

Examples of the perfusion maps generated by the vendor software. In each row, the perfusion maps from a different vendor software (A-C) are shown for a single slice of the phantom. In each column, a different perfusion map is shown for each vendor software. Ideally, each column should be the same in all its rows. CBF is cerebral blood flow, CBV is cerebral blood volume, MTT is mean transit time, TMAX is time to maximum, and TTP is time to peak. The color schemes were left unadjusted. The examples are the first noise realization from the representative scan protocols A|4, B|6, and C|1 (see Figure 1).

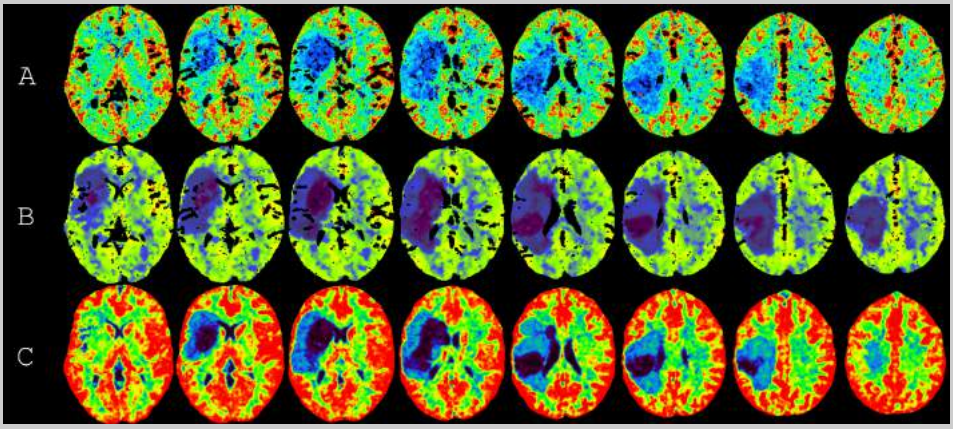

Figure 4

Examples of the cerebral blood flow parameter map generated by the vendor software. In each row, the cerebral blood flow from a different vendor software (A-C) is shown for all slices of the phantom. Ideally, each column should be the same in all its rows. The color schemes were left unadjusted. The examples are the first noise realization from the representative scan protocols A/4, B/6, and C/1 (see Figure 1).

Assessment of CTP imaging

Figure 5 shows boxplots of the perfusion parameters for one (representative) scan protocol per vendor software. We refer to the Supplementary Material for a similar overview of all the scan protocols. Figure 6 shows the boxplots of the volumes of the estimated ischemic stroke regions for each scan protocol (additional boxplots can be found in the Supplementary Material). The median, first quartile, and third quartile error of the volumes estimated by the vendor software and by the standardized method are given in Table 3.

Figure 6 demonstrates that the differences between centers were mainly due to the vendor software. Vendor software A estimated the largest infarct cores and was the most sensitive to different noise realizations of the phantom. Vendor software B and C were both much less sensitive to the different noise realizations. Vendor software B estimated smaller infarct cores than vendor software C. Hence, three groups of estimated volumes according to vendor software clearly emerged.

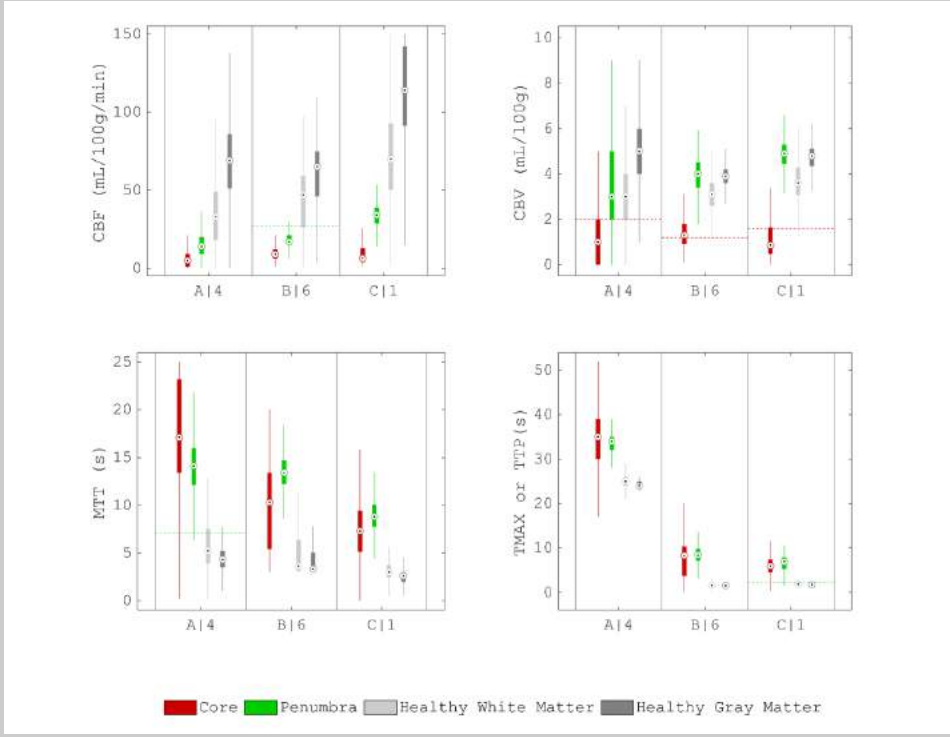

Figure 5

Boxplots of the perfusion parameters estimated by the vendor software. We pooled the ten noise realizations of the phantom for each scan protocol and show the results for scan protocol A/4, B/6, and C/1. The dashed horizontal colored lines indicate the thresholds given in Table 1, for which relative values were calculated as relative to the median value of the perfusion parameter in healthy matter. CBF is cerebral blood flow, CBV is cerebral blood volume, MTT is mean transit time, TMAX is time to maximum, and TTP is time to peak.

Albeit much less than the vendor software, the scan acquisition protocol impacted the estimated volumes in some cases (Figure 6). Scan protocols A|1 and A|5, with a longer interval between frames during contrast enhancement, resulted in volumes that deviated the most. Too few frames before contrast arrival may have increased the variance in the estimated infarct core for scan protocols A|7 and C|2 because of an increased noise in the CBV [25].

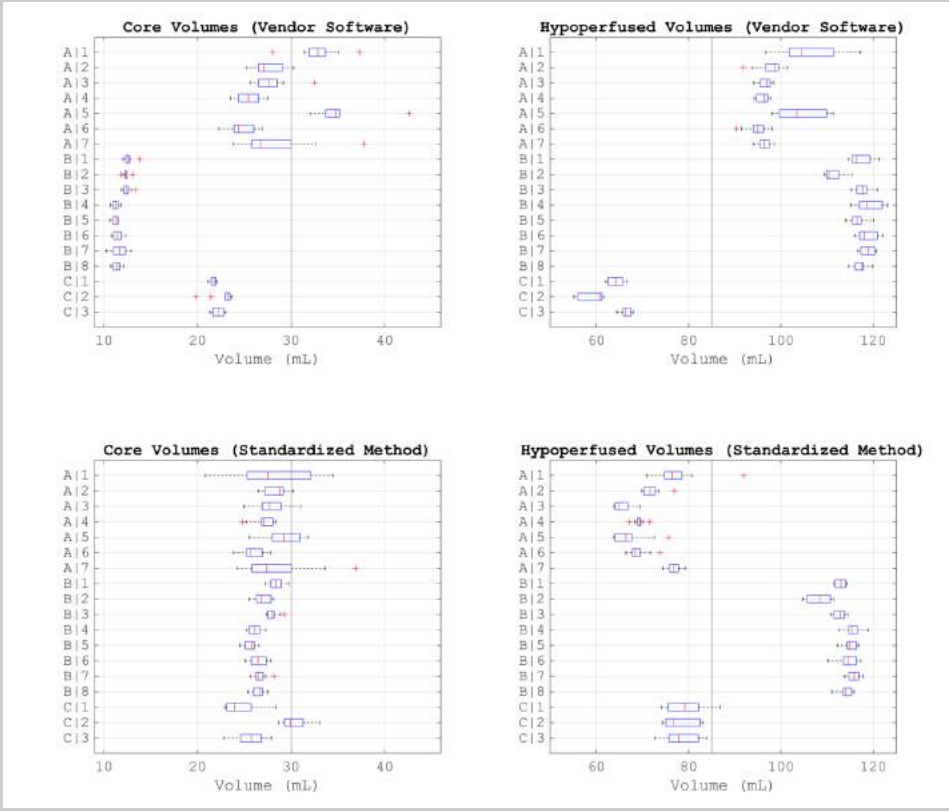

Figure 6

Boxplots of the volumes of the ischemic stroke regions estimated by the vendor software and by the standardized method. Eighteen scan protocols (A|1-C|3) were analyzed with center-specific software from one of three vendors (A-C). The vertical black lines indicate the ground truth volumes.

The estimated volumes of the infarct core were aligned between vendor software and scan protocols after standardization (Figure 6 and Table 3). The estimated volumes of the hypoperfused region were still segregated, mainly between vendor software B and vendor software A and C (Figure 6). The standardized method overestimated the hypoperfused region for vendor software B, which could be expected from the perfusion maps and which resulted in a wider interquartile range for the hypoperfused volumes (Figure 4 and Table 3).

Table 3

Median [first quartile, third quartile] error of the volumes of the ischemic stroke regions estimated by the vendor software and by the standardized method. We pooled all noise realizations of the phantom. A positive error indicates overestimation.

Ischemic region	Vendor software	Standardized method
Core (mL)	-8.2 [-18.1, -3.5]	-3.1 [-4.2, -1.7]
Hypoperfused (mL)	18.4 [10.2, 32.0]	-3.2 [-12.5, 28.8]

Discussion

Our study evaluated CTP stroke imaging in a real-world setting and found that the estimated ischemia varied greatly between centers. The primary source of this variation was the perfusion software rather than the acquisition protocol. Previous research has already shown for patient data that vendor software can cause large differences in estimated ischemia and our study supports these findings with homogeneous phantom data representative of clinical variation [11, 26, 27]. The homogeneous nature of our data, combined with the disparate outcome, suggests that multicenter CTP data and prevailing clinical guidelines may in fact hold limited validity. Hence, patients are likely evaluated variously at present, with both scientific and clinical consequences, depending on the software used to analyze their CTP scans.

Much of the variation between vendor software was due to the estimation of ischemia. While the perfusion maps were both qualitatively and quantitatively dissimilar, the standardized method resulted in a harmonized estimation of ischemia. This feasibility of harmonization implies that the perfusion parameters from the different vendor software actually contain a comparable level of information and can be equally valuable on the whole when properly assessed. We opted for a logistic model to standardize vendor software because of its ability to combine multiple perfusion parameters when characterizing ischemia, while being insusceptible to multicollinearity in its predictions, so that each vendor software could be assessed fairly based on all of their perfusion data [28]. Additionally, a logistic model is relatively easy to implement by vendors. Although similar models have been proposed in the past, they have not been applied in the context of harmonization [13, 24, 29–31]. Some variation in the estimated ischemia remained, demonstrating a desirable sensitivity to the acquisition and processing protocol. As a clear example, the overestimated hypoperfusion

from vendor software B rightly resulted in divergent volumes. Thus, variability in CTP imaging resulted mainly from the vendor software but could be compensated for when estimating ischemia.

The acquisition protocol may require minimal guidelines to ensure consistent CTP imaging. Previous studies have already shown that acquisition settings can affect CTP images separately [4–7]. By examining existent acquisition protocols integrally, our findings suggest that the timing of the frames is the most consequential aspect of present scan protocols. Minimal requirements on this timing, such as a maximum interval during contrast enhancement and a minimum number of frames before contrast arrival, may be sufficient to level the variation that was due to the scan protocol. Hence, only little standardization of the acquisition protocol seems necessary to secure a harmonized CTP outcome when the same perfusion software is used.

Our study has some limitations. It is based on phantom data, which may not directly translate to patient data. Emulating anthropomorphic perfusion data and generating realistic scanner noise are both challenging tasks. Additionally, scanner-specific features such as the reconstruction algorithm are difficult to incorporate in a digital phantom. Besides, we did not consider the contrast medium injection protocol, which has been shown to affect CTP imaging as well and which may combine with aspects of the scan protocol [32]. For instance, shorter injection times may require shorter frame intervals to not overpass the contrast enhancement phase. Finally, an identical treatment of each vendor software was hampered by their different implementations, for example in the set, the size, and the value of the exported DICOM images, limiting the veracity of the standardization of the vendor software.

Conclusion

We evaluated CTP imaging in a real-world setting and found that ischemia was estimated disparately between centers. The perfusion software, rather than the acquisition protocol, was the main cause of this variation. Still, the variation in estimated ischemia could be reconciled by incorporating all available perfusion data in a consistent way. Accordingly, we advocate for the harmonization of CT perfusion imaging by standardizing the estimation of ischemia.

References

1 Nogueira RG, Jadhav AP, Haussen DC, et al (2018) Thrombectomy 6 to 24 hours after stroke with a mismatch between deficit and infarct. New England Journal of Medicine 378:11–21. https://doi.org/10.1056/NEJMoa1706442

2 Albers GW, Marks MP, Kemp S, et al (2018) Thrombectomy for stroke at 6 to 16 hours with selection by perfusion imaging. New England Journal of Medicine 378:708–718. https://doi.org/10.1056/NEJMoa1713973

3 Shankar JJS (2021) Variation in CT perfusion protocol has implications on defining irreversibly damaged ischemic brain parenchyma. Eur Radiol 31:8315–8316. https://doi.org/10.1007/s00330-021-08209-w

4 Wintermark M, Maeder P, Verdun FR, et al (2000) Using 80 kVp versus 120 kVp in perfusion CT measurement of regional cerebral blood flow. American Journal of Neuroradiology 21:1881–1884

5 Murphy A, So A, Lee TY, et al (2014) Low dose CT perfusion in acute ischemic stroke. Neuroradiology 56:1055–1062. https://doi.org/10.1007/s00234-014-1434-z

6 Manniesing R, Oei MTH, Van Ginneken B, Prokop M (2016) Quantitative dose dependency analysis of whole-brain CT perfusion imaging. Radiology 278:190–197. https://doi.org/10.1148/radiol.2015142230

7 van Ommen F, Kauw F, Bennink E, et al (2019) Effect of prolonged acquisition intervals for CT-perfusion analysis methods in patients with ischemic stroke. Med Phys 46:3156–3164. https://doi.org/10.1002/mp.13559

8 Fahmi F, Marquering HA, Borst J, et al (2014) 3D movement correction of CT brain perfusion image data of patients with acute ischemic stroke. Neuroradiology 56:445–452. https://doi.org/10.1007/s00234-014-1358-7

9 Ferreira RM, Lev MH, Goldmakher G V., et al (2010) Arterial Input Function Placement for Accurate CT Perfusion Map Construction in Acute Stroke. American Journal of Roentgenology 194:1330–1336. https://doi.org/10.2214/AJR.09.2845

10 Mendrik AM, Vonken EJ, Van Ginneken B, et al (2011) TIPS bilateral noise reduction in 4D CT perfusion scans produces high-quality cerebral blood flow maps. Phys Med Biol 56:3857–3872. https://doi.org/10.1088/0031-9155/56/13/008

11 Kudo K, Sasaki M, Yamada K, et al (2010) Differences in CT perfusion maps generated by different commercial software: Quantitative analysis by using identical source data of acute stroke patients. Radiology 254:200–209. https://doi.org/10.1148/radiol.254082000

12 Konstas AA, Lev MH (2010) CT perfusion imaging of acute stroke: The need for arrival time, delay insensitive, and standardized postprocessing algorithms? Radiology 254:22–25. https://doi.org/10.1148/radiol.09091610

13 Flottmann F, Broocks G, Faizy TD, et al (2017) CT-perfusion stroke imaging: a threshold free probabilistic approach to predict infarct volume compared to traditional ischemic thresholds. Sci Rep 7:6679. https://doi.org/10.1038/s41598-017-06882-w

14 Peerlings D, van Ommen F, Bennink E, et al (2022) Probability maps classify ischemic stroke regions more accurately than CT perfusion summary maps. Eur Radiol 32:6367–6375. https://doi.org/10.1007/s00330-022-08700-y

15 Koopman MS, Hoving JW, van Voorst H, et al (2022) Cost-effectiveness of CT perfusion for patients with acute ischemic stroke (CLEOPATRA)-Study protocol for a healthcare evaluation study. Eur Stroke J. https://doi.org/10.1177/23969873221092535

16 Chalos V, Van De Graaf RA, Roozenbeek B, et al (2020) Multicenter randomized clinical trial of endovascular treatment for acute ischemic stroke. The effect of periprocedural medication: Acetylsalicylic acid, unfractionated heparin, both, or neither (MR CLEAN-MED). Rationale and study design. Trials 21:1–17. https://doi.org/10.1186/s13063-020-04514-9

17 Treurniet KM, LeCouffe NE, Kappelhof M, et al (2021) MR CLEAN-NO IV: intravenous treatment followed by endovascular treatment versus direct endovascular treatment for acute ischemic stroke caused by a proximal intracranial occlusion—study protocol for a randomized clinical trial. Trials 22:1–15. https://doi.org/10.1186/s13063-021-05063-5

18 Pirson FAV (Anne), Hinsenveld WH, Goldhoorn R-JB, et al (2021) MR CLEAN Late study protocol. Trials 15:1–13

19 Riordan AJ, Prokop M, Viergever MA, et al (2011) Validation of CT brain perfusion methods using a realistic dynamic head phantom. Med Phys 38:3212–3221. https://doi.org/10.1118/1.3592639

20 Lira D, Padole A, Kalra MK, Singh S (2015) Tube potential and CT radiation dose optimization. AJR Am J Roentgenol 204:W4–W10. https://doi.org/10.2214/AJR.14.13281

21 Ebrahimi Kalan M, Jebai R, Zarafshan E, Bursac Z (2021) Distinction Between Two Statistical Terms: Multivariable and Multivariate Logistic Regression. Nicotine Tob Res 23:1446–1447. https://doi.org/10.1093/ntr/ntaa055

22 van Seeters T, Biessels GJ, van der Schaaf IC, et al (2014) Prediction of outcome in patients with suspected acute ischaemic stroke with CT perfusion and CT angiography: the Dutch acute stroke trial (DUST) study protocol. BMC Neurol 14:37. https://doi.org/10.1186/1471-2377-14-37

23 Bennink E, Oosterbroek J, Kudo K, et al (2016) Fast nonlinear regression method for CT brain perfusion analysis. Journal of Medical Imaging 3:026003. https://doi.org/10.1117/1.jmi.3.2.026003

24 Peerlings D, Ommen F Van, Bennink E, et al (2022) Probability maps classify ischemic stroke regions more accurately than CT perfusion summary maps. C:

25 Li K, Chen G-H (2016) Noise characteristics of CT perfusion imaging: how does noise propagate from source images to final perfusion maps? Medical Imaging 2016: Physics of Medical Imaging 9783:978310. https://doi.org/10.1117/12.2216293

26 Koopman MS, Berkhemer OA, Geuskens RREG, et al (2019) Comparison of three commonly used CT perfusion software packages in patients with acute ischemic stroke. J Neurointerv Surg 11:1249–1256. https://doi.org/10.1136/neurintsurg-2019-014822

27 Fahmi F, Marquering HA, Streekstra GJ, et al (2012) Differences in CT perfusion summary maps for patients with acute ischemic stroke generated by 2 software packages. American Journal of Neuroradiology 33:2074–2080. https://doi.org/10.3174/ajnr.A3110

28 Farrar DE, Glauber RR (1967) Multicollinearity in Regression Analysis : The Problem Revisited. The Review of Economic and Statistics 49:92–107

29 Kemmling A, Flottmann F, Forkert ND, et al (2015) Multivariate Dynamic Prediction of Ischemic Infarction and Tissue Salvage as a Function of Time and Degree of Recanalization. Journal of Cerebral Blood Flow & Metabolism 35:1397–1405. https://doi.org/10.1038/jcbfm.2015.144

30 Goyal M, Ospel JM, Menon B, et al (2020) Challenging the Ischemic Core Concept in Acute Ischemic Stroke Imaging. Stroke 3147–3155. https://doi.org/10.1161/STROKEAHA.120.030620

31 Goyal M, McTaggart R, Ospel JM, et al (2022) How can imaging in acute ischemic stroke help us to understand tissue fate in the era of endovascular treatment and cerebroprotection? Neuroradiology 64:1697–1707. https://doi.org/10.1007/s00234-022-03001-z

32 Peerlings D, Bennink E, Dankbaar JW, et al (2021) Variation in arterial input function in a large multicenter computed tomography perfusion study. Eur Radiol 31:8317–8325. https://doi.org/10.1007/s00330-021-08067-6

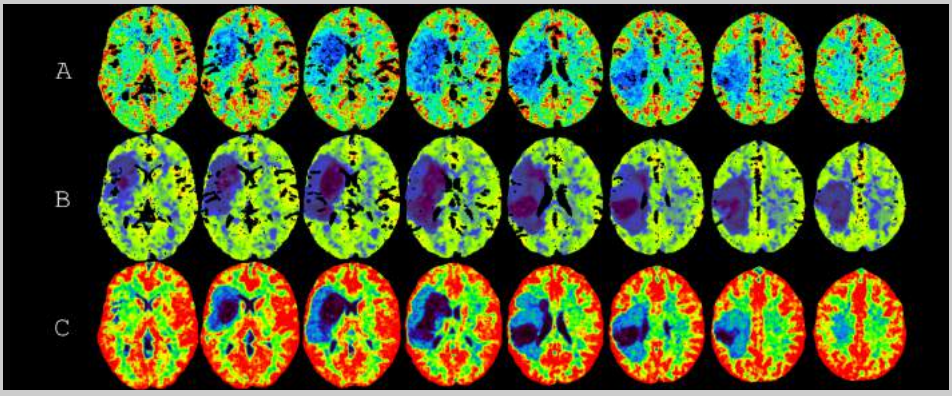

Figure 7

Examples of the cerebral blood flow parameter map generated by the vendor software. In each row, the cerebral blood flow from a different vendor software (A-C) is shown for all slices of the phantom. The color schemes were left unadjusted. The examples are the first noise realization from the representative scan protocols A|4, B|6, and C|1 (see Figure 1).

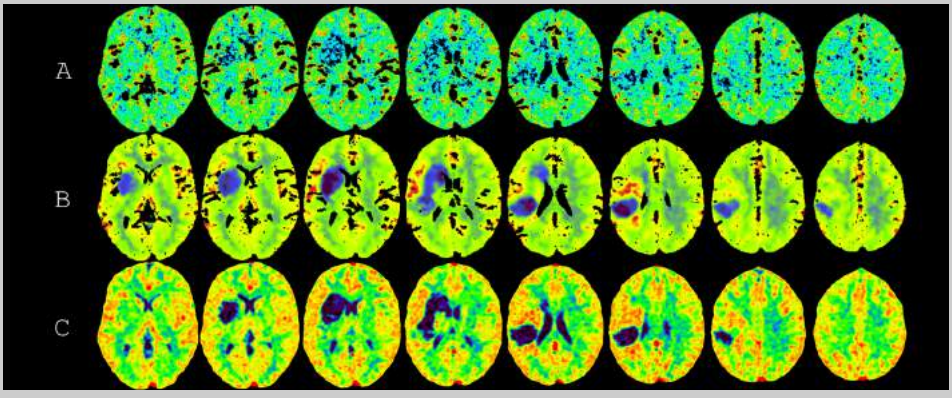

Supplementary Figure 1

Examples of the cerebral blood volume parameter map generated by the vendor software. In each row, the cerebral blood volume from a different vendor software (A-C) is shown for all slices of the phantom. The color schemes were left unadjusted. The examples are the first noise realization from the representative scan protocols A|4, B|6, and C|1 (see Figure 1).

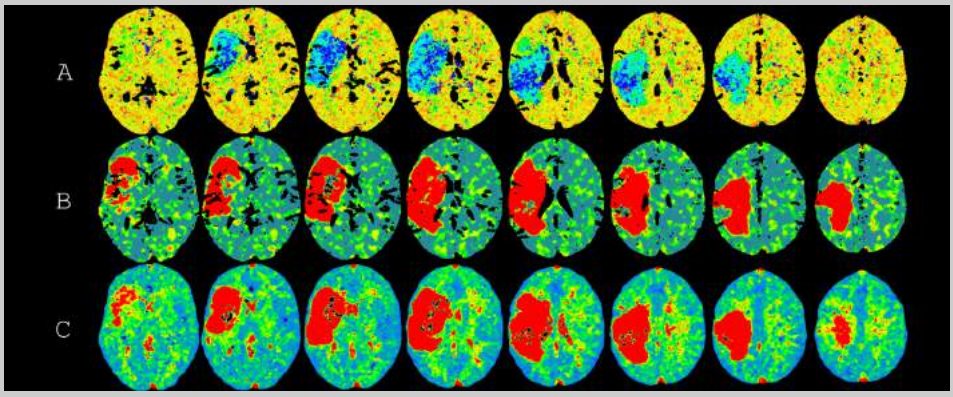

Supplementary Figure 2

Examples of the mean transit time parameter map generated by the vendor software. In each row, the mean transit time from a different vendor software (A-C) is shown for all slices of the phantom. The color schemes were left unadjusted. The examples are the first noise realization from the representative scan protocols A|4, B|6, and C|1 (see Figure 1).

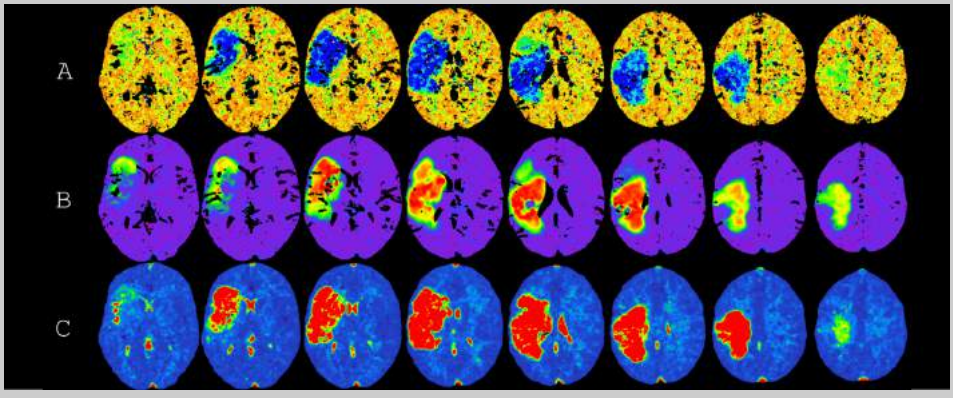

Supplementary Figure 3

Examples of the time to maximum or time to peak parameter map generated by the vendor software. In the first row, the time to peak from vendor software A and, in the second and third row, the time to maximum from vendor software B and C are shown for all slices of the phantom. The color schemes were left unadjusted. The examples are the first noise realization from the representative scan protocols A|4, B|6, and C|1 (see Figure 1).

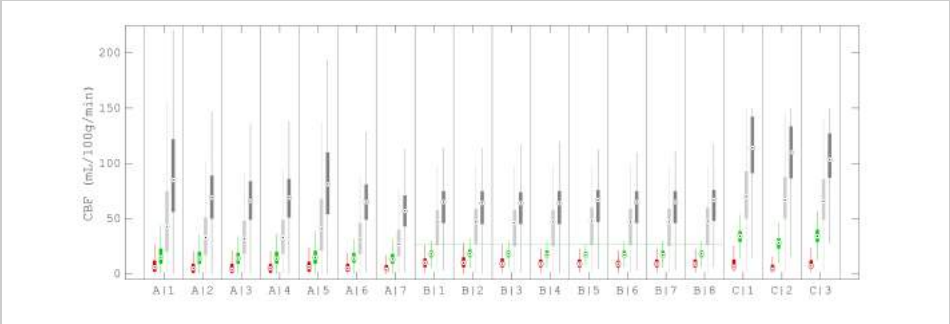

Supplementary Figure 4

Boxplots of the cerebral blood flow (CBF) estimated by the vendor software for each scan protocol (A|1-C|3). We pooled the ten noise realizations of the phantom for each scan protocol. The dashed horizontal colored lines indicate the thresholds given in Table 1, for which relative values were calculated as relative to the median value of the perfusion parameter in healthy matter.

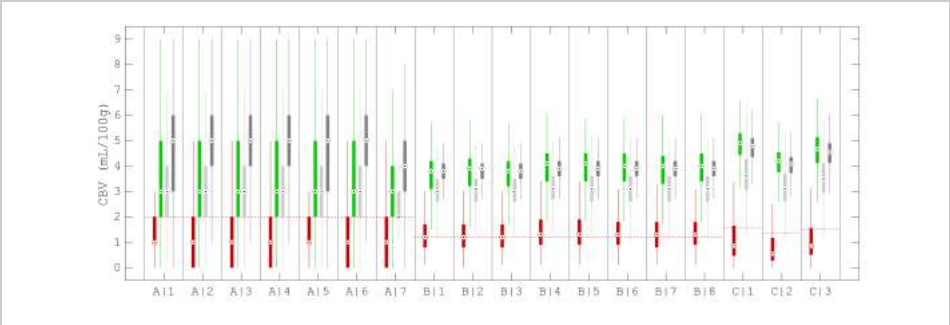

Supplementary Figure 5

Boxplots of the cerebral blood volume (CBV) estimated by the vendor software for each scan protocol (A|1-C|3). We pooled the ten noise realizations of the phantom for each scan protocol. The dashed horizontal colored lines indicate the thresholds given in Table 1, for which relative values were calculated as relative to the median value of the perfusion parameter in healthy matter.

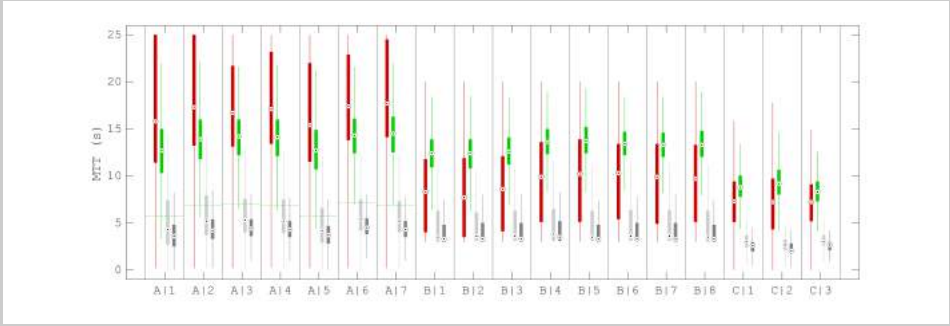

Supplementary Figure 6

Boxplots of the mean transit time (MTT) estimated by the vendor software for each scan protocol (A|1-C|3). We pooled the ten noise realizations of the phantom for each scan protocol. The dashed horizontal colored lines indicate the thresholds given in Table 1, for which relative values were calculated as relative to the median value of the perfusion parameter in healthy matter.

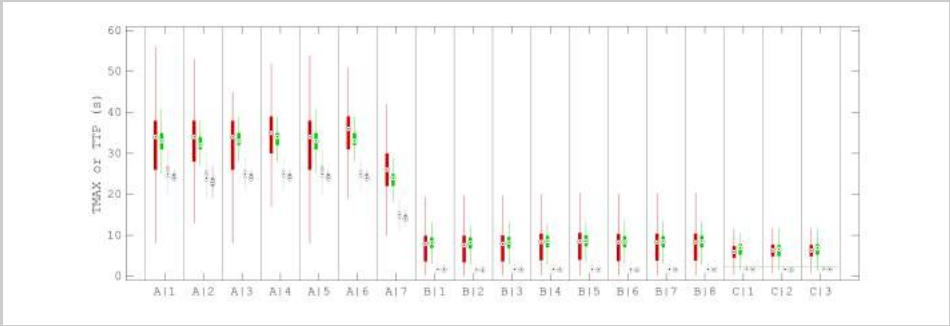

Supplementary Figure 7

Boxplots of the time to maximum (TMAX) or the time to peak (TTP) estimated by the vendor software for each scan protocol (A|1-C|3). For vendor software A, the TTP is shown. For vendor software B and C, the TMAX is shown. We pooled the ten noise realizations of the phantom for each scan protocol. The dashed horizontal colored lines indicate the thresholds given in Table 1, for which relative values were calculated as relative to the median value of the perfusion parameter in healthy matter.

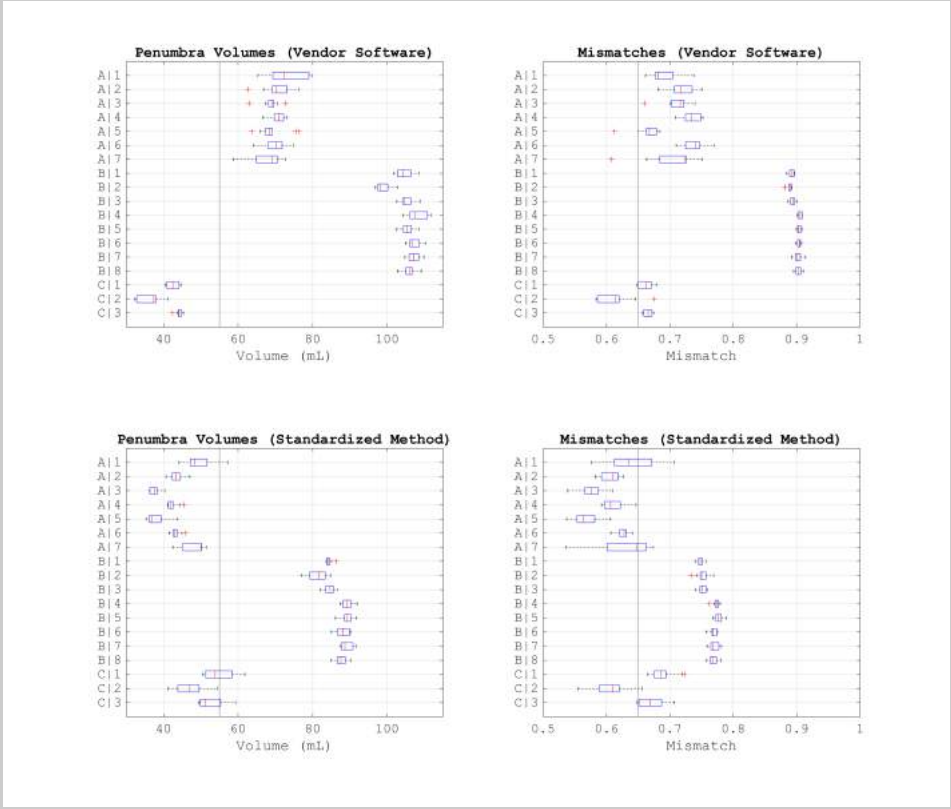

Supplementary Figure 8

Boxplots of the mismatches and the volumes of the penumbra estimated by the vendor software and by the standardized method. The mismatch is defined as the volume of the penumbra over the volume of the hypoperfused tissue. Eighteen scan protocols (A|1-C|3) were analyzed with center-specific software from one of three vendors (A-C). The vertical black lines indicate the ground truth volumes.

Supplementary Table 1

Median [first quartile, third quartile] error of the mismatches and the volumes of the penumbra estimated by the vendor software and by the standardized method. We pooled all noise realizations of the phantom. A positive error indicates overestimation.

Ischemic region	Vendor software	Standardized method
Penumbra (mL)	19.1 [12.5, 50.3]	-1.1 [-11.2, 31.6]
Mismatch (%)	9.8 [3.3, 25.1]	3.9 [-3.5, 11.6]

Chapter 4

CT perfusion (CTP) imaging yields crucial quantitative information on the infarct for management of acute ischemic stroke patients. Given the technical complexity and variability of CTP protocols across centers, there is a need for calibration and image quality control. No physical phantom is available that realistically includes all relevant features of CTP imaging. To this end, we developed an anthropomorphic physical phantom to provide CTP imaging quality control in acute ischemic stroke.

We propose a phantom that generates realistic brain features by stacking contrast agent printed sheets. By moving the phantom through the CT field of view, a dynamic effect is achieved, enabling a realistic simulation of contrast inflow and egress. The physical phantom was a printed version of an anthropomorphic digital phantom, which thus provided the ground truth. The final design of the phantom was scanned in slices of 5 mm thickness and analyzed with the perfusion software CT Brain Perfusion (IntelliSpace Portal, Philips Healthcare).

The perfusion maps of the physical phantom were visually similar to those of the digital phantom. The ischemia was estimated similarly as well with a Dice similarity coefficient of 0.96 for the infarct core an 0.92 for the penumbra. However, the tissue enhancement curves themselves were biased due to technical imperfections in the phantom.

We showed the feasibility of mimicking anthropomorphic brain tissue perfusion with a physical phantom. In its current state, the phantom still has limitations, such as the need for post-processing before the perfusion analysis and suboptimal contrast enhancement in the brain tissue.

Constructing a physical phantom

Based on 'Daan Peerlings, Edwin Bennink, Jan W Dankbaar, Hugo WAM de Jong.
An anthropomorphic physical phantom for CT perfusion imaging in acute ischemic stroke.'
Ongoing research.

Introduction

CT perfusion (CTP) imaging is critical to evaluate acute ischemic stroke patients. The objective of CTP scanning is to come to quantitative volume measures for the infarct core and penumbra. The treatment decision is typically based on these volumes, underlining the importance of quantitative accuracy. However, the CTP imaging protocol is complicated, consisting of a diverse array of injection, scanning, and processing methodologies employed across stroke centers, all of which can lead to significant variations in the estimated ischemia [1]. Despite recognition of these complexities and their clinical implications, there is currently no quality control for the quantitative accuracy of CTP outcome measures.

Quality control is already established in other quantitative imaging situations, where dedicated phantoms have become instrumental. The National Electrical Manufacturers Association's (NEMA) NU 2 image quality phantom, for example, has been used to assess the quantitative performance of PET/CT systems and to harmonize multicenter studies [2]. For dual-energy X-ray absorptiometry, comparable methodologies are in place [3, 4]. Likewise, phantoms may facilitate harmonization and optimization of the CTP imaging protocol; providing a way to check the consistency and performance of CT scanner hardware and CTP software between and within centers.

Ideally, a CTP image quality phantom meets the following requirements. Firstly, it can mimic the dynamic behavior of contrast agent through the tissue. This inflow and egress, which can be depicted in time attenuation curves, is the basis on which perfusion measurements are based and should be representative of a clinical brain scan. Secondly, the phantom has anthropomorphic features such that the automatic analysis of clinical software can be evaluated for the accuracy of infarct volume measurements in standard clinical settings. Lastly, the phantom should be relatively easy to operate and yield reproducible results. To our knowledge no phantom exists that meets these requirements. A few phantoms are available that provide some dynamic contrast features, such as a phantom that moves rods with varying radiopacity and a phantom that employs a pump to perfuse a plastic tissue mimicking compartment [5, 6]. Still, both phantoms lack anthropomorphic features so that a clinically meaningful CTP analysis, with a volume measurement of ischemia, cannot be tested.

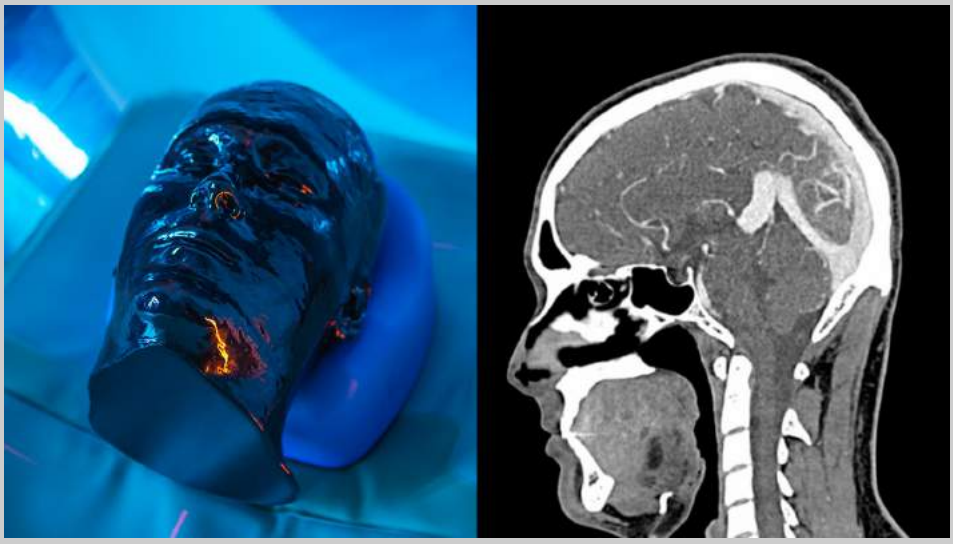

Figure 1

The normal radiopaque printing process of PhantomX. The head CT phantom on the left consists of paper sheets that were printed on with contrast agent, cut out, stacked together with adhesive in the axial direction, and coated. The phantom can be scanned to obtain anatomically accurate CT scans as on the right. Reprinted with permission from phantomx.de

Radiopaque printing has made it possible to construct realistically anthropomorphic physical CT phantoms (Figure 1). In radiopaque printing, attenuating materials are printed to simulate human anatomy. Radiopaque printed phantoms have, so far, been designed to evaluate human-reader diagnostics, to train medical professionals, or to plan surgical procedures [7-9]. We propose a CTP phantom based on radiopaque printing consisting of a number of sections representing different contrast transition phases that, combined with a translation mechanism, creates a dynamic effect in the CT scanner's field of view. This way, a dynamic process can be simulated accurately enough to perform a perfusion analysis and serve as method for quality control. In this study, the development of the phantom and the current performance status is reported on.

Methods

Concept of the phantom

The concept of the phantom is depicted in Figure 2. CTP imaging can be considered as a series of scans of different time frames of the same anatomical volume. One scan typically takes 0.5 seconds and the time between frames is typically 1 to 4 seconds. In the phantom, every CTP frame corresponds to a stack of printed sheets, which we will refer to as a CTP frame volume. As the number of time frames in a typical CTP series is between thirty and sixty, our phantom also contains this number of CTP frame volumes, which are stacked in a large cylinder. The idea is that, after a CTP frame volume is scanned, the phantom is automatically moved in the time between frames, to place the next CTP frame volume in the scanner's field of view. This creates the perception of a dynamic change of the anthropomorphic frames.

Constructing the phantom includes a number of challenges. The amplitude of time attenuation curves depends on the anatomical location (voxel) of contrast measurement. In an artery, the contrast ranges from around 0 HU, when the voxel contains blood without contrast agent, to 500 HU, when the voxel is completely filled with contrast and the maximum of the bolus passes through. In healthy brain tissue, where only a fraction of the voxel will be filled with contrast agent, the contrast ranges between 25 HU and 35 HU for white matter and between 30 HU and 50 HU for gray matter. In ischemic brain tissue, these contrast ranges are reduced, possibly to only a couple Hounsfield units. In order for all time attenuation curves to be accurately represented in the phantom, a resolution of approximately 2 HU should be attained, which requires a high printing quality. In addition, the background contrast from the paper sheets should ideally be below this resolution of 2 HU, as spurious variation of the background may result in unrealistic time attenuation curves.

Paper phantom prototype

The envisioned paper stack phantom consists of approximately 15 to 30 thousand paper sheets, with every CTP time frame volume consisting of 500 printed sheets, corresponding to a thickness of 5 mm per CTP time frame volume. The total stack, which is 30 to 60 cm in length, is to be translated with a stepping device.

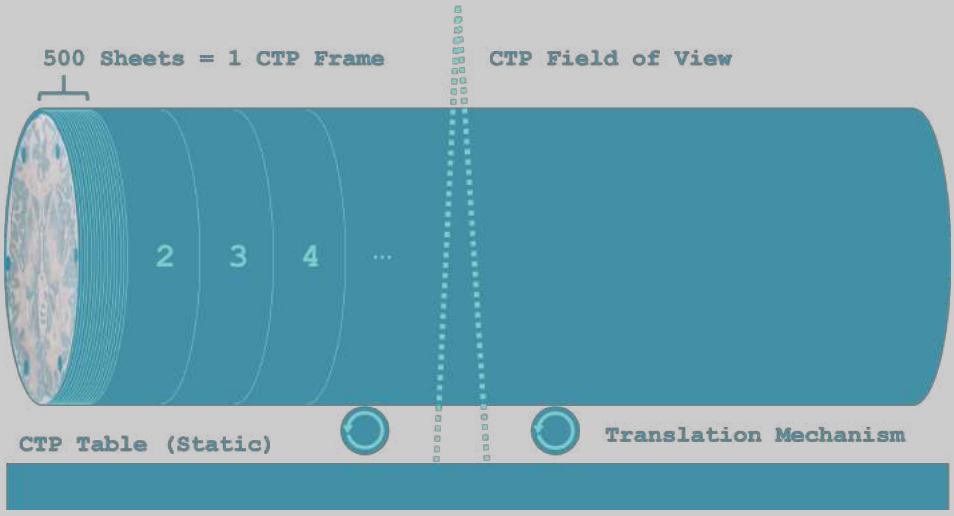

Figure 2

The concept of the radiopaque printed CT perfusion (CTP) phantom. Each 500 sheets, which add to a thickness of 5 mm, represent the same anatomical volume but a different time frame. In the time between frames, the phantom should be moved 5 mm to create the perception of a dynamic change as the phantom moves through the CTP field of view.

To investigate the uniformity and contrast resolution of such a stacked paper phantom, we tested a block phantom provided by PhantomX, a company specialized in printing iodinated contrast agent (Figure 3). The block phantom consisted of a grid with contrast enhancement curves, of varying heights and widths, for brain tissue and a single arterial enhancement curve. The block phantom also included regions that were not printed (no contrast agent). The unprinted paper had a standard deviation of 5.0 HU, which meant that the paper background was not uniform enough to measure the signal of approximately 15 HU from contrast enhancement curves for brain tissue. However, the signal of 500 HU from the arterial enhancement curve could be accurately replicated (Figure 3).

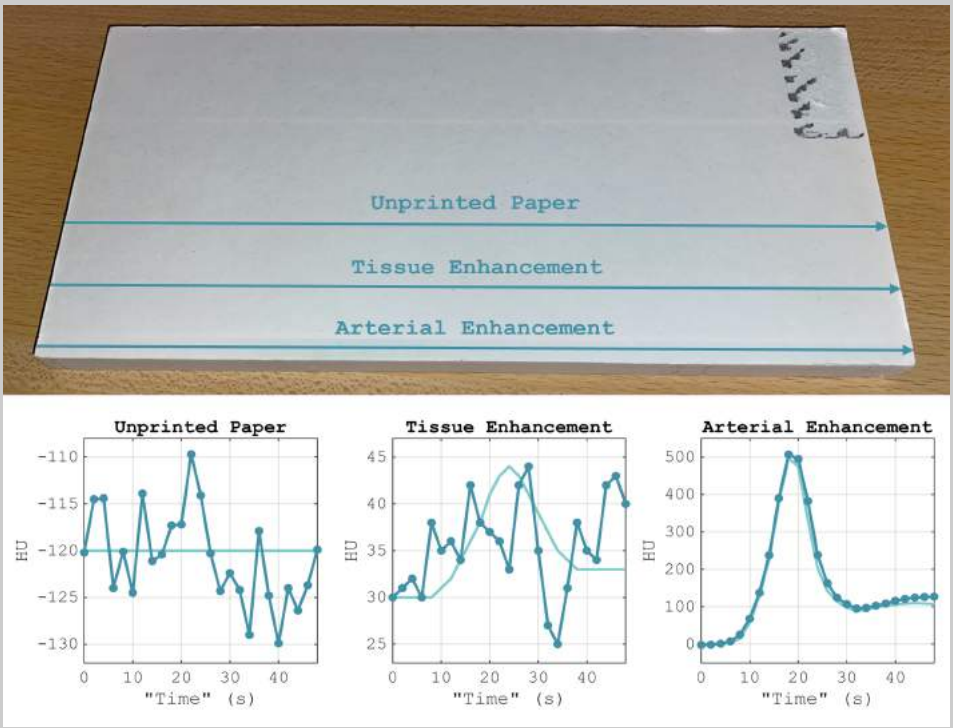

Figure 3

Block phantom for testing. On the top, the direction from left to right simulates time. The bottom left shows the HU for paper that is not printed on. The bottom right shows the arterial enhancement curve that was printed in the block phantom. The curves represent scanning at 80 kVp and 500 mAs, with each point in the graphs corresponding to a region of 5 mm x 5 mm x 5 mm.

PMMA phantom prototype

As the paper stack approach could not replicate contrast enhancement curves for brain tissue, an alternative approach was proposed. In this approach, a single anatomical CTP time frame volume was not printed on a stack of paper sheets but instead on one paper sheet. The printed sheet was placed between two disks of polymethyl methacrylate (PMMA). By scanning a single CT slice with a collimation of 5 mm, the acquired CT image was an average of the paper with the PMMA disks. On one hand, this limited our phantom to time frames consisting of two-

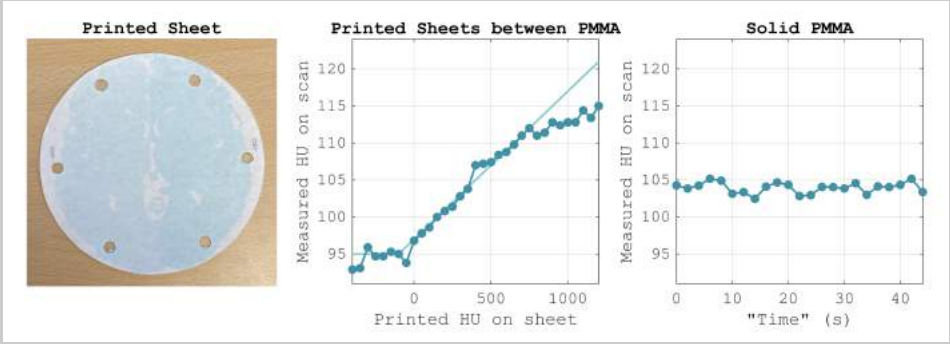

Figure 4

Calibration phantom with polymethyl methacrylate (PMMA) disks as background. An unprinted paper sheet between PMMA disks in a slice of 5 mm thickness resulted in a measured attenuation of 95 HU. The measured attenuation increased linearly as expected until the measured attenuation dropped off compared to the expectation. At earlier points, the measured attenuation also occasionally deviated from the expectation.

dimensional volumes, but also came with a number of advantages. First of all, the PMMA has an improved uniformity over stacked papers, reducing the standard deviation of the background to 0.7 HU (Figure 4), which allows more subtle and realistic tissue time attenuation curves. Secondly, instead of printing more than 10 thousand paper sheets, only one sheet per time frame is to be printed, improving the flexibility of the phantom and costs. And lastly, averaging out the contrast on the single printed sheet with PMMA converts a large contrast range with a limited contrast resolution into a small range with a high contrast resolution, which is required to replicate the contrast enhancement curves for brain tissue.

To investigate the resolution of the printed contrast for the new approach, a test phantom was constructed (Figure 4). The test phantom consisted of sheets with a printed brain mask, for which each hemisphere had a specific printed HU. In total, 20 such sheets were printed, ranging from -400 to 1200 HU in steps of 50 HU, and were placed in between PMMA disks, which had a thickness of 1 cm and a diameter of 15 cm. The printed sheets between the PMMA were scanned in 5 mm slices. Figure 4 shows the uniformity of solid PMMA as well as the linearly increasing contrast enhancement, with a sufficient resolution to print contrast enhancement curves for brain tissue.

Anthropomorphic phantom

After this an anthropomorphic version of the phantom was constructed (Figure 5). We designated the anthropomorphic physical phantom to be a printed version of our anthropomorphic digital phantom [10]. Only the brain tissue of the digital phantom was printed. We printed the brain tissue on 151 separate paper sheets, for 0 to 75 seconds in steps of 0.5 seconds. By selecting printed sheets to put in between the PMMA disks, we can tailor to specific scan protocols. To test the phantom, we chose a scan protocol from 0 to 60 seconds with frames every 2 seconds, for which we thus used 31 of the 151 available sheets. We scanned the phantom at 80 kVp and 150 mAs on a dual-energy IQon Spectral CT scanner (Philips Healthcare). The scan was reconstructed in 1 mm axial slices and was exported as DICOM file.

The exported scan required post-processing to look like a CTP scan. The PMMA disks resulted in a relatively dense background of 95 HU (Figure 4). While this may not obstruct a CTP analysis in theory, clinical software may not expect such dense soft tissue and exclude these regions from the analysis. Therefore, we subtracted 69 HU to reach the baseline intensity as seen in real CTP scans. On the positions of the paper sheets, we averaged five slices of 1 mm thickness to a single slice of 5 mm thickness. The resulting 31 slices of 5 mm thickness were transformed rigidly to the first slice. Finally, we synthetically added the remaining tissue, like the vessels, cerebrospinal fluid, and skull, from a digital phantom, because our dynamic printing range was limited to brain tissue.

The post-processed scan was analyzed with CT Brain Perfusion (arrival-time-sensitive algorithm) from IntelliSpace Portal (ISP) version 10.1 (Philips Healthcare). This gave perfusion maps of the cerebral blood flow (CBF), cerebral blood volume (CBV), mean transit time (MTT), and time to peak (TTP). From these perfusion maps, the summary map was determined by estimating the infarct core as tissue with both a CBV < 2.0 mL/100g and a relative MTT $> 150\%$, and by estimating the penumbra as tissue with a relative MTT $> 150\%$ not estimated as infarct core.

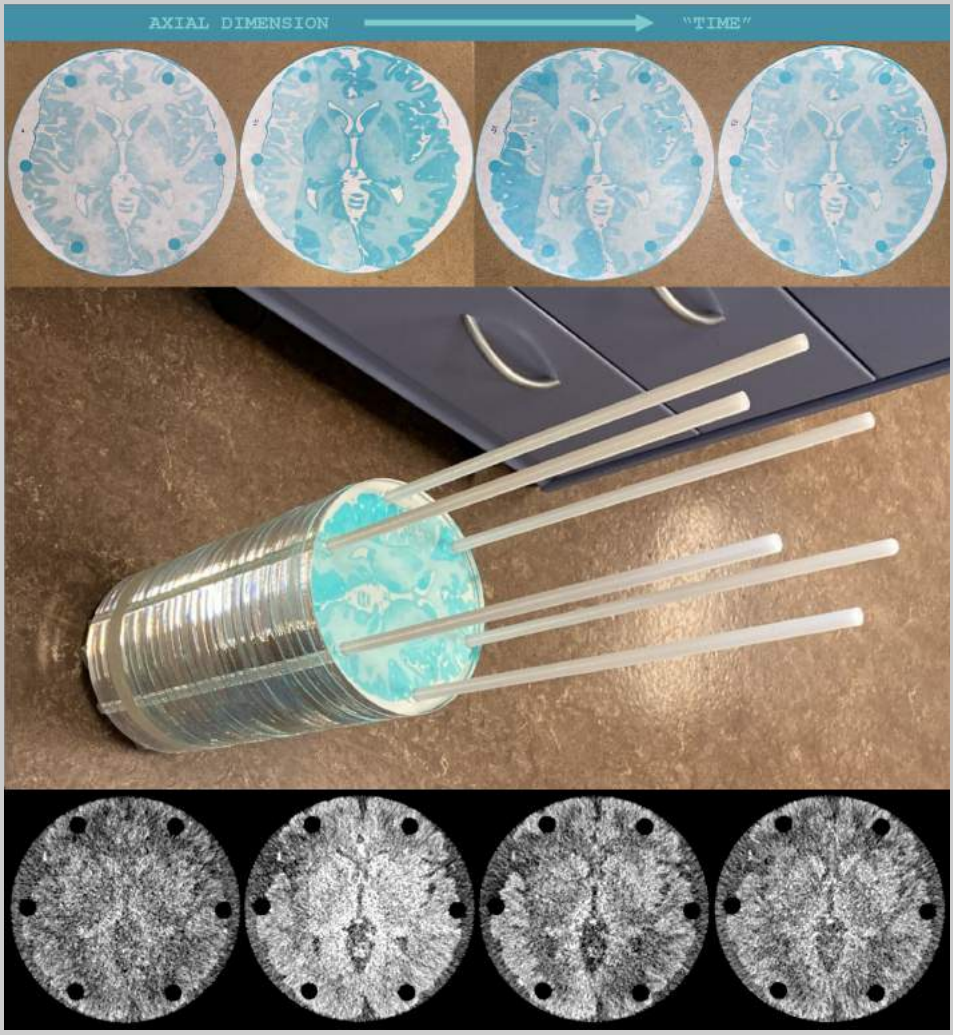

Figure 5

Final design of the anthropomorphic physical phantom while under construction. The axial direction simulates time. On the top, single paper sheets were printed on with different concentrations of contrast agent. In the middle, the printed sheets were put in between disks of polymethyl methacrylate and were joined together with plastic bolts and nuts. On the bottom, the phantom was scanned at 80 kVp and 150 mAs, and the slices were averaged to 5 mm thickness. The slices are shown in a window of 80 to 120 HU.

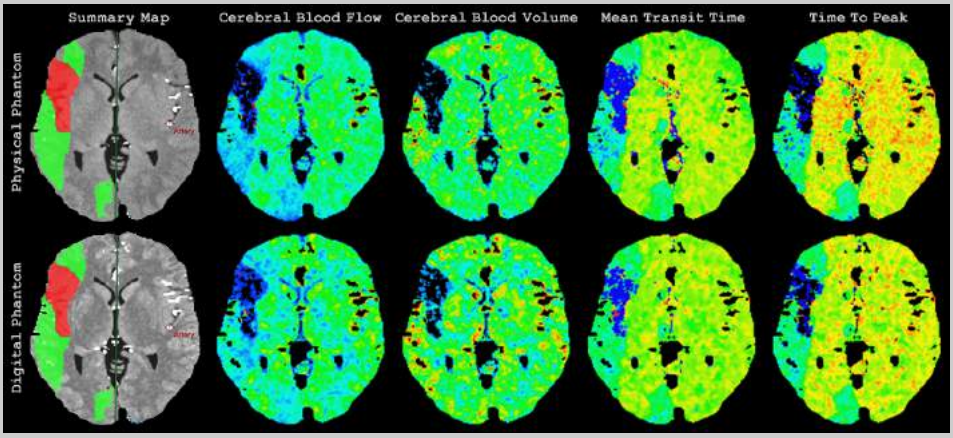

Figure 6

Screenshots of the perfusion maps and summary map for the anthropomorphic physical phantom. The maps are from IntelliSpace Portal (Philips). On the top, the results are shown for the anthropomorphic physical phantom scanned at 80 kVp and 150 mAs. On the bottom, for comparison, the results are shown for the anthropomorphic digital phantom with noise corresponding to 80 kVp and 150 mAs.

Results

Figure 6 shows screenshots of the perfusion maps and the summary map generated by ISP for the physical phantom and, for comparison, the digital phantom. The summary map shows the estimated infarct core and penumbra on a maximum intensity projection. The maximum intensity projection and the perfusion maps of the CBF and CBV show that the contrast enhancement of gray matter was insufficient. The estimated infarct core and penumbra of the physical phantom were very close to those of the digital phantom, with Dice similarity coefficients of 0.96 and 0.92 respectively.

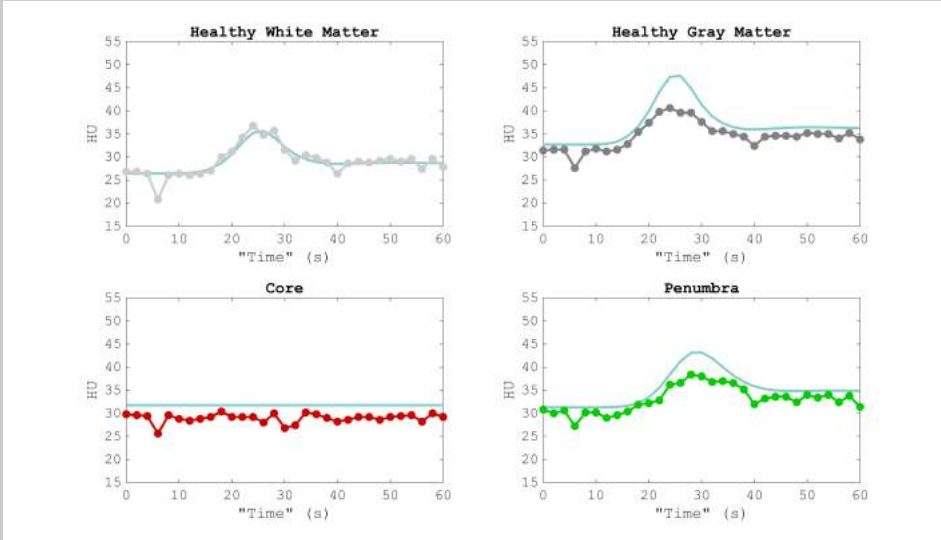

Figure 7

Average contrast enhancement curves for different regions in the anthropomorphic physical phantom. Apart from the healthy white matter, the contrast enhancement is lower than expected.

Figure 7 shows the average enhancement curve for different regions in the brain. For healthy white matter, the shape of the contrast enhancement curve was replicated well, while for healthy gray matter, the contrast enhancement was lower than the ground truth (also see Figure 4). The contrast enhancement correctly vanished for the infarct core and was correctly delayed and prolonged for the penumbra, but was too low on average for both regions, as each region contained gray matter.

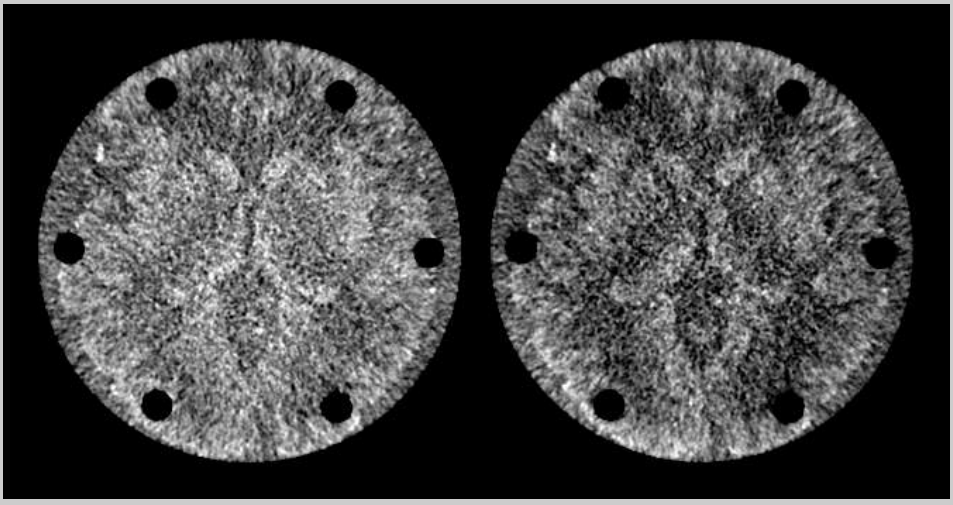

Figure 8

The third (left) and fourth (right) frame of the scanned physical phantom. In the fourth frame, the attenuation is lower because of air in between the two disks of polymethyl methacrylate (also see Figure 7). The phantom was scanned at 80 kVp and 150 mAs, and the slices were averaged to 5 mm thickness. The slices are shown in a window of 80 to 120 HU.

Figure 8 shows the third and fourth frame of the scanned phantom, to exemplify an issue that arises when stacking PMMA disks. The third and fourth frame should look similar to each other, but the fourth frame deviated from its expectation (Figure 7). For the fourth frame, air in between the two PMMA disks lowered the attenuation; the attenuation of air (-1000 HU) divided by the slice thickness (5000 micrometer) results in decrease of 0.2 HU per micrometer of air between the disks. The air in between the PMMA disks was the result of slightly hollow disks. The PMMA disks turned out not to be perfectly flat because they were molded, a technique where liquid is hardened in a mold.

Discussion

We developed an anthropomorphic physical CTP phantom that simulated a dynamic process accurately enough for a perfusion analysis with clinical software. The perfusion maps and summary map for the physical phantom were visually similar to its digital counterpart. However, the tissue enhancement curves for brain tissue were biased due to technical imperfections in the phantom, and the scanned phantom required post-processing to look like a CTP scan. Still, this proof-of-concept study showed the feasibility of mimicking anthropomorphic brain tissue perfusion with a physical phantom.

In its current state, the phantom still has several issues. Mainly, we could not reproduce the perfusion of gray matter; our range was insufficient, most clearly illustrated in Figure 4, where the measured HU drops off compared to what was expected. We suspected beam hardening caused this drop-off, because the printed sheets themselves had a high attenuation and because scanning at higher tube voltages reduced the issue. Beam hardening occurs when very dense material attenuates the beam, which is a negative consequence of using a single printed sheet with high contrast averaged out by PMMA disks. Putting two printed sheets between the PMMA disks, which allows a less concentrated attenuation by doubling the amount of printed contrast agent, also reduced the drop-off. However, these adaptations introduced complications: it became notably more difficult to confine stacked sheets to a 5 mm slice, as it was already difficult to align the phantom accurately enough for a single sheet, and a higher tube voltage would deviate from the most common tube voltage in CTP imaging as well as require differently calibrated radiopaque printing [11].

In addition to the insufficient range to print brain tissue, we were limited to print only brain tissue because we traded in dynamic range for sub-Hounsfield-unit accuracy when printing iodine. Regions with a higher attenuation than brain tissue, such as the skull and contrast enhanced vessels, and regions with a lower attenuation than brain tissue, such as the cerebrospinal fluid (CSF), were implemented digitally. These regions need to be realized physically to test CTP protocols integrally, as the perfusion software required a skull for image registration, needed an arterial input function for the perfusion analysis, and confused CSF for infarcted white matter. In an attempt to solve these issues, we laser engraved the CSF on the PMMA disks, lowering the attenuation by substituting PMMA by air, and added aluminum plates on the disks to increase the attenuation for the skull, but adding an aluminum casing around the phantom seemed a constructional challenge and laser engraving lacked precision. Contrast enhanced vessels, such as the arterial input function, pivotal in a

perfusion analysis, are even more of a challenge because of their dynamics. To replicate the arterial input function, we could revert to the original paper stack solution that we demonstrated was adequate for these curves and combine that with the PMMA solution. This could be achieved by inserting small cylinders, each printed with a certain attenuation with PhantomX' normal printing process and placed over a length of 5 mm for each slice.

Further, the background provided by the PMMA disks was unstable across frames because of how the disks fit together, given they were not perfectly flat. We tried to bore the phantom's fourth frame flat, but this roughened the surfaces of the PMMA disks, resulting in more noise and an even lower average attenuation. A more precise process to machine plastic may solve this.

Finally, we did not implement the device to automatically move the phantom through the field of view. The phantom was not scanned through time, but as a long axial scan and made to look like a CTP scan through post-processing. To select a preset CTP protocol on a scanner, the phantom would need to be moved in between frames, which may be accomplished, for example, by placing the phantom on a construction with rolling tires that automatically move the phantom a centimeter each couple of seconds.

Conclusion

We have developed a radiopaque printed anthropomorphic physical phantom for CTP imaging quality control. Despite limitations, the phantom showed realistic brain tissue perfusion, which resulted in realistically estimated ischemia. A CTP imaging quality control phantom could harmonize and optimize the evaluation of acute ischemic stroke patients across stroke centers.

References

1 Shankar JJS (2021) Variation in CT perfusion protocol has implications on defining irreversibly damaged ischemic brain parenchyma. Eur Radiol 31:8315–8316. https://doi.org/10.1007/s00330-021-08209-w

2 Boellaard R, Delgado-Bolton R, Oyen WJG, et al (2015) FDG PET/CT: EANM procedure guidelines for tumour imaging: version 2.0. Eur J Nucl Med Mol Imaging 42:328–354

3 Tsai SY, Chen CY, Lee JS, Chen JC (2013) Evaluation of effective dose using TLDs with different weighted PMMA phantoms undergoing coronary artery calcium computed tomography examination. IEEE Trans Nucl Sci 60:2147–2154. https://doi.org/10.1109/TNS.2013.2258175

4 Tseng HC, Liu WS, Tsai HH, et al (2015) Radiation dose for normal organs by helical tomotherapy for lung cancer. Applied Radiation and Isotopes 102:35–41. https://doi.org/10.1016/j.apradiso.2015.04.007

5 Peladeau-Pigeon M, Coolens C (2013) Computational fluid dynamics modelling of perfusion measurements in dynamic contrast-enhanced computed tomography: Development, validation and clinical applications. Phys Med Biol 58:6111–6131. https://doi.org/10.1088/0031-9155/58/17/6111

6 Jacobsen MC, Schellingerhout D, Wood CA, et al (2018) Intermanufacturer comparison of dual-energy CT iodine quantification and monochromatic attenuation: A phantom study. Radiology 287:224–234. https://doi.org/10.1148/radiol.2017170896

7 Jahnke P, Schwarz FB, Ziegert M, et al (2018) A radiopaque 3D printed, anthropomorphic phantom for simulation of CT-guided procedures. Eur Radiol 28:4818–4823. https://doi.org/10.1007/s00330-018-5481-4

8 Jahnke P, Conzelmann J, Genske U, et al (2021) Task-based assessment of neck CT protocols using patient-mimicking phantoms—effects of protocol parameters on dose and diagnostic performance. Eur Radiol 31:3177–3186. https://doi.org/10.1007/s00330-020-07374-8

9 Conzelmann J, Genske U, Emig A, et al (2022) Comparison of low-contrast detectability between uniform and anatomically realistic phantoms—influences on CT image quality assessment. Eur Radiol 32:1267–1275. https://doi.org/10.1007/s00330-021-08248-3

10 Riordan AJ, Prokop M, Viergever MA, et al (2011) Validation of CT brain perfusion methods using a realistic dynamic head phantom. Med Phys 38:3212–3221. https://doi.org/10.1118/1.3592639

11 Wintermark M, Maeder P, Verdun FR, et al (2000) Using 80 kVp versus 120 kVp in perfusion CT measurement of regional cerebral blood flow. American Journal of Neuroradiology 21:1881–1884

Chapter 5

We aimed to compare single parameter thresholding with multivariable probabilistic classification of ischemic stroke regions in the analysis of computed tomography perfusion (CTP) parameter maps.

Patients were included from two multicenter trials and were divided into two groups based on their modified arterial occlusive lesion grade. CTP parameter maps were generated with three methods – a commercial method (ISP), block-circulant singular value decomposition (bSVD), and non-linear regression (NLR). Follow-up non-contrast CT defined the follow-up infarct region. Conventional thresholds for individual parameter maps were established with a receiver operating characteristic curve analysis. Probabilistic classification was carried out with a logistic regression model combining the available CTP parameters into a single probability.

A total of 225 CTP data sets were included, divided into a group of 166 patients with successful recanalization and 59 with persistent occlusion. The precision and recall of the CTP parameters were lower individually than when combined into a probability. The median difference [interquartile range] in mL between the estimated and follow-up infarct volume was 29/23/23 [52/50/52] (ISP/bSVD/NLR) for conventional thresholding and was 4/6/11 [31/25/30] (ISP/bSVD/NLR) for the probabilistic classification.

Multivariable probability maps outperform thresholded CTP parameter maps in estimating the infarct lesion as observed on follow-up non-contrast CT. A multivariable probabilistic approach may harmonize the classification of ischemic stroke regions.

Standardizing the estimation of ischemic regions

Published as 'Daan Peerlings, Fasco van Ommen, Edwin Bennink, Jan W Dankbaar, Birgitta K Velthuis, Bart J Emmer, Jan W Hoving, Charles BLM Majoie, Henk A Marquering, Hugo WAM de Jong. Probability maps classify ischemic stroke regions more accurately than CT perfusion summary maps. *European Radiology* 32.9 (2022): 6367-6375.'

Introduction

Since endovascular treatment revolutionized acute ischemic stroke care, baseline imaging has become ever more relevant to select patients for treatment [1–3]. Personalized selection criteria may be provided by computed tomography perfusion (CTP) imaging.

For a patient with acute ischemic stroke, a CTP scan should estimate the irreversibly damaged tissue (i.e. the infarct core) and the salvageable tissue (i.e. the penumbra), which together form the total hypoperfused region. To classify these regions, the CTP scan is processed with dedicated software to produce four perfusion maps: the cerebral blood flow (CBF), cerebral blood volume (CBV), mean transit time (MTT), and time to peak (TTP/Tmax). Subsequently, a predefined threshold can be applied to outline the ischemic core and the penumbra.

However, different approaches in CTP processing software and analysis between vendors have led to a variety of threshold values for ischemia in stroke imaging (Table 1). These different thresholds may partly contribute to the discordance between vendors in CTP results, hampering multicenter CTP studies. A standardized classification method could increase harmony in CTP results between different processing methods.

Probabilistic classification of ischemic stroke regions has been proposed as an alternative to threshold-based classification [4, 5]. Probability maps can combine parameters and can indicate certainty of ischemia [4, 6]. Volumes obtained from probability maps were already validated against conventional threshold-based volumes for probability models that include a single perfusion parameter [4]. However, the chosen perfusion parameter may still differ between vendors and the disregarded maps may contain additional – unused – information. Also, a multivariable probabilistic classification has been compared to single parameter thresholding, but only for different CTP software between the two classification methods [7]. Probabilistic classification has not yet been compared to threshold-based classification for a probability map that combines multiple perfusion parameters readily available within any single CTP software.

This study tests the hypothesis that a multivariable probabilistic analysis of perfusion maps is superior to single variable thresholding in predicting the ischemic core and total hypoperfused region.

Table 1

Clinical definitions of ischemic core and penumbra that are currently implemented in varying commercially available perfusion software packages. CBF is cerebral blood flow, CBV is cerebral blood volume, MTT is mean transit time, and TTP/Tmax is time to peak. Values relative to the opposite hemisphere are indicated by an 'r'.

Software	Ischemic core	Penumbra
IntelliSpace Portal (Philips Healthcare)	CBV < 2.0 mL/100g & rMTT > 150%	rMTT > 150%
Syngo.via (Siemens Healthineers)	CBV < 1.2 mL/100g	CBF < 27.0 mL/100g/min
Vitrea (Toshiba/Canon Medical Systems)	rCBV < 41%	TTP > 6.8 s
RAPID (iSchemaView)	rCBF < 30%	Tmax > 6 s

Methods

Acquisition of imaging data

Both the Dutch acute stroke (DUST) study, in which fourteen stroke centers participated, and the Multicenter Randomized Clinical Trial of Endovascular Treatment for Acute Ischemic Stroke in the Netherlands (MRCLEAN), in which seventeen stroke centers participated, contributed their data to this study [8, 9]. All included DUST participants ($n = 182$) and included MRCLEAN participants ($n = 43$) gave informed consent for the use of their clinical and imaging data.

The DUST study protocol design describes acquisition of the admission CTP scan at 80 kVp and 150 mAs on 40- to 320-detector CT scanners (GE Healthcare, Philips, Siemens, Toshiba) with a two-second interval for a duration of 50 seconds and reconstructed to a slice thickness of 5 mm. The advised injection protocol was a 40 mL contrast bolus injected at a rate of 6 mL/s followed by a saline flush of 40 mL injected at a rate of 6 mL/s. Patients eligible for treatment received intravenous thrombolysis, intra-arterial thrombolysis, and/or mechanical thrombectomy. For this study, the necessary follow-up imaging consisted of a non-contrast CT (NCCT) as well as a CT angiography (CTA) scan within three days.

In the MRCLEAN trial, centers could adhere to their own acquisition and injection protocol. Patients eligible for treatment received intravenous thrombolysis, intra-arterial thrombolysis, and/or mechanical thrombectomy. The necessary follow-up imaging again consisted of a NCCT as well as a CTA scan and was acquired after 24 hours.

Processing of imaging data

For the data from the DUST study, a radiologist with 6 years of experience manually segmented the follow-up NCCT of each patient to define the follow-up infarct region. In the MRCLEAN trial, the follow-up NCCT of each patient was segmented automatically using a convolutional neural network [10]. Because our study compared two classification methods, any inconsistencies in the follow-up infarct regions were the same for both these methods.

The total patient population ($n = 225$) was divided into a patient group with successful recanalization (REC, $n = 166$) and a patient group with persistent occlusion (OCC, $n = 59$), based on the modified arterial occlusive lesion (mAOL) grade determined from the follow-up CTA (REC: mAOL grade 3; OCC: mAOL grade 0 and 1) [11]. Subsequently, each patient group was divided 2:1 into a REC/OCC training patient group ($n = 110/n = 39$) and a REC/OCC test patient group ($n = 56/n = 20$).

Patients were divided into a REC and OCC patient group because the segmentation on the follow-up NCCT should resemble the infarct core at the time of admission imaging for the REC patient group (since the recanalization should have saved the penumbra) whereas the segmentation on the follow-up NCCT should resemble the total hypoperfused region at the time of admission imaging for the OCC patient group (since the occlusion should have infarcted the penumbra). Hence, the REC patient group was used to train and test the classification of the infarct core, whereas the OCC patient group was used to train and test the classification of the total hypoperfused region.

To assess the robustness and universality of our method, perfusion maps were generated with three perfusion processing methods, all providing a CBF, CBV, MTT, and TTP map. The first is a commercial method in which the CTP scan was analyzed with the arrival time sensitive algorithm in IntelliSpace Portal (ISP; Brain Perfusion, IntelliSpace Portal 10.1, Philips Healthcare). The second is an in-house developed method, which uses a block-circulant singular value decomposition (bSVD) [12] algorithm. The third is an in-house model-based nonlinear regression (NLR) method [13].

Prior to perfusion analysis, the CTP scans were processed the same way for both in-house methods (bSVD and NLR), as described previously [14]. For ISP, the IntelliSpace Portal Brain Perfusion application was used to filter the CTP image data as well as to automatically select the arterial input function (AIF) and venous output function (VOF). All further data processing and analysis was carried out with MATLAB (MATLAB, R2019b: The Mathworks Inc.).

Determining thresholds

To determine thresholds, we followed (and refer to) the procedure on which the current clinical thresholds of ISP are based [15]. To summarize, a receiver operating characteristic (ROC) curve is produced for each perfusion parameter. The perfusion parameter yielding the largest AUC of its ROC curve is chosen as the parameter to define either the ischemic core (for the REC training patient group) or the total hypoperfused region (for the OCC training patient group). The threshold value for this perfusion parameter is then found by maximizing the Youden index [16].

Determining probability models

To determine the probability models, we performed logistic regression by maximum likelihood estimation on all four perfusion parameters with follow-up tissue outcome as response variable. This resulted in a logistic model for the ischemic core (from the REC training patient group) and for the total hypoperfused region (from the OCC training patient group):

$$P(\text{CORE}) = 1 / (1 + e^{(C_{\text{INT, REC}} + C_{\text{CBF,REC}} \times \text{CBF} + C_{\text{CBV,REC}} \times \text{CBV} + C_{\text{MTT,REC}} \times \text{MTT} + C_{\text{TTP,REC}} \times \text{TTP})}) ,$$

$$P(\text{HYPOPERFUSED}) = 1 / (1 + e^{(C_{\text{INT,OCC}} + C_{\text{CBF,OCC}} \times \text{CBF} + C_{\text{CBV,OCC}} \times \text{CBV} + C_{\text{MTT,OCC}} \times \text{MTT} + C_{\text{TTP,OCC}} \times \text{TTP})}) .$$

Once the coefficients for the intercept (C_{INT}), the CBF (C_{CBF}), the CBV (C_{CBV}), the MTT (C_{MTT}), and the TTP (C_{TTP}) were determined from the training patient groups, the CBF, CBV, MTT and TTP of a voxel gave the probability P(CORE) that this voxel belonged to the ischemic core (based on the REC training patient group) and the probability P(HYPOPERFUSED) that this voxel belonged to the total hypoperfused region (based on the OCC training patient group). Calculating these probabilities for all voxels resulted in a probability map for the ischemic core and a probability map for the total hypoperfused region.

Training data set

The training data set was prepared the same way for both the ROC curve analysis and the logistic regression analysis. Because the ROC curve can show bias towards the majority class in imbalanced data (in our case the class of healthy voxels against the class of ischemic voxels) [17], the training data set was limited to the collection of parenchymal voxels in the ischemic hemisphere of slices with a segmentation of the follow-up infarct region. To minimize the impact of high leverage voxels on logistic regression (in our case voxels with normal perfusion in the segmented region on the ground truth map and voxels with reduced perfusion outside this region) [18], voxels with an outlier in one of the perfusion parameters were removed. An outlier was defined as a data point more than 1.5 times the interquartile range below the first quartile or above the third quartile [19].

Determining volumes

A threshold-based volume followed from a summary map by summing the voxel volumes of all voxels in a classified region. Before determining a volume, the summary map was morphologically opened and then morphologically closed, both with a spherical structure element of 5 mm in diameter, to reduce noise artefacts.

A probabilistic volume follows from a probability map by summing the probabilities, multiplied by the voxel volume, of the left and right hemisphere separately and taking the absolute difference between these two sums. Noise artefacts are automatically accounted for in the comparison between the two hemispheres.

Classification performance

The classification performance of both methods was assessed on the level of voxels as well as on the level of patients. On the level of voxels, a precision-recall curve was produced for each perfusion parameter and for the probability. These curves show the precision and the recall for different thresholds of a perfusion parameter or of the probability. On the level of patients, the predicted threshold-based volume and the predicted probabilistic volume were compared to the follow-up infarct volume for each patient. Both assessments were carried out on the total ischemic hemisphere.

Table 2

Thresholds following from a receiver operating characteristic (ROC) curve analysis for three processing methods (ISP, bSVD, NLR) based on a training patient group with successful recanalization (REC) and a training patient group with persistent occlusion (OCC). CBF stands for cerebral blood flow, MTT for mean transit time, TTP for time to peak, and AUC for area under the curve.

Method	Training patient group	Threshold	AUC of ROC curve	Youden index
ISP	REC	CBF < 14.0 mL/100g/min	0.68	0.29
	OCC	MTT > 11.0 s	0.75	0.44
bSVD	REC	CBF < 9.0 mL/100g/min	0.74	0.38
	OCC	TTP > 6.0 s	0.79	0.49
NLR	REC	CBF < 10.0 mL/100g/min	0.78	0.41
	OCC	TTP > 6.5 s	0.82	0.54

A precision-recall curve was used to visualize classification performance because of considerable class imbalance between the ischemic and healthy tissue in the total ischemic hemisphere [17]. In the context of classifying ischemic regions, the precision is the percentage of the classified region that is truly ischemic core or hypoperfused and the recall is the percentage of the true ischemic core or hypoperfused region that is correctly classified.

The predicted volume was compared to the follow-up infarct volume because the final infarct volume is a principal predictor of functional outcome [20–22]. The volume difference between the predicted volume and the ground truth volume was defined as the predicted volume minus the ground truth volume. A boxplot of the volume difference was made for each patient group (i.e. REC and OCC), each CTP processing method (i.e. ISP, bSVD, and NLR), and each classification method (i.e. threshold-based and probabilistic). The mean volume differences of the threshold-based classification and probabilistic classification were compared with a paired *t*-test for each patient group and for each CTP processing method. The level of significance was defined as a two-tailed $P < 0.05$.

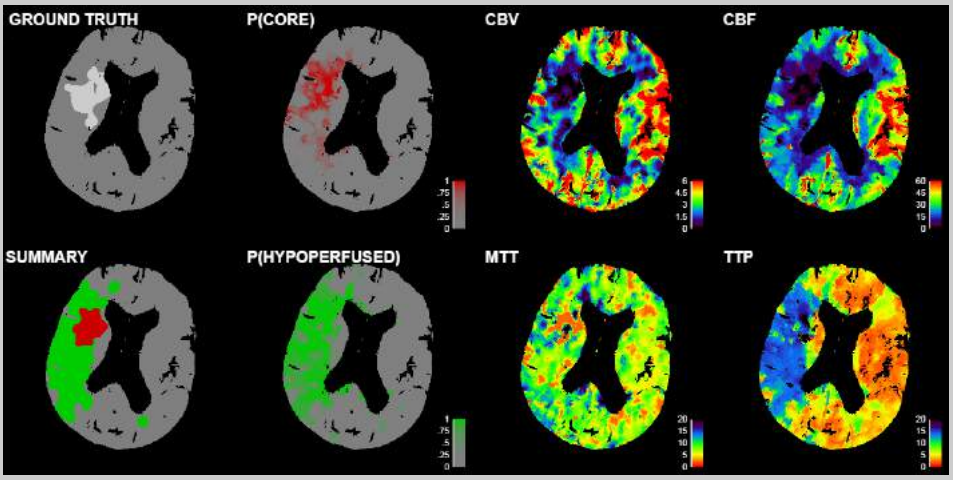

Figure 1

The ground truth map (i.e. manual segmentation from a follow-up non-contrast CT scan, in this case from the REC patient group), summary map (obtained from thresholding according to Table 2, in this case for the bSVD processing method), the probability map P(CORE) in case of successful recanalization (REC; obtained from the logistic model in Table 3, in this case for the bSVD processing method), the probability map P(HYPOPERFUSED) in case of persistent occlusion (OCC; obtained from the logistic model in Table 3, in this case for the bSVD processing method), and the perfusion maps. The cerebral blood flow (CBF) is in mL/100g/min, the cerebral blood volume (CBV) is in mL/100g, the mean transit time (MTT) is in seconds, and the time to peak (TTP) is in seconds.

Results

Threshold-based classification of ischemic regions

Based on the REC training patient group (to acquire the optimal threshold for the ischemic core), the CBF was the parameter with the highest AUC of its ROC curve for each processing method (Table 2). Based on the OCC training patient group (to acquire the optimal threshold for the total hypoperfused region), the MTT had the highest AUC of its ROC curve for the ISP processing method and the TTP had the highest AUC of its ROC curve for both in-house processing methods (Table 2). For these parameters, the threshold value was determined by maximizing the Youden index. Figure 1 shows an example summary map.

Table 3

Coefficients following from a logistic regression analysis for three processing methods (ISP, bSVD, NLR) based on a training patient group with successful recanalization (REC) and a training patient group with persistent occlusion (OCC). The coefficient for the CBF (C_{CBF}) is in $(mL/100g/min)^{-1}$, the coefficient for the CBV (C_{CBV}) is in $(mL/100g)^{-1}$, the coefficient for the MTT (C_{MTT}) is in $(seconds)^{-1}$, and the coefficient for the TTP (C_{TTP}) is in $(seconds)^{-1}$.

Method	Patient group	C_{INT}	C_{CBF}	C_{CBV}	C_{MTT}	C_{TTP}
ISP	REC	2.31	0.06	0.26	-0.09	-0.08
	OCC	3.98	0.04	0.12	-0.21	-0.17
bSVD	REC	2.58	0.13	0.57	-0.14	-0.32
	OCC	3.09	0.08	0.30	-0.16	-0.38
NLR	REC	3.45	0.14	0.66	-0.15	-0.39
	OCC	4.16	0.09	0.28	-0.17	-0.48

Probabilistic classification of ischemic regions

Table 3 shows the coefficients from a logistic regression analysis to acquire probability maps. The positive model coefficients for the CBF and CBV reflect that the CBF and CBV decrease in an ischemic region. The negative model coefficients for the MTT and TTP reflect that the MTT and TTP increase in an ischemic region. For the CBF and CBV, the coefficient from the REC patient group is higher than the coefficient from the OCC patient group for each of the three processing methods. For the MTT and TTP, the coefficient from the OCC patient group is lower than the coefficient from the REC patient group for each of the three processing methods. This implies that the CBF and CBV were more important for predicting the ischemic core, whereas the MTT and TTP were more important for predicting the total hypoperfused region. Figure 1 shows an example probability map in case of successful recanalization, and in case of persistent occlusion.

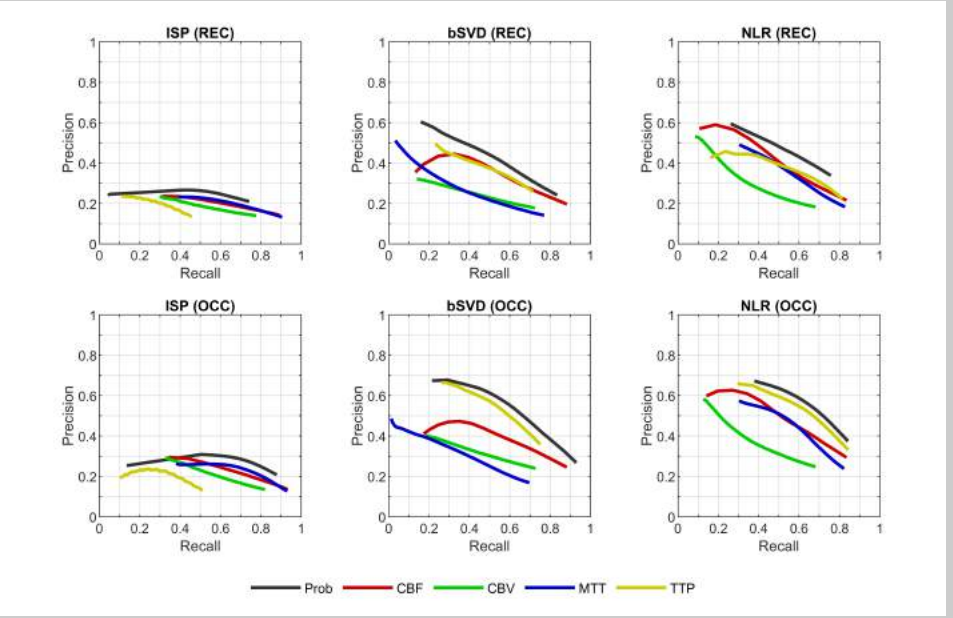

Figure 2

Precision-recall curves of the perfusion and probability maps for three processing methods (ISP, bSVD, NLR) following from a test patient group with successful recanalization (REC) and a test patient group with persistent occlusion (OCC). CBF stands for cerebral blood flow, CBV for cerebral blood volume, MTT for mean transit time, TTP for time to peak, and Prob for the probability (corresponding to the patient group).

Classification performance

The precision-recall curve of the probability generally lies above the precision-recall curves of the perfusion parameters (Figure 2), indicating a better classification performance. For ISP, low values of the CBF and CBV may have a higher precision in predicting the total hypoperfused region (i.e. in the OCC patient group) than the probability at the same (low) level of recall. Clinically, however, these low values of the CBF and CBV are not so relevant for predicting the total hypoperfused region because of the low recall.

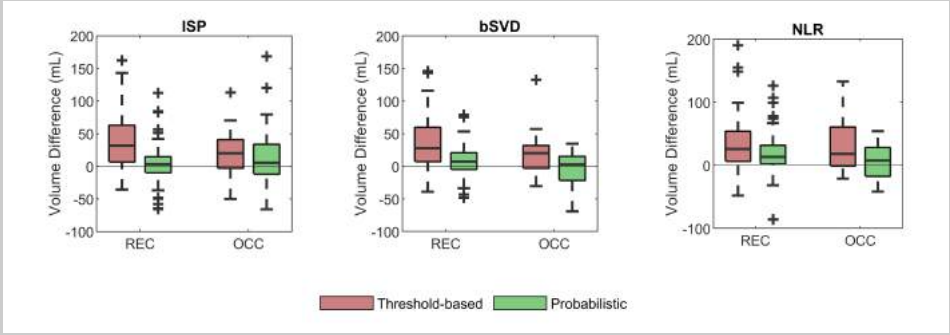

Figure 3

Boxplots of the volume difference between the ground truth volume and the predicted volume (either threshold-based or probabilistic) for three processing methods (ISP, bSVD, NLR) following from a test patient group with successful recanalization (REC) and a test patient group with persistent occlusion (OCC).

For ISP, the curve for the CBF was calculated for 1 to 40 mL/100g/min in steps of 2 mL/100g/min, the curve for the CBV for 0.1 to 4.0 mL/100g in steps of 0.2 mL/100g, the curve for the MTT for 25 to 5 s in steps of 1 s, the curve for the TTP for 15 to 5 s in steps of 1 s, and the curve for the probability for 95 to 5% in steps of 5%. For the in-house processing methods, the curve for the CBF was calculated for 1 to 20 mL/100g/min in steps of 1 mL/100g/min, the curve for the CBV for 0.1 to 2.0 mL/100g in steps of 0.1 mL/100g, the curve for the MTT for 25 to 5 s in steps of 1 s, the curve for the TTP for 15 to 5 s in steps of 0.5 s, and the curve for the probability for 95 to 5% in steps of 5%.

Threshold-based classification led to an overall overestimation of the follow-up infarct volume within the test patient groups. For the REC and OCC test patient groups combined, the median volume difference [Q1, Q3] in mL was 29 [4, 56]/23 [3, 53]/23 [4, 56] (ISP/bSVD/NLR) for threshold-based classification and was 4 [-10, 21]/6 [-7, 18]/11 [0, 30] (ISP/bSVD/NLR) for probabilistic classification. For each test patient group separately, the volume difference following from the probabilistic classification was lower than from the threshold-based classification (Figure 3).

Between threshold-based classification and probabilistic classification, the mean ischemic core volume difference differed significantly for each processing method ($P < 0.001$). The mean hypoperfused region volume difference differed significantly for bSVD ($P = 0.003$) as well as for NLR ($P = 0.002$) but not for ISP ($P = 0.24$). A scatter plot of the volumes and a Bland-Altman plot of the volumes can be found in the Supplementary Material.

Discussion

Our results show that combining perfusion parameters in a logistic model improved the precision-recall curve and that probabilistic volumes were significantly more accurate than threshold-based volumes in estimating the infarct volume on follow-up non-contrast CT obtained within three days. This study suggests that multivariable probability maps classify ischemic stroke regions more accurately than CTP summary maps.

Fixed single parameter thresholds do not use the available information to its full potential, because of their limitation to incorporate multiple (perfusion) parameters as well as their limitation to show the certainty of predicted ischemia; a voxel is classified as either completely healthy or not, regardless of its proximity to the defined threshold or the value of the other perfusion parameters [4, 6, 23]. Moreover, the existence of a universal pathophysiological cut-off value to determine final tissue state is questionable due to oversimplification [4, 5].

For a logistic model with four perfusion parameters, we showed that the precision and recall of the probability map are better than that of the individual perfusion maps. The precision-recall curve of a probability map that follows from a logistic model with a single perfusion parameter, is identical to the precision-recall curve of the perfusion parameter itself. Therefore, the inclusion of multiple perfusion parameters in a logistic model improved the model. However, we have not compared the probabilistic volumes following from our multivariable logistic model with probabilistic volumes following from single variable logistic models. Instead, we have tested the multivariable logistic model against single variable thresholding because in the current clinical setting, thresholds are typically applied to single perfusion maps.

A strength of our study is that data was used from two different multicenter trials with multiple CT vendors and was divided into a training and test patient group, which gives generalizable results. The data also included small and large follow-up infarct volumes. Our analysis has strengths as well. First, the validation with three CTP processing methods

demonstrated the translatability of our method of probabilistic classification. Second, we compared the predicted volumes of both methods next to a voxel-wise comparison – as represented by the precision-recall curve – because the final infarct volume is characterized as pivotal in determining functional outcome [20, 21, 24].

Several limitations to our study should be noted. First, NCCT was used as follow-up imaging method since better methods such as diffusion-weighted MR imaging was not generally available for our data. For patients from the MRCLEAN trial, the infarct was sometimes poorly visible on the follow-up NCCT after 24 hours. Additionally, the centers in the MRCLEAN trial could adhere to their own acquisition and injection protocol, which introduces variability to the CTP results [25–27]. For the REC patient group, the ischemic core may have grown between the time of admission imaging and recanalization, especially for patients who received intravenous thrombolytic therapy. As a result, the ground truth maps for the REC patient group may cover substantial parts of the penumbra at the time of imaging. The resulting probability maps should therefore be interpreted as an estimation of the ischemic core at time of reperfusion [6]. Also, for all patients, the ground truth map could be influenced by brain shift due to edema.

There are weaknesses to our analysis as well. First, class imbalance, although minimized by the choice of our sample space, can lead to low predictive accuracy for the class of ischemic voxels in both classification methods [17]. Second, regarding probabilistic classification in specific, the decision to include all four perfusion maps may not be optimal for logistic regression because of correlation between the perfusion parameters. Third, we interpreted the probabilities as volume fractions and estimated the ischemic core and total hypoperfused region volumes by taking the difference between both hemispheres, but this approach may leave room for improvement. Fourth, relative values of the perfusion parameters were not studied both because relative perfusion parameter maps could not be exported from ISP and because no clear definition of relative values exists.

Conclusion

Multivariable probability maps outperform conventional CTP summary maps in estimating the follow-up infarct lesion, as observed on follow-up non-contrast CT obtained within three days. Clinically, an improved classification benefits the selection to treat acute ischemic stroke patients. Probability maps may provide an improved and standardized classification of ischemic regions in CTP stroke imaging.

References

1 Nogueira RG, Jadhav AP, Haussen DC, et al (2018) Thrombectomy 6 to 24 hours after stroke with a mismatch between deficit and infarct. New England Journal of Medicine 378:11–21. https://doi.org/10.1056/NEJMoa1706442

2 Albers GW, Marks MP, Kemp S, et al (2018) Thrombectomy for stroke at 6 to 16 hours with selection by perfusion imaging. New England Journal of Medicine 378:708–718. https://doi.org/10.1056/NEJMoa1713973

3 Borst J, Berkhemer OA, Roos YBWEM, et al (2015) Value of computed tomographic perfusion-based patient selection for intra-arterial acute ischemic stroke treatment. Stroke 46:3375–3382. https://doi.org/10.1161/STROKEAHA.115.010564

4 Flottmann F, Broocks G, Faizy TD, et al (2017) CT-perfusion stroke imaging: a threshold free probabilistic approach to predict infarct volume compared to traditional ischemic thresholds. Sci Rep 7:6679. https://doi.org/10.1038/s41598-017-06882-w

5 Goyal M, Ospel JM, Menon B, et al (2020) Challenging the Ischemic Core Concept in Acute Ischemic Stroke Imaging. Stroke 3147–3155. https://doi.org/10.1161/STROKEAHA.120.030620

6 Kemmling A, Flottmann F, Forkert ND, et al (2015) Multivariate Dynamic Prediction of Ischemic Infarction and Tissue Salvage as a Function of Time and Degree of Recanalization. Journal of Cerebral Blood Flow & Metabolism 35:1397–1405. https://doi.org/10.1038/jcbfm.2015.144

7 Nael K, Tadayon E, Wheelwright D, et al (2019) Defining ischemic core in acute ischemic stroke using CT perfusion: A multiparametric Bayesian-based model. American Journal of Neuroradiology 40:1491–1497. https://doi.org/10.3174/ajnr.A6170

8 van Seeters T, Biessels GJ, van der Schaaf IC, et al (2014) Prediction of outcome in patients with suspected acute ischaemic stroke with CT perfusion and CT angiography: the Dutch acute stroke trial (DUST) study protocol. BMC Neurol 14:37. https://doi.org/10.1186/1471-2377-14-37

9 Fransen PSS, Beumer D, Berkhemer OA, et al (2014) MR CLEAN, a multicenter randomized clinical trial of endovascular treatment for acute ischemic stroke in the Netherlands: Study protocol for a randomized controlled trial. Trials 15:. https://doi.org/10.1186/1745-6215-15-343

10 Barros RS, Tolhuisen ML, Boers AMM, et al (2020) Automatic segmentation of cerebral infarcts in follow-up computed tomography images with convolutional neural networks. Journal of NeuroInterventional Surgery 12:848–852. https://doi.org/10.1136/neurintsurg-2019-015471

11 Zaidat OO, Yoo AJ, Khatri P, et al (2013) Recommendations on Angiographic Revascularization Grading Standards for Acute Ischemic Stroke: A Consensus Statement and for the Cerebral Angiographic Revascularization, Grading (CARG) Collaborators, STIR Revascularization working group, and STIR Thrombol. Stroke 44:2630–2663. https://doi.org/10.1161/STROKEAHA.113.001972.Recommendations

12 Kudo K, Christensen S, Sasaki M, et al (2013) Accuracy and Reliability Assessment of CT and MR Perfusion Analysis Software Using a Digital Phantom. Radiology 267:201–211. https://doi.org/10.1148/radiol.12112618

13 Bennink E, Oosterbroek J, Kudo K, et al (2016) Fast nonlinear regression method for CT brain perfusion analysis. Journal of Medical Imaging 3:026003. https://doi.org/10.1117/1.jmi.3.2.026003

14 van Ommen F, Kauw F, Bennink E, et al (2019) Effect of prolonged acquisition intervals for CT-perfusion analysis methods in patients with ischemic stroke. Medical Physics 46:3156–3164. https://doi.org/10.1002/mp.13559

15 Wintermark M, Flanders AE, Velthuis B, et al (2006) Perfusion-CT Assessment of Infarct Core and Penumbra. Stroke 37:979–985. https://doi.org/10.1161/01.STR.0000209238.61459.39

16 Youden WJ (1950) Index for rating diagnostic tests. Cancer 3:32–35. https://doi.org/10.1002/1097-0142(1950)3:1<32::AID-CNCR2820030106>3.0.CO;2-3

17 Guo X, Yin Y, Dong C, et al (2008) On the class imbalance problem. Proceedings - 4th International Conference on Natural Computation, ICNC 2008 4:192–201. https://doi.org/10.1109/ICNC.2008.871

18 Imon AHMR, Hadi AS (2013) Identification of multiple high leverage points in logistic regression. Journal of Applied Statistics 40:2601–2616. https://doi.org/10.1080/02664763.2013.822057

19 Hoaglin DC, Iglewicz B, Tukey JW (1986) Performance of some resistant rules for outlier labeling. Journal of the American Statistical Association 81:991–999. https://doi.org/10.1080/01621459.1986.10478363

20 Campbell BCV, Majoie CBLM, Albers GW, et al (2019) Penumbral imaging and functional outcome in patients with anterior circulation ischaemic stroke treated with endovascular thrombectomy versus medical therapy: a meta-analysis of individual patient-level data. The Lancet Neurology 18:46–55. https://doi.org/10.1016/S1474-4422(18)30314-4

21 Yoo AJ, Chaudhry ZA, Nogueira RG, et al (2012) Infarct volume is a pivotal biomarker after intra-arterial stroke therapy. Stroke 43:1323–1330. https://doi.org/10.1161/STROKEAHA.111.639401

22 Boers AMM, Jansen IGH, Beenen LFM, et al (2018) Association of follow-up infarct volume with functional outcome in acute ischemic stroke: A pooled analysis of seven randomized trials. Journal of NeuroInterventional Surgery 10:1137–1142. https://doi.org/10.1136/neurintsurg-2017-013724

23 Pennig L, Thiele F, Goertz L, et al (2020) Comparison of Accuracy of Arrival-Time-Insensitive and Arrival-Time-Sensitive CTP Algorithms for Prediction of Infarct Tissue Volumes. Sci Rep 10:9252. https://doi.org/10.1038/s41598-020-66041-6

24 Berkhemer OA, Fransen PSS, Beumer D, et al (2015) A Randomized Trial of Intraarterial Treatment for Acute Ischemic Stroke. New England Journal of Medicine 372:11–20. https://doi.org/10.1056/nejmoa1411587

25 Peerlings D, Bennink E, Dankbaar JW, et al (2021) Variation in arterial input function in a large multicenter computed tomography perfusion study. Eur Radiol 31:8317–8325. https://doi.org/10.1007/s00330-021-08067-6

26 Shankar JJS (2021) Variation in CT perfusion protocol has implications on defining irreversibly damaged ischemic brain parenchyma. Eur Radiol 31:8315–8316. https://doi.org/10.1007/s00330-021-08209-w

27 Wintermark M, Albers GW, Broderick JP, et al (2013) Acute stroke imaging research roadmap II. Stroke 44:2628–2639. https://doi.org/10.1161/STROKEAHA.113.002015

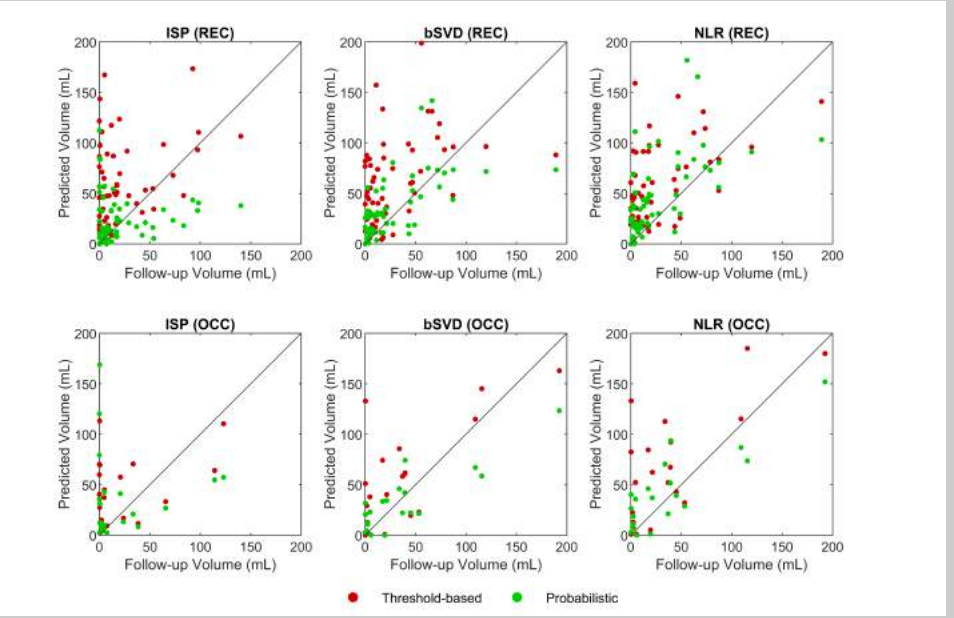

Supplementary Figure 1

Scatter plot of threshold-based and probabilistic volumes for three processing methods (ISP, bSVD, NLR) following from a test patient group with successful recanalization (REC) and a test patient group with persistent occlusion (OCC).

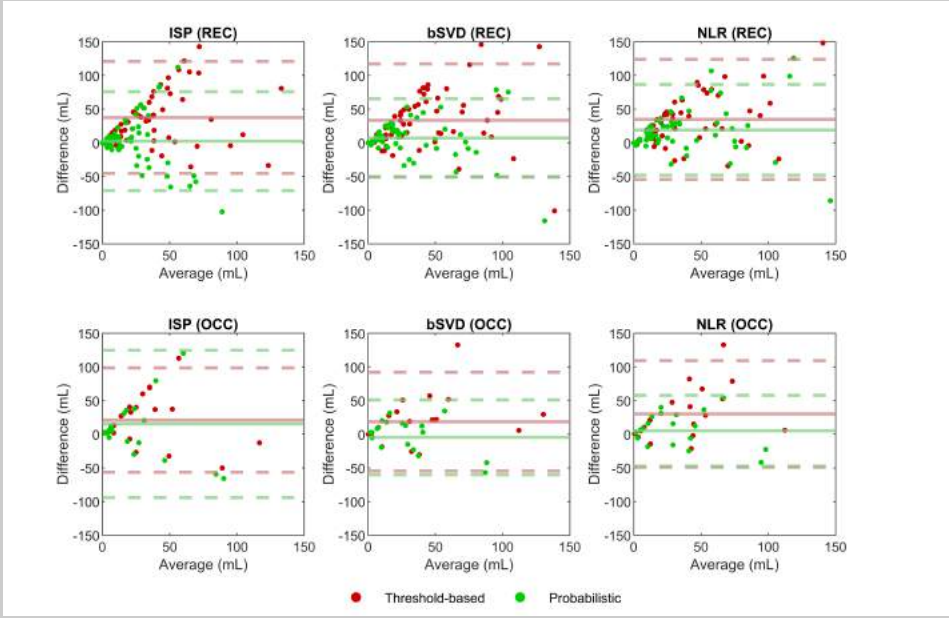

Supplementary Figure 2

Bland-Altman plot of threshold-based and probabilistic volumes for three processing methods (ISP, bSVD, NLR) following from a test patient group with successful recanalization (REC) and a test patient group with persistent occlusion (OCC). The difference and average are between the predicted volume and the follow-up volume. The continuous line represents the mean volume difference, which is positive for an overestimation of predicted volumes. The dashed lines represent the mean volume difference plus or minus 1.96 times the standard deviation.

Chapter 6

We aimed to demonstrate the diagnostic value of CTP imaging in a best-case scenario.

CTP data sets from a local cohort of the CLEOPATRA (cost-effectiveness of CTP for patients with acute ischemic stroke) healthcare evaluation were included retrospectively if acute MR diffusion imaging was available. The CTP data sets were processed with a widely used vendor software (syngoVIA, Siemens Healthineers) to produce perfusion maps. We manually segmented the perfusion maps and compared the volume and location of the manual segmentations with segmentations that were derived from the MR diffusion imaging. Additionally, we examined the segmentations produced by the vendor software itself and by an in-house method, which was based on a logistic model.

Fifteen patients, all with anterior circulation stroke, were included. Median time between CTP imaging and MR imaging was 61 minutes. The MR segmentation volumes ranged from 0.4 to 118 mL. The manual segmentations each overlapped with the MR segmentation and had a mean absolute volume difference of 15 mL. Performance varied with the segmentation method: for the manual segmentations, the vendor segmentations, and the in-house segmentations, we observed a mean Dice similarity coefficient of 0.44, 0.26, and 0.48, a mean precision of 0.61, 0.38, and 0.49, and a mean recall of 0.41, 0.25, and 0.54, respectively.

CTP imaging seems diagnostically valuable by resembling MR diffusion imaging in the acute phase of ischemic stroke. Still, the volume and location of the estimated ischemia varied substantially with different segmentation methods.

Benchmarking the estimation of ischemic regions

Based on 'Daan Peerlings, Hugo WAM de Jong, Edwin Bennink, Jan W Dankbaar, Henk A Marquering, Bart J Emmer, Lucas de Vries, Charles BLM Majoie. CT perfusion imaging resembles MR diffusion imaging in the acute phase of ischemic stroke.' *Submitted*.

Introduction

The infarct core volume and its ratio to the volume of the penumbra have been the main selection criteria for multiple large acute ischemic stroke trials and have been included in clinical guidelines accordingly [1–4]. In current clinical practice, the infarct core and penumbra are most frequently estimated, in the acute phase, with CT perfusion (CTP) imaging.

Although CTP imaging is standard practice, its validation has remained challenging. The estimated infarct core and penumbra vary greatly between various software in use and are difficult to verify because of the lack of a reliable ground truth reference [5, 6]. Typically, the ground truth infarct core and penumbra are derived from follow-up imaging obtained after a couple of days and grouped by the success of recanalization [7–9]. However, the ischemia can change considerably in this time and depends on the level of reperfusion and collateral blood supply. MR diffusion imaging is sensitive to acute infarction and could therefore provide a ground truth reference for CTP imaging in the acute phase of ischemic stroke [10, 11]. However, MR diffusion imaging is challenging to acquire in the acute phase, limiting the amount of available data to compare CTP imaging with.

In this study, we investigated the diagnostic value of CTP imaging in a best-case scenario by comparing manually segmented CTP images with lesion segmentations from acute MR diffusion imaging. Additionally, we considered automatic segmentations of the CTP images from the clinical perfusion software and from an in-house segmentation model.

Methods

Data acquisition

Retrospective data were used from a local cohort at Amsterdam University Medical Centers (location AMC) relating to the nationwide multicenter healthcare evaluation CLEOPATRA (cost-effectiveness of CTP for patients with acute ischemic stroke) [12]. The study population and image acquisition for this cohort are described by Hoving et al. in more detail [13]. Patients from the CTP cohort were included in our study if they had MR diffusion imaging within 4 hours of CTP imaging.

The CTP protocol consisted of scanning at 70 kVp and 200 mAs on a dual source 192-slice CT scanner (SOMATOM Force, Siemens Healthineers, Forchheim, Germany) with 15 frames 1.5 seconds apart followed by 15 frames 3 seconds apart. The scans were reconstructed as 5 mm axial slices. The injection protocol consisted of a 35 mL contrast bolus (Iomeron 300, iomeprol, 300 mg iodine/mL; Bracco Imaging Deutschland GmbH, Konstanz, Germany) injected at a rate of 6 mL/s followed by a saline flush of 40 mL injected at a rate of 6 mL/s. The MR diffusion images ($b = 0$ s/mm^2 and $b = 1000$ s/mm^2) were acquired on a 1.5 T scanner (MAGNETOM Avanto fit, Siemens Healthcare, Erlangen, Germany) or a 3.0 T scanner (Ingenia 3.0T, Philips Healthcare, Best, The Netherlands), both with a slice thickness of 5 mm.

MR segmentations of severe ischemia

For each patient, we aligned the MR diffusion images with the CTP images by a rigid transformation with a mean square error metric using Elastix [14]. The aligned MR diffusion images were segmented employing a convolutional neural network and were adjusted manually where necessary [15]. We considered the segmentations from the acute MR diffusion imaging as the ground truth for severe ischemia, but refer to them as MR segmentations. Additionally, we prefer severe ischemia instead of infarct core because this study aims to compare the visible ischemia on CTP imaging with the lesion on acute MR diffusion imaging and is thus not concerned with follow-up imaging.

Vendor segmentations of severe ischemia

All CTP scans were analyzed with the perfusion software CT Neuro Perfusion from syngoVIA version VB40A-HF02 (Siemens Healthineers) and additional smoothing was applied following recommendations to minimize artifacts [16]. The arterial input function was determined automatically. The software calculated perfusion maps of the cerebral blood flow (CBF), the cerebral blood volume (CBV), the mean transit time (MTT), and the time to maximum (TMAX). Subsequently, severe ischemia was segmented with the default threshold of CBV < 1.2 mL/100g.

Manual segmentations of severe ischemia

We manually segmented the exported perfusion maps using ITK-SNAP 4.0.0 [17]. The perfusion maps were viewed with a jet color map windowed 0-50 mL/100g/min for the CBF, 0-5 mL/100g for the CBV, 0-20 seconds for the MTT, and 0-15 seconds for the TMAX. We applied a conservative strategy by looking primarily for both a low CBV and a high TMAX, but we inspected all the perfusion parameters and deliberated the geometry of the ischemic region as well. First, an imaging scientist, with three years of experience in perfusion imaging,

segmented the images. Then, two expert neuroradiologists, with at least fifteen years of experience, checked the segmentations and gave feedback. This process was repeated until consensus was reached. All observers were blinded to everything other than the perfusion maps.

In-house segmentations of severe ischemia

Because logistic models have been shown to outperform threshold-based segmentation, we also considered automatic segmentations that followed from an in-house developed logistic model [9]. The training data and the model design are explained in detail by Peerlings et al. [18]. The in-house model takes in the perfusion parameters of a voxel and puts out the probability that the voxel is infarct core, penumbra, or healthy. The logistic model, with weights specific to the perfusion software from syngoVIA, reads:

$$P_{CORE} = 10^{S_{CORE}} / (1 + 10^{S_{CORE}} + 10^{S_{PENUMBRA}}) ,$$

$$P_{PENUMBRA} = 10^{S_{PENUMBRA}} / (1 + 10^{S_{CORE}} + 10^{S_{PENUMBRA}}) ,$$

$$P_{HEALTHY} = 1 - P_{CORE} - P_{PENUMBRA} ,$$

where

$$S_{CORE} = 20.7 - 0.7049 \times CBF - 8.00 \times CBV - 0.29 \times MTT + 2.9 \times TMAX ,$$

and

$$S_{PENUMBRA} = -13.7 - 0.0045 \times CBF + 0.54 \times CBV + 0.33 \times MTT + 2.9 \times TMAX .$$

The in-house segmentations of severe ischemia were obtained by considering P_{CORE} within a region of interest to eliminate false positives. This region of interest was automatically determined from the probabilities as follows. The voxels for which P_{CORE} was greater than $P_{PENUMBRA}$ and $P_{HEALTHY}$ constituted an initial segmentation. This initial segmentation, having false positive regions that were similar in both hemispheres, was mirrored over the midline of the brain. After subtracting the mirrored segmentation from the initial segmentation, we took the largest connected component, which we subsequently opened and closed morphologically. The morphological operations were performed with a spherical structure element that had a diameter equal to the slice thickness. The resulting region of interest was intersected with the initial segmentation to obtain the in-house segmentation of severe ischemia.

Table 1

Relevant patient information. The patients (A-O) are ordered according to their MR segmentation volume.

Patient	MR volume (mL)	Occlusion	NIHSS	Time onset-CTP (min)	Time CTP-MR (min)	Reason for MR	Time spent for manual segmentation (min)
A	0.4	M2	2	785	39	Uncertain age of infarct	32
B	0.9	M2	6	995	32	Wake-up	53
C	1.5	M3	11	455	61	Wake-up	9
D	2.1	M4	5	126	252	Strong suspicion of endocarditis	20
E	3.1	M2	10	645	100	Wake-up	24
F	5.3	M1	15	451	65	Wake-up	277
G	13	M3	-	720	62	Wake-up	32
H	26	M2	13	474	47	Wake-up	56
I	34	ICA	18	917	50	Wake-up	70
J	43	M2/A2	8	544	59	Wake-up	35
K	83	M1	16	590	37	Wake-up	129
L	84	M1	18	295	47	Wake-up	58
M	101	M1	17	303	128	Doubtful indication for thrombectomy	120
N	106	ICA	23	275	65	Confirmation of CT findings for treatment decision	240
O	118	ICA/M1	-	-	227	Wake-up	284

Performance assessment of perfusion-based segmentations

For each patient, we determined the volume of the MR segmentation. For the CTP based segmentations, we determined the volume inside and outside the MR segmentation. From this, we calculated the precision by dividing the volume inside the MR segmentation by the total volume of the perfusion-based segmentation, the recall by dividing the volume inside the MR segmentation by the total volume of the MR segmentation, and the Dice similarity coefficient (DSC) by taking the harmonic mean of the precision and the recall.

Results

Fifteen patients, all with anterior circulation stroke, were included (Table 1). Median (first quartile, third quartile) time between CTP and MR imaging was 61 (47, 100) minutes. We named the patients A through O, according to an increasing MR segmentation volume. The volumes of the segmentations are depicted in Figure 1. Table 2 presents their precision, recall, and DSC. In Figure 2, we plotted the precision, recall, and DSC against the MR volume, demonstrating that the precision, recall, and DSC improved for larger MR volumes. Figures 3-6 illustrate the general findings. In Figures 3-5, the ischemia on CTP imaging resembled the lesion on MR diffusion imaging. In the Supplementary Material, we have included boxplots of the perfusion parameters in the different segmentations for each patient.

Vendor segmentations of severe ischemia

The vendor segmentations overestimated the smaller MR volumes and underestimated the larger MR volumes, with a mean absolute volume difference of 25 mL, and resulted in the lowest mean precision (0.38), the lowest mean recall (0.25), and the lowest mean DSC of the three segmentation methods (Figure 1, Table 2). For four of the five smallest MR volumes, the recall was very low (< 0.08) and the precision was near zero (< 0.02). The precision for larger MR volumes was the best feature of the vendor segmentations. The overestimation of smaller MR volumes and the underestimation of larger MR volumes resulted in a lack of differentiation between the patients; the patients C, G, H, and O had MR volumes of 1.5 mL, 13 mL, 26 mL, and 118 mL, respectively, and estimated volumes of 10 mL, 32 mL, 8.5 mL, and 36 mL, respectively.

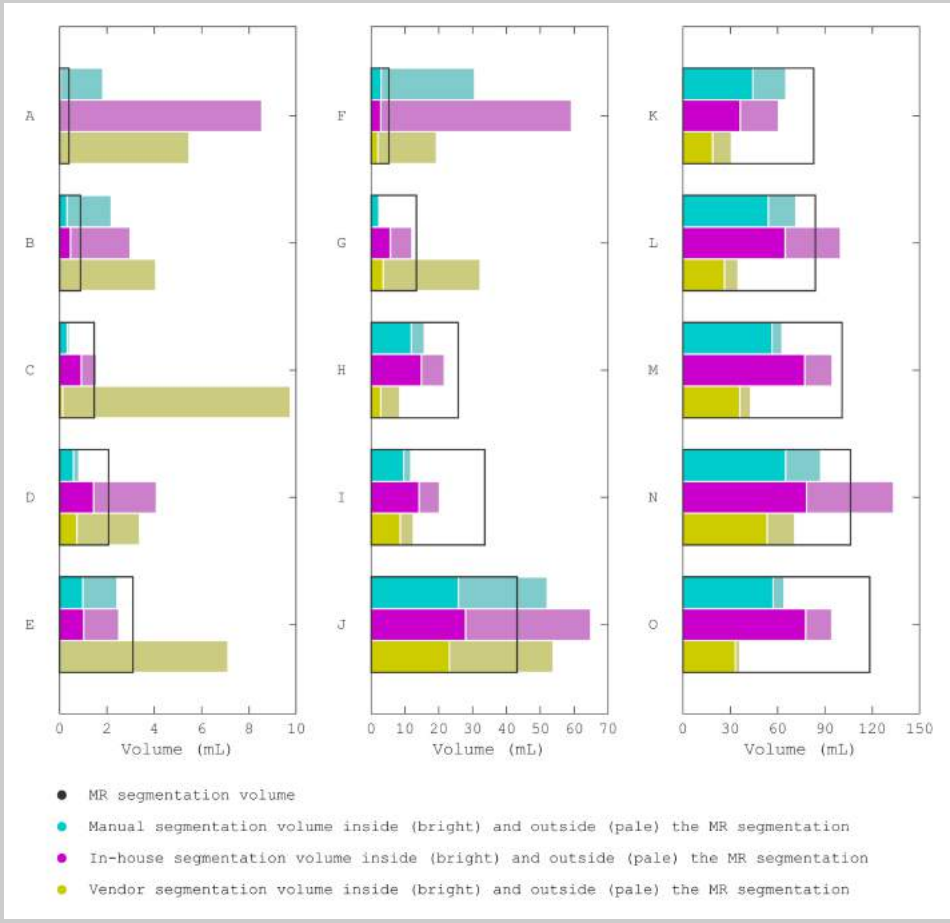

Figure 1

Volumetric agreement of the perfusion-based segmentations with the MR segmentations for patients A to O, who were ordered to MR volume. The black outline is the volume of the MR segmentation. The stacked bar graphs indicate the volume inside (bright) and outside (pale) the MR segmentation for the perfusion-based segmentations. The volume ranges on the horizontal axes differ in the three charts.

Table 2

Spatial agreement of the perfusion-based segmentations with the MR segmentations. The patients (A-O) are ordered according to their MR segmentation volume.

	Precision			Recall			Dice similarity coefficient		
Patient	**Manual**	**In-house**	**Vendor**	**Manual**	**In-house**	**Vendor**	**Manual**	**In-house**	**Vendor**
Mean	0.61	0.49	0.38	0.41	0.54	0.25	0.44	0.48	0.26
A	0.03	0	0	0.13	0	0	0.05	0	0
B	0.14	0.15	0	0.35	0.52	0.01	0.21	0.24	0
C	0.77	0.58	0.01	0.22	0.62	0.08	0.35	0.60	0.02
D	0.70	0.35	0.22	0.28	0.70	0.36	0.40	0.47	0.27
E	0.40	0.41	0	0.32	0.33	0	0.36	0.36	0
F	0.10	0.05	0.10	0.57	0.54	0.37	0.17	0.09	0.16
G	0.94	0.47	0.11	0.18	0.43	0.27	0.30	0.45	0.16
H	0.75	0.69	0.34	0.46	0.58	0.11	0.57	0.63	0.17
I	0.82	0.70	0.69	0.29	0.42	0.26	0.43	0.53	0.38
J	0.49	0.43	0.43	0.60	0.65	0.54	0.54	0.52	0.48
K	0.68	0.60	0.61	0.53	0.44	0.23	0.60	0.51	0.33
L	0.75	0.65	0.75	0.64	0.77	0.31	0.69	0.70	0.44
M	0.90	0.81	0.84	0.56	0.76	0.36	0.69	0.79	0.50
N	0.74	0.59	0.75	0.61	0.74	0.50	0.67	0.65	0.60
O	0.89	0.82	0.92	0.48	0.66	0.28	0.63	0.73	0.43

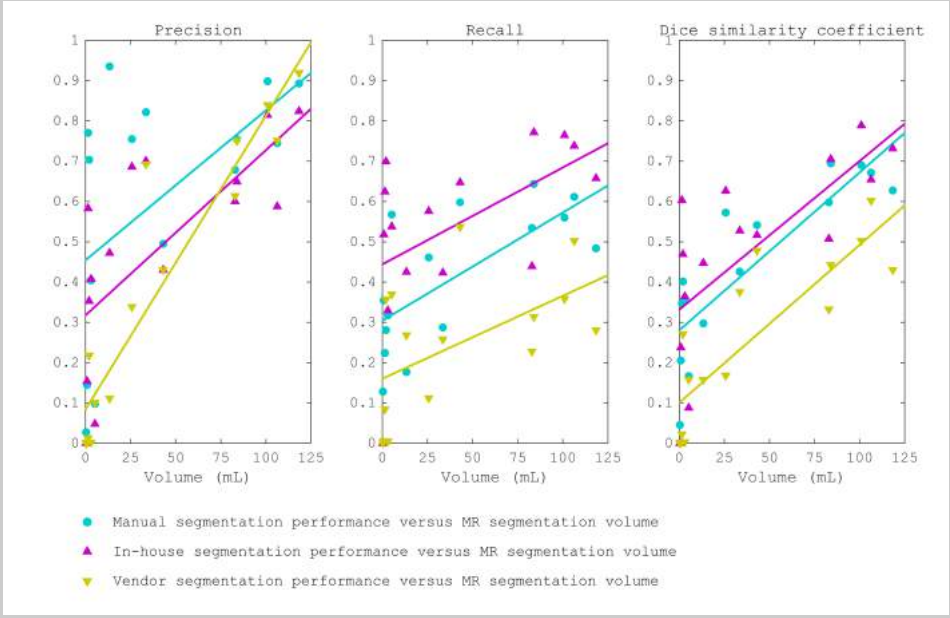

Figure 2

Performance measures plotted against the MR segmentation volume. The line of best fit shows the trend of increased performance for larger MR volumes.

Manual segmentations of severe ischemia

The manual segmentations generally underestimated the MR volumes, with a mean absolute volume difference of 15 mL, and resulted in a mean precision (0.61) that was higher than the mean recall (0.41), yielding a mean DSC of 0.44 (Figure 1, Table 2). The manual segmentations had a non-zero recall for each patient. Besides being time consuming (Table 1), it was not always obvious what to segment. Examples are the area with a lower TMAX inside the MR segmentation in Figure 3 and the area with a higher CBV inside the MR segmentation in Figure 5. We also note that the vendor segmentations sometimes differed completely from the manual segmentations (Figure 3).

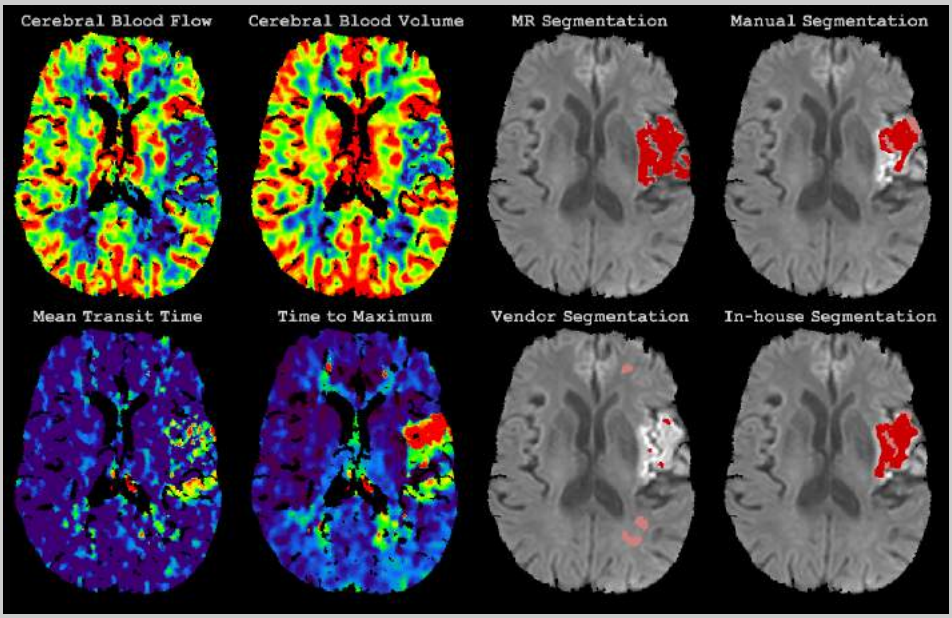

Figure 3

The perfusion maps, MR diffusion scan, and segmentations of severe ischemia for patient H. For the segmentations, the bright red regions are inside the MR segmentation whereas the pale red regions are outside the MR segmentation.

It was remarked, during its manual segmentation, that patient F may had been spontaneously recanalized given the hyperperfusion in the basal ganglia (Figure 6). The manual segmentation for patient F resulted in the largest overestimation compared to the other patients (Figure 1). The CTP imaging and MR diffusion imaging are dissimilar for this patient (Figure 6).

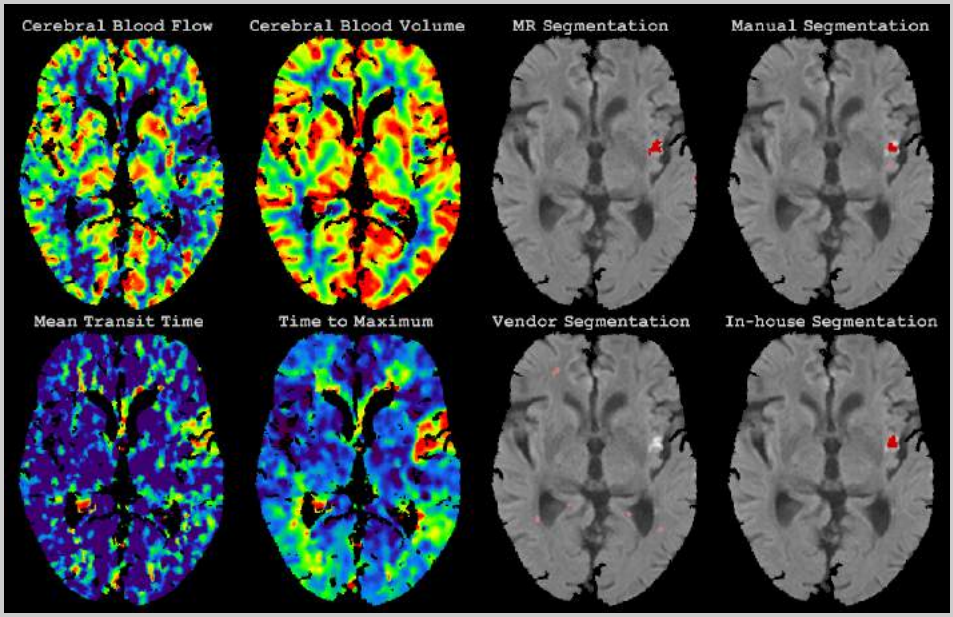

Figure 4

The perfusion maps, MR diffusion scan, and segmentations of severe ischemia for patient B. For the segmentations, the bright red regions are inside the MR segmentation whereas the pale red regions are outside the MR segmentation.

In-house segmentations of severe ischemia

The in-house segmentations had a mean absolute volume difference of 14 mL and resulted in a mean precision of 0.49, a mean recall of 0.54, and a mean DSC of 0.48 (Figure 1, Table 2). The mean DSC of the in-house segmentations was similar to the mean DSC of the manual segmentations, but the in-house segmentations resulted in a lower mean precision and a higher mean recall than the manual segmentations. Were we to take the manual segmentations as our ground truth, then the in-house segmentations would give a mean DSC of 0.58 with a mean precision of 0.49 and a mean recall of 0.82. Indeed, the in-house segmentations appeared to enclose the manual segmentations (Figures 3-6).

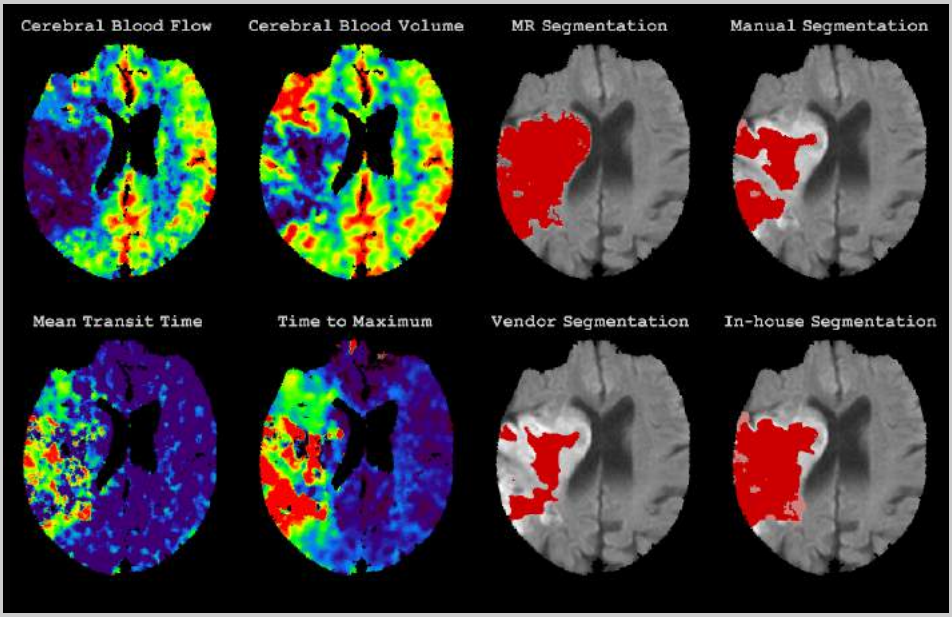

Figure 5

The perfusion maps, MR diffusion scan, and segmentations of severe ischemia for patient M. For the segmentations, the bright red regions are inside the MR segmentation whereas the pale red regions are outside the MR segmentation.

Discussion

The manual segmentations demonstrated that CTP imaging resembles MR diffusion imaging in the acute phase of ischemic stroke. The manual segmentations were in the right place for each patient and were generally of the right size. For one patient, the overestimation may have been the result of a spontaneous recanalization that was recognized with CTP imaging. While the in-house segmentations were as good as the manual segmentations, the vendor segmentations were worse. Together, these results imply that CTP imaging can be of diagnostic value, but that the estimation of ischemia needs to be critically evaluated.

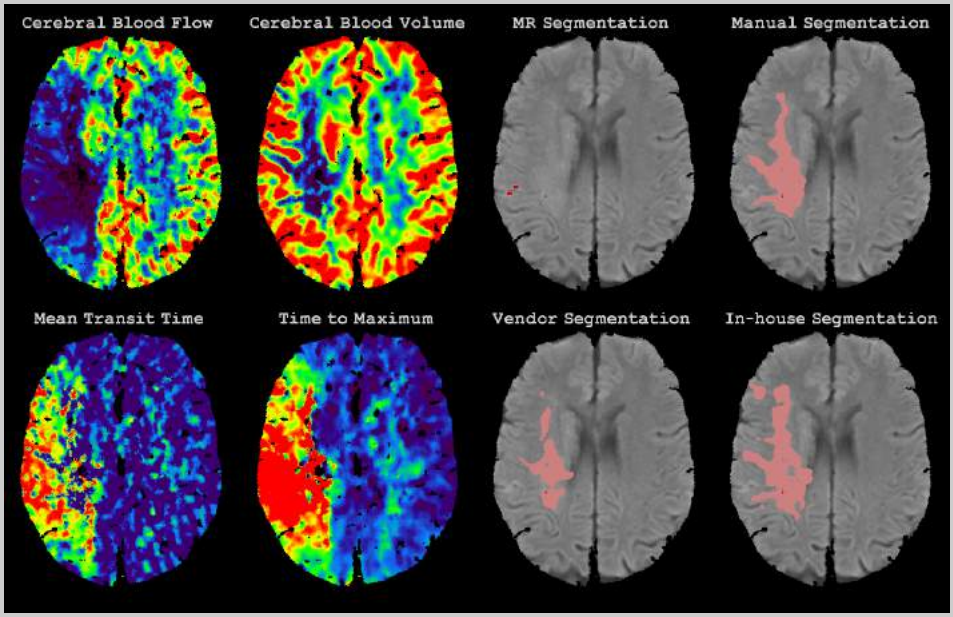

Figure 6

The perfusion maps, MR diffusion scan, and segmentations of severe ischemia for patient F. For the segmentations, the bright red regions are inside the MR segmentation whereas the pale red regions are outside the MR segmentation. The hyperperfusion of the basal ganglia visible on the perfusion maps may indicate that the patient was spontaneously recanalized.

We considered CTP imaging in a best-case scenario with manual segmentations and acute MR diffusion imaging. To our knowledge, this is the first study to consider manual segmentations for CTP imaging. CTP imaging has been compared to acute MR diffusion imaging before in the ISLES (Ischemic Stroke Lesion Segmentation) challenge, a machine learning competition for stroke lesion analysis [19]. In this challenge, the best Dice similarity coefficient was 0.51 and the best mean absolute volume difference was 10 mL, comparable to our performance. As we considered a best-case scenario, this performance seems to be limited, since roughly only half of each segmentation overlapped the MR segmentation and vice versa on average. We also struggled to consistently segment the perfusion maps manually, we observed a different performance for the manual and in-house segmentations, and severe ischemia on CTP imaging appeared viable for a patient who may had been recanalized already. These observations are in line with an earlier study that outlined conceptual and practical

challenges that arise when estimating ischemia from perfusion imaging [6]. In addition, the practical utility of CTP imaging to select patients for treatment is increasingly contested, as thrombectomy proves to be an effective treatment for a broadening range of patients [20-22]. Still, this study shows that ischemia estimated with CTP imaging can be of diagnostic value, considering its resemblance to acute MR diffusion imaging.

Our study has limitations. Firstly, we used MR diffusion imaging to provide a ground truth for severe ischemia. However, a diffusion lesion does not always result in complete infarction [23]. It is also possible, although unlikely, for infarction not to show up as a diffusion lesion [24]. Additionally, the time between CTP imaging and MR diffusion imaging, although limited, allowed the infarct to grow so that the diffusion lesion may have been smaller at the time of CTP imaging. Also, the small number of patients with acute MR diffusion imaging makes our study less generalizable. Secondly, we were biased to segment at least some tissue based on the patient selection. Therefore, our manual segmentations were somewhat inconsistent across patients, because we were more willing to segment tissue with ambiguous perfusion for smaller ischemic regions than for larger ischemic regions. Thirdly, we only considered severe ischemia and not the total ischemic region, which is clinically important as well. To validate CTP imaging, future studies might focus on manual segmentations of perfusion maps. These manual segmentations may be considered the acute ground truth and could be used to develop automatic segmentation methods. This approach would facilitate the availability of data for both the severely ischemic and the total ischemic tissue, and would make it possible to account for uncertainty by making manual segmentations with different levels of confidence.

Conclusion

Ischemia can be estimated with CTP imaging in a diagnostically valuable way. Manually segmented ischemia on CTP imaging resembled lesions on MR diffusion imaging in the acute phase of ischemic stroke. Still, the estimated ischemia varied based on the segmentation method. Estimating ischemia in a consistent way can help to diagnose acute ischemic stroke patients accurately, and to advance stroke healthcare.

References

1 Nogueira RG, Jadhav AP, Haussen DC, et al (2018) Thrombectomy 6 to 24 hours after stroke with a mismatch between deficit and infarct. New England Journal of Medicine 378:11–21. https://doi.org/10.1056/NEJMoa1706442

2 Albers GW, Marks MP, Kemp S, et al (2018) Thrombectomy for stroke at 6 to 16 hours with selection by perfusion imaging. New England Journal of Medicine 378:708–718. https://doi.org/10.1056/NEJMoa1713973

3 Campbell BCV, Mitchell PJ, Kleinig TJ, et al (2015) Endovascular Therapy for Ischemic Stroke with Perfusion-Imaging Selection. New England Journal of Medicine 372:1009–1018. https://doi.org/10.1056/nejmoa1414792

4 Ma H, Campbell BCV, Parsons MW, et al (2019) Thrombolysis Guided by Perfusion Imaging up to 9 Hours after Onset of Stroke. New England Journal of Medicine 380:1795–1803. https://doi.org/10.1056/nejmoa1813046

5 Shankar JJS (2021) Variation in CT perfusion protocol has implications on defining irreversibly damaged ischemic brain parenchyma. Eur Radiol 31:8315–8316. https://doi.org/10.1007/s00330-021-08209-w

6 Goyal M, Ospel JM, Menon B, et al (2020) Challenging the Ischemic Core Concept in Acute Ischemic Stroke Imaging. Stroke 3147–3155. https://doi.org/10.1161/STROKEAHA.120.030620

7 Pennig L, Thiele F, Goertz L, et al (2020) Comparison of Accuracy of Arrival-Time-Insensitive and Arrival-Time-Sensitive CTP Algorithms for Prediction of Infarct Tissue Volumes. Sci Rep 10:9252. https://doi.org/10.1038/s41598-020-66041-6

8 Wintermark M, Flanders AE, Velthuis B, et al (2006) Perfusion-CT Assessment of Infarct Core and Penumbra. Stroke 37:979–985. https://doi.org/10.1161/01.STR.0000209238.61459.39

9 Peerlings D, van Ommen F, Bennink E, et al (2022) Probability maps classify ischemic stroke regions more accurately than CT perfusion summary maps. Eur Radiol 32:6367–6375. https://doi.org/10.1007/s00330-022-08700-y

10 Simonsen CZ, Madsen MH, Schmitz ML, et al (2015) Sensitivity of diffusion-and perfusion-weighted imaging for diagnosing acute ischemic stroke is 97.5%. Stroke 46:98–101. https://doi.org/10.1161/STROKEAHA.114.007107

11 Powers WJ, Rabinstein AA, Ackerson T, et al (2019) Guidelines for the early management of patients with acute ischemic stroke: 2019 update to the 2018 guidelines for the early management of acute ischemic stroke a guideline for healthcare professionals from the American Heart Association/American Stroke Association. Stroke 50:E344–E418

12 Koopman MS, Hoving JW, van Voorst H, et al (2022) Cost-effectiveness of CT perfusion for patients with acute ischemic stroke (CLEOPATRA)-Study protocol for a healthcare evaluation study. Eur Stroke J. https://doi.org/10.1177/23969873221092535

13 Hoving JW, Koopman MS, Tolhuisen ML, et al (2022) Accuracy of CT perfusion ischemic core volume and location estimation: A comparison between four ischemic core estimation approaches using syngo.via. PLoS One 17:. https://doi.org/10.1371/journal.pone.0272276

14 Klein S, Staring M, Murphy K, et al (2010) elastix: A Toolbox for Intensity-Based Medical Image Registration. IEEE Trans Med Imaging 29:196–205. https://doi.org/10.1109/TMI.2009.2035616

15 Kamnitsas K, Ledig C, Newcombe VFJ, et al (2017) Efficient multi-scale 3D CNN with fully connected CRF for accurate brain lesion segmentation. Med Image Anal 36:61–78. https://doi.org/10.1016/j.media.2016.10.004

16 Koopman MS, Berkhemer OA, Geuskens RREG, et al (2019) Comparison of three commonly used CT perfusion software packages in patients with acute ischemic stroke. J Neurointerv Surg 11:1249–1256. https://doi.org/10.1136/neurintsurg-2019-014822

17 Yushkevich PA, Piven J, Hazlett HC, et al (2006) User-guided 3D active contour segmentation of anatomical structures: Significantly improved efficiency and reliability. Neuroimage 31:1116–1128. https://doi.org/10.1016/j.neuroimage.2006.01.015

18 Peerlings D, Bennink E, Dankbaar JW, et al (2023) Standardizing the estimation of ischemic regions can harmonize CT perfusion stroke imaging. Eur Radiol. https://doi.org/10.1007/s00330-023-10035-1

19 Hakim A, Christensen S, Winzeck S, et al (2021) Predicting Infarct Core from Computed Tomography Perfusion in Acute Ischemia with Machine Learning: Lessons from the ISLES Challenge. Stroke 2328–2337. https://doi.org/10.1161/STROKEAHA.120.030696

20 Nogueira RG, Haussen DC, Liebeskind D, et al (2021) Stroke Imaging Selection Modality and Endovascular Therapy Outcomes in the Early and Extended Time Windows. Stroke 491–497. https://doi.org/10.1161/STROKEAHA.120.031685

21 Huo X, Ma G, Tong X, et al (2023) Trial of Endovascular Therapy for Acute Ischemic Stroke with Large Infarct. N Engl J Med. https://doi.org/10.1056/NEJMoa2213379

22 Sarraj A, Hassan AE, Abraham MG, et al (2023) Trial of Endovascular Thrombectomy for Large Ischemic Strokes. N Engl J Med. https://doi.org/10.1056/NEJMoa2214403

23 Labeyrie M-A, Turc G, Hess A, et al (2012) Diffusion Lesion Reversal After Thrombolysis. Stroke 43:2986–2991. https://doi.org/10.1161/STROKEAHA.112.661009

24 Edlow BL, Hurwitz S, Edlow JA (2017) Diagnosis of DWI-negative acute ischemic stroke A meta-analysis

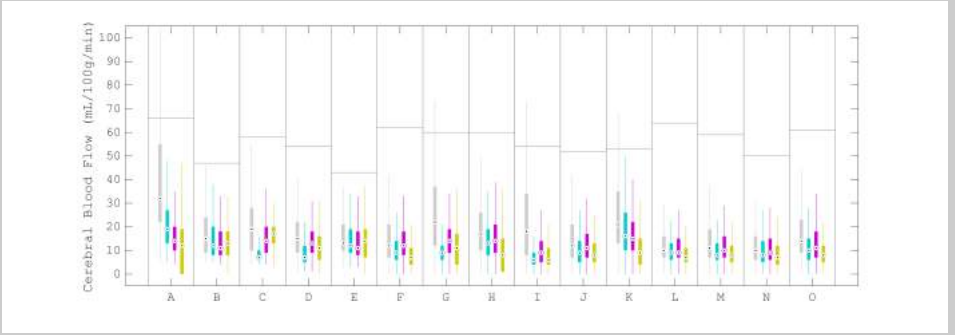

Supplementary Figure 1

Boxplots of the cerebral blood flow in different segmentations for each patient (A-O). The MR segmentation is in white, the manual segmentation in cyan, the in-house segmentation in magenta, and the vendor segmentation in yellow. The horizontal black lines indicate the median value in the contralateral hemisphere.

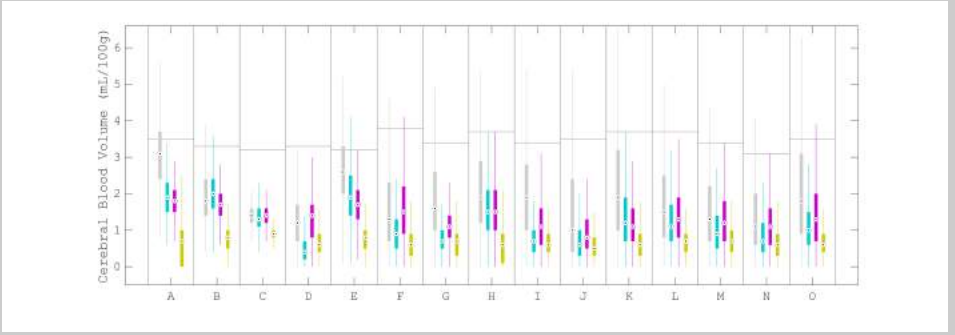

Supplementary Figure 2

Boxplots of the cerebral blood volume in different segmentations for each patient (A-O). The MR segmentation is in white, the manual segmentation in cyan, the in-house segmentation in magenta, and the vendor segmentation in yellow. The horizontal black lines indicate the median value in the contralateral hemisphere.

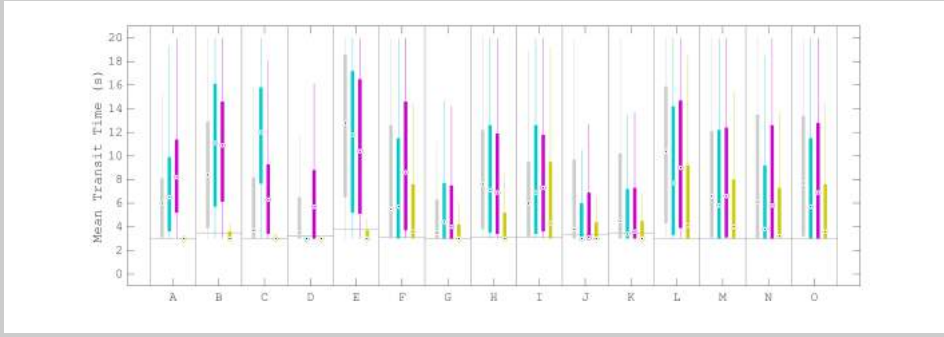

Supplementary Figure 3

Boxplots of the mean transit time in different segmentations for each patient (A-O). The MR segmentation is in white, the manual segmentation in cyan, the in-house segmentation in magenta, and the vendor segmentation in yellow. The horizontal black lines indicate the median value in the contralateral hemisphere.

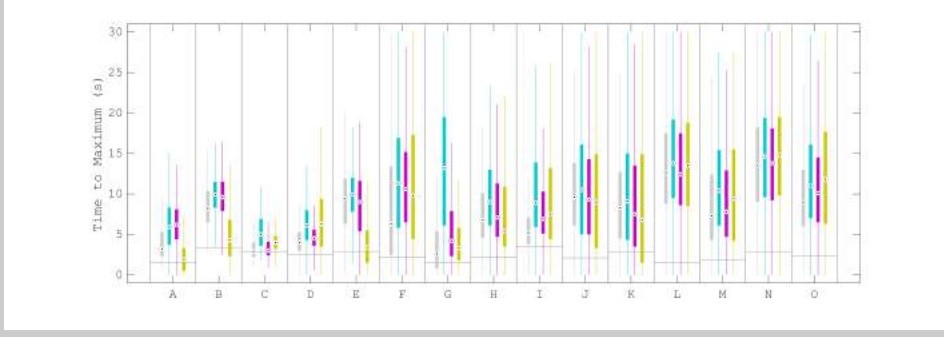

Supplementary Figure 4

Boxplots of the time to maximum in different segmentations for each patient (A-O). The MR segmentation is in white, the manual segmentation in cyan, the in-house segmentation in magenta, and the vendor segmentation in yellow. The horizontal black lines indicate the median value in the contralateral hemisphere.

Chapter 7

Locating a vessel occlusion is important for the clinical decision support in stroke healthcare. The advent of endovascular thrombectomy beyond proximal large vessel occlusions spurs alternative approaches to locate vessel occlusions. We explore whether CT perfusion (CTP) data can help to automatically locate vessel occlusions.

We composed an atlas with the downstream regions of particular vessel segments. Occlusion of these segments should result in the hypoperfusion of the corresponding downstream region. We differentiated between seven vessel occlusion locations (ICA, proximal M1, distal M1, M2, M3, ACA, and posterior circulation). We included 596 patients from the Dutch acute stroke (DUST) multicenter study. Each patient CTP data set was processed with perfusion software to determine the hypoperfused region. The downstream region with the highest overlap with the hypoperfused region was considered to indicate the vessel occlusion location. We assessed the indications from CTP against expert annotations from CT angiography (CTA) imaging.

Our atlas-based model had a mean accuracy of 86% and could achieve substantial agreement with the annotations from CTA according to Cohen's kappa coefficient (up to 0.68). In particular, anterior large vessel occlusions and occlusions in the posterior circulation could be located with an accuracy of 80% and 92%, respectively.

The spatial layout of the hypoperfused region can help to automatically indicate the vessel occlusion location for acute ischemic stroke patients. However, variation in vessel architecture between patients seemed to limit the capacity of CTP data to distinguish between vessel occlusion locations more accurately.

Locating the vessel occlusion

Published as 'Daan Peerlings, Hugo WAM de Jong, Edwin Bennink, Jan W Dankbaar, Birgitta K Velthuis, Bart J Emmer, Charles BLM Majoie, Henk A Marquering. Spatial CT perfusion data helpful in automatically locating vessel occlusions for acute ischemic stroke patients. *Frontiers in Neurology* 14 (2023): 1136232.'

Introduction

The location of a vessel occlusion is central to the clinical decision support of acute ischemic stroke patients. To diagnose these patients, multimodal CT imaging is performed, consisting of non-contrast CT, CT angiography (CTA), and CT perfusion (CTP). Non-contrast CT can be used to exclude hemorrhagic stroke and stroke mimics, after which CTP can be used to distinguish the infarcted tissue from the salvageable tissue, and CTA can be used to locate the vessel occlusion [1].

Mechanical thrombectomy has become the standard of care for patients suffering from acute ischemic stroke due to anterior circulation proximal large vessel occlusions [2]. Recent advancements in stent retriever technology and thromboaspiration devices may widen the eligibility criteria for endovascular treatment by considering occlusions in smaller and more distal vessels [3]. It is a prerequisite for endovascular treatment to locate the vessel occlusion.

Reading CTA to locate vessel occlusions can be challenging. The more distal the vessel occlusion, the harder this task becomes because the occlusion is smaller, has delayed opacification, can be concealed behind cortical veins, and can be found in a larger number of vessels that exhibit more anatomical variability [4, 5]. Moreover, while less experienced readers are likely on call in the emergency setting, they do not perform as well as experienced readers in giving fast and accurate evaluations [6, 7]. Therefore, the advent of endovascular treatment beyond proximal large vessel occlusions spurs alternative approaches to locate vessel occlusions [8].

CTP provides a way to locate vessel occlusions because a vessel occlusion results in a perfusion deficit in the downstream region of the occluded vessel [3, 5, 9, 10]. As such, it has been shown that experienced readers of CTP can accurately discern patients with a distal vessel occlusion from patients without a vessel occlusion [5]. Moreover, the addition of CTP to CTA has expedited and improved the detection of vessel occlusions on CTA in previous studies [9, 10]. Hence, CTP data may contain information that is helpful in locating vessel occlusions.

CTP data on its own are often regarded as complex because it consists of several physiological parameters. Although the presence of a perfusion deficit suffices to detect a vessel occlusion, assessing this deficit to locate the vessel occlusion requires additional physiological and neuroanatomical expertise. Therefore, an automatic evaluation of CTP data may facilitate the support of CTP in reading CTA.

In this study, we explore the potential of CTP to automatically locate vessel occlusions. We present an atlas-based method in which CTP data are used to indicate the vessel occlusion location. These indicated vessel occlusion locations were compared with annotated vessel occlusion locations from expert readings of CTA.

Methods

Acquiring imaging data from the patient population

Retrospective data were obtained from the Dutch acute stroke (DUST) study, in which 14 stroke centers in the Netherlands participated [11]. All included DUST participants gave informed consent for the use of their imaging and clinical data. Patients that were admitted to the DUST study were suspected of an ischemic stroke and underwent non-contrast CT, CTP, and CTA imaging within 9 h after symptom onset. Only patients with both an annotated vessel occlusion location (obtained from CTA) and a perfusion deficit (obtained from CTP) were considered in this study.

The CTP protocol consisted of scanning at 80 kVp and 150 mAs on 40- to 320-detector CT scanners (GE Healthcare, Philips, Siemens, or Toshiba) with a 2 s interval for a duration of 50 s. The scans were reconstructed as 5 mm contiguous axial slices. The advised injection protocol was a 40 mL contrast bolus injected at a rate of 6 mL/s followed by a saline flush of 40 mL injected at a rate of 6 mL/s.

For the CTA, a 50–70 mL contrast bolus was injected at a rate of 6 mL/s followed by a saline flush of 40 mL injected at a rate of 6 mL/s. Centers could adhere to their own scanning protocol (such as setting the kVp and the mAs). The CTA scan delay after contrast injection was determined on a per patient basis either from the time to peak arterial enhancement on CTP or by a trigger based on a threshold for the attenuation measured in the aortic arch during contrast enhancement.

The multicenter DUST data were processed centrally in the University Medical Center Utrecht. The CTA scans were examined with commercially available software on an Extended Brilliance Workstation (IntelliSpace Portal 4.5, Philips Healthcare). All further data processing and analysis were carried out with MATLAB (MATLAB, R2019b: The Mathworks Inc.).

Vessel occlusion location	Vasculature (CTA)	Downstream region (CTP)
ICA	Up to the bifurcation of the internal carotid artery.	The collection of neuroanatomical regions from the M1p downstream region and either the ACA downstream region or the PC downstream region.
M1p (proximal M1)	From the bifurcation of the internal carotid artery up to the end of the lateral lenticulostriate arteries.	The collection of neuroanatomical regions from the M1d downstream region together with the neuroanatomical regions that are supplied by the anterior choroidal artery (entorhinal region, parahippocampus, hippocampus, and amygdala) and the neuroanatomical regions that are supplied by the lateral lenticulostriate arteries (caudate, pallidum, putamen, anterior limb of internal capsule, retrolenticular part of internal capsule, posterior limb of external capsule, and external capsule).
M1d (distal M1)	From the end of the lateral lenticulostriate arteries to the bifurcation of the middle cerebral artery.	The collection of neuroanatomical regions from the M2 downstream regions (anterior and posterior).
M2 (anterior)	From the bifurcation of the middle cerebral artery to where arteries exit the Sylvian fissure. (The annotations from CTA did not specify between different M2 branches.)	Rostral middle frontal region, caudal middle frontal region, pars orbitalis of inferior frontal region, pars opercularis of inferior frontal region, pars triangularis of inferior frontal region, precentral region, insular region, frontal white matter, anterior corona radiata, superior corona radiata, superior fronto-occipital fasciculus, and uncinate fasciculus.
M2 (posterior)	From the bifurcation of the middle cerebral artery to where arteries exit the Sylvian fissure. (The annotations from CTA did not specify between different M2 branches.)	Postcentral region, supramarginal region, superior parietal region, inferior parietal region, superior temporal region, transverse temporal region, middle temporal region, inferior temporal region, parietal white matter, temporal white matter, posterior corona radiata, and superior longitudinal fasciculus.
M3	Distal to where arteries exit the Sylvian fissure. (The annotations from CTA did not specify between different M3 branches.)	The individual neuroanatomical regions from the M1d downstream region.
ACA	The anterior cerebral artery.	Superior frontal region, lateral division of orbitofrontal region, medial division of orbitofrontal region, paracentral region, anterior cingulate region, posterior cingulate region, isthmus cingulate, accumbens area, and corpus callosum.
PC	The arteries of the posterior circulation i.e. the vertebral arteries, the basilar artery, and the posterior cerebral artery.	Mesencephalon, pons, medulla oblongate, vermis, precuneal region, cuneal region, pericalcarine region, lingual region, lateral occipital region, fusiform region, thalamus, cerebellum, occipital white matter, and corticospinal tract.

Table 1

The definitions of the vessel occlusion locations and their downstream regions. The regions from a neuroanatomical CT-MRI brain atlas specific to the stroke population were grouped to constitute downstream regions that correspond to vessel occlusion locations [12]. We adhere to the nomenclature of the atlas to indicate the neuroanatomical regions.

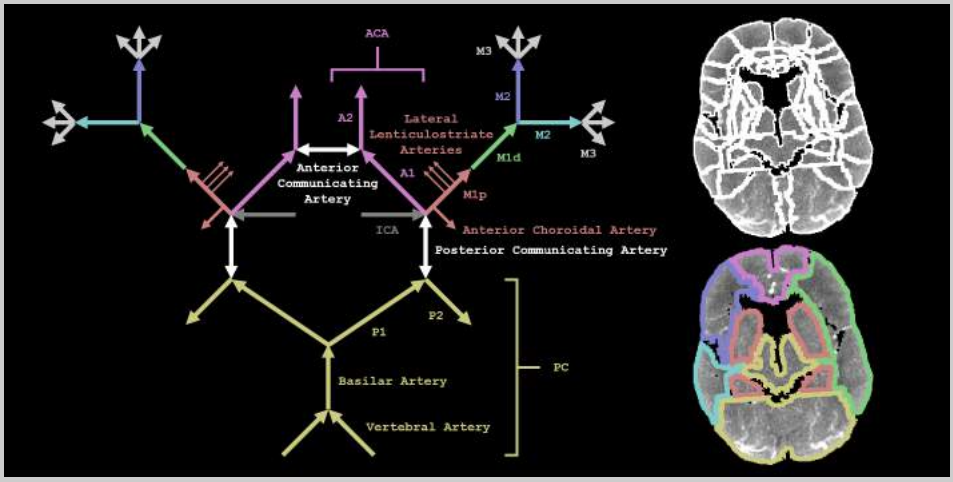

Figure 1

A visual representation of our methods. On the left is a schematic depiction of the arterial blood supply of the brain. The annotations from CTA did not specify between different M2 (or M3) branches. On the top right, we show the regions from a neuroanatomical CT-MRI brain atlas specific to the stroke population (registered to the CT perfusion scan of a patient) [12]. On the bottom right, the neuroanatomical regions (shown on the top right) are grouped to constitute downstream regions that correspond to the vessel occlusion locations (shown on the left). We show the M1d downstream region in the left hemisphere and the two M2 downstream regions in the right hemisphere.

Annotating vessel occlusion locations with CTA

The vessel occlusion locations on CTA were defined as shown in Table 1 (also see Figure 1) and were termed ICA, M1p, M1d, M2 (anterior and posterior), M3, ACA, and PC. An expert reader (from a pool of three readers with at least five years of experience in neurovascular imaging) annotated the CTA images with the most proximal vessel occlusion location by reviewing thin slice CTA data with adjustable maximum intensity projection and multiplanar reformatting. The reader was blind to all clinical information other than the side of the symptoms. In Table 1, we differentiated between anterior M2 and posterior M2 occlusions because these have different downstream regions, but both were annotated as M2 on the CTA images.

Defining downstream regions for vessel occlusion locations

We adopted a neuroanatomical CT-MRI brain atlas specific to the stroke population from Kaffenberger et al. to define the downstream regions corresponding to the vessel occlusion locations [12]. The neuroanatomical regions in the atlas were grouped to constitute these downstream regions in each hemisphere separately as shown in Table 1 (see Figure 1).

Determining hypoperfused regions with CTP

The CTP scans were first corrected for motion by a three-dimensional rigid registration on the skull with Elastix [13]. Subsequently, the registered CTP scans were smoothed using a bilateral filter with a kernel of size 3 mm x 3 mm x 3 mm x 20 HU. The arterial input function was determined automatically as described elsewhere [14]. An in-house developed model-based non-linear regression method generated the perfusion maps of the cerebral blood flow, the cerebral blood volume, the mean transit time, and the time to peak [15]. From these perfusion maps, a logistic model (that is described elsewhere) determined the hypoperfused region (i.e. the infarct core and the penumbra taken together) [16].

Indicating vessel occlusion locations with CTP

For each patient, we aligned the atlas with the downstream regions to the CTP scan by an affine transformation using Elastix. For each downstream region, we calculated the intersection-over-union with the hypoperfused region, i.e. the volume of the region that is both the downstream region and the hypoperfused region (the intersection) divided by the volume of the region that is either the downstream region or the hypoperfused region or both (the union). The downstream region with the highest intersection-over-union with the hypoperfused region was considered to indicate the vessel occlusion location. We restricted the calculation of the intersection-over-union to slices with a perfusion deficit, and we used the Zadeh operators to determine the intersection and the union [17].

Assessing classification with performance metrics

We compared the indicated vessel occlusion locations from CTP and the annotated vessel occlusion locations from CTA with a confusion matrix (also known as an error matrix), considering the annotations from CTA as the reference class and the indications from CTP as the predicted class. To elicit some properties of our atlas-based model, we also looked at two (separate) variations of this confusion matrix. The first variation was to consider both the best and second-best downstream regions in order to examine the extent of wrong indications. For example, if the annotation was M1p, the best indication was M1d, and the second-best indication was M1p, then we would count the classification as correct. The second variation was a dichotomization of vessel occlusion locations into anterior large vessel occlusions and other vessel occlusions because CTP has been shown to improve the detection of CTA of vessel occlusions that are not anterior large vessel occlusions [9, 10]. Anterior large vessel occlusions were defined as ICA, M1p, M1d, and the first segment of the ACA (A1). We visualized the confusion matrices with stacked bar graphs.

We derived several performance metrics from the confusion matrices. The accuracy is the number of matching annotations and indications divided by the number of patients. For each vessel occlusion location, we determined the precision and the recall. Given an indication, the precision is the probability that it matches the annotation. Given an annotation, the recall is the probability that it matches the indication.

To indicate the agreement between annotations and indications, we computed Cohen's kappa coefficient (with its 95% confidence interval). Cohen's kappa coefficient is a statistic that measures the overall agreement between two different categorizations of the same data. Mathematically, Cohen's kappa is defined as one minus the quotient of the relative observed disagreement and the hypothetical probability of chance disagreement. We evaluated Cohen's kappa coefficient qualitatively according to the levels of agreement: poor (<0.00), slight (0.00–0.20), fair (0.21–0.40), moderate (0.41–0.60), substantial (0.61–0.80), and almost perfect (0.81–1.00) [18].

Results

A total of 620 patients was included. The included patients had a mean age of 67 years (SD: 15 years), a median NIHSS quintile of 4 (Q1-Q3: 3-5), a mean time from onset to imaging of 148 minutes (SD: 121 minutes), a median 3-month follow-up mRS of 3 (Q1-Q3: 1-4), and 57% were male (N: 353).

Table 2

The confusion matrix for the annotated vessel occlusion locations from CT angiography (CTA) and the indicated vessel occlusion locations from CT perfusion (CTP). We considered the annotations from CTA as the reference class and the indications from CTP as the predicted class. The percentages in square brackets are over the columns. The overall accuracy was 48% (299/620).

	ICA (CTA)	M1p (CTA)	M1d (CTA)	M2 (CTA)	M3 (CTA)	ACA (CTA)	PC (CTA)
ICA (CTP)	14 [13%]	14 [19%]	7 [5%]	5 [3%]	1 [3%]	1 [7%]	1 [1%]
M1p (CTP)	25 [24%]	38 [52%]	22 [16%]	5 [3%]	1 [3%]	0 [0%]	2 [2%]
M1d (CTP)	23 [22%]	13 [18%]	82 [60%]	32 [20%]	0 [0%]	0 [0%]	0 [0%]
M2 (CTP)	22 [21%]	4 [5%]	16 [12%]	76 [47%]	13 [36%]	3 [21%]	0 [0%]
M3 (CTP)	9 [9%]	1 [1%]	4 [3%]	31 [19%]	16 [44%]	2 [14%]	8 [9%]
ACA (CTP)	1 [1%]	0 [0%]	1 [1%]	1 [1%]	1 [3%]	6 [43%]	5 [5%]
PC (CTP)	7 [7%]	1 [1%]	4 [3%]	9 [6%]	1 [3%]	2 [14%]	67 [72%]
None (CTP)	4 [4%]	2 [3%]	0 [0%]	4 [2%]	3 [8%]	0 [0%]	10 [11%]

Table 2 shows the confusion matrix for the annotations and indications. The annotations and indications matched for 48% (299/620) of the included patients. Based on chance alone, the classification of seven categories would result in an accuracy of 14% (=1/7). For 23 patients (4%), there was no hypoperfused region.

Table 3 presents the accuracy, Cohen's kappa, precision, and recall for each vessel occlusion location. The mean accuracy for these location-specific performance assessments was 86%, the mean precision was 46%, and the mean recall was 47%. Overall, Cohen's kappa coefficient [95% confidence interval] was 0.39 [0.35, 0.44], which indicates fair agreement. Figures 2-5 show examples of the downstream regions and the hypoperfused region for different annotations and indications.

Table 3

The accuracy, Cohen's kappa, precision, and recall for each vessel occlusion location. We considered the annotated vessel occlusion locations from CT angiography as the reference class and the indicated vessel occlusion locations from CT perfusion as the predicted class. The mean accuracy was 86%, the mean precision was 46%, and the mean recall was 47%.

	ICA	M1p	M1d	M2	M3	ACA	PC
Accuracy	81%	85%	80%	77%	88%	97%	92%
Kappa	0.10	0.38	0.45	0.36	0.24	0.40	0.68
Precision	33%	41%	55%	57%	23%	40%	74%
Recall	13%	52%	60%	47%	44%	43%	72%

Table 4 shows the confusion matrix for considering both the best and second-best downstream regions. The precision and the recall for the vessel occlusion locations can be found in the Supplementary Material. This allowance yielded 410/620 correct matches, a mean accuracy of 91%, a mean precision of 64%, a mean recall of 64%, and an overall Cohen's kappa coefficient [95% confidence interval] of 0.62 [0.57, 0.67], which indicates substantial agreement.

Table 5 shows the confusion matrix for the dichotomization of vessel occlusion locations into anterior large vessel occlusions and other vessel occlusions. The precision and the recall for the vessel occlusion locations can be found in the Supplementary Material. This dichotomization yielded an accuracy of 80% (479/597), a mean precision of 80%, a mean recall of 80%, and a Cohen's kappa coefficient [95% confidence interval] of 0.61 [0.54, 0.67], which indicates substantial agreement.

Figure 6 shows the stacked bar graphs corresponding to the confusion matrices of Table 2, Table 4, and Table 5.

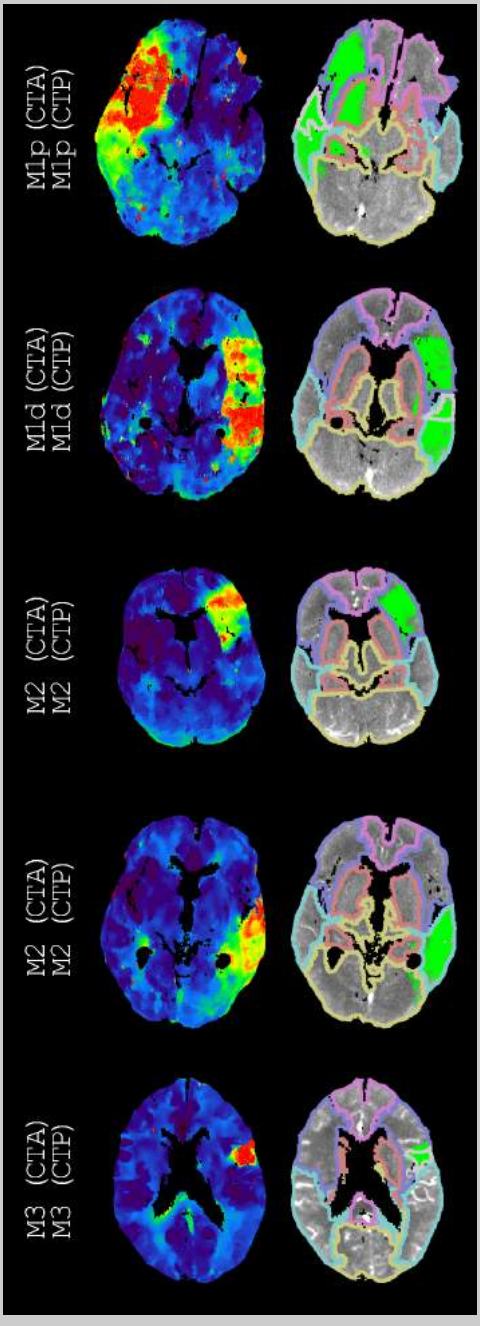

Figure 2

Examples of annotations (CTA) and indications (CTP) that match for different segments of the middle cerebral artery. On the left, time-to-peak perfusion maps are shown. On the right, the hypoperfused regions and the downstream regions (according to Figure 1) are shown. For each example, we only regarded the M3 downstream region with the highest intersection-over-union. If displayed, these M3 downstream regions are the superior temporal region, the superior temporal region, and the precentral region (from top to bottom).

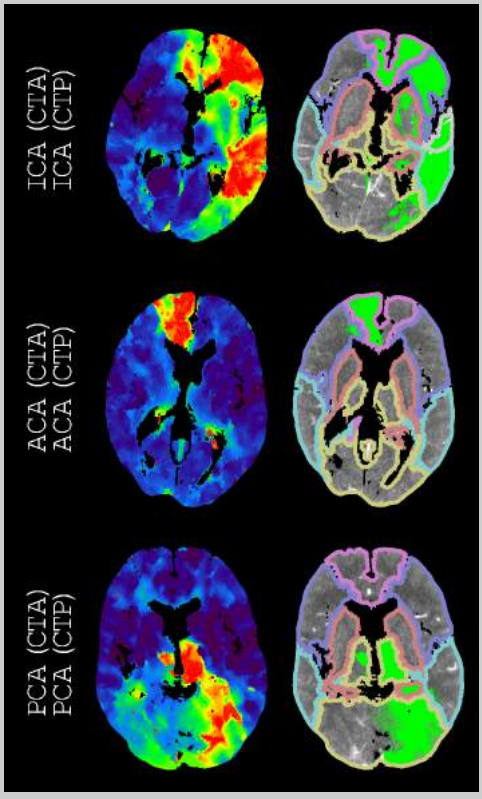

Figure 3

Examples of annotations (CTA) and indications (CTP) that match for arteries other than the middle cerebral artery. On the left, time-to-peak perfusion maps are shown. On the right, the hypoperfused regions and the downstream regions (according to Figure 1) are shown. For each example, we only regarded the M3 downstream region with the highest intersection-over-union. The only displayed M3 downstream region is the superior temporal region.

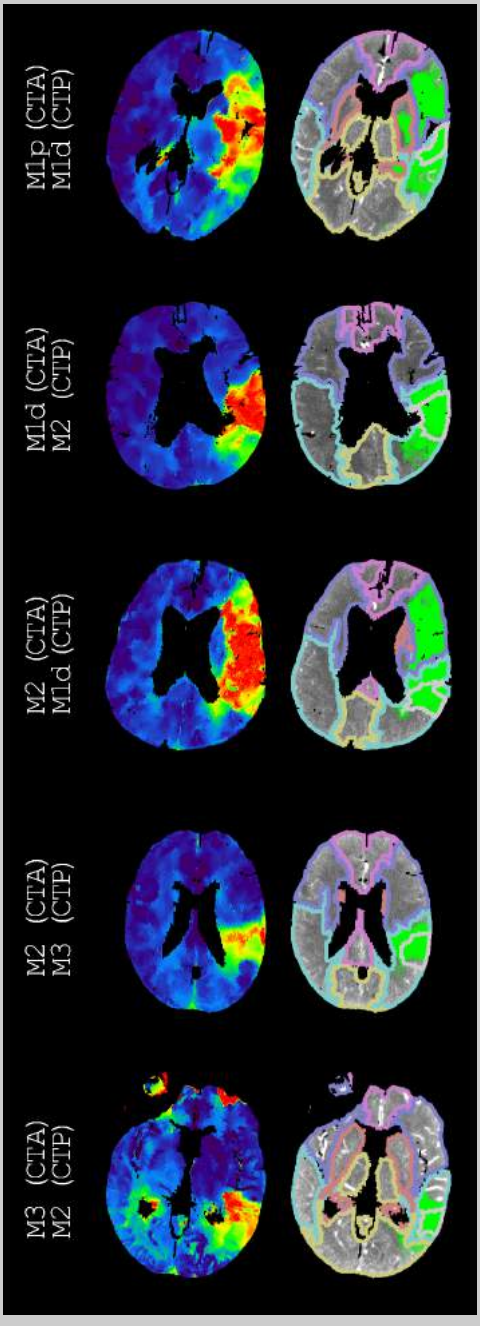

Figure 4

Examples of annotations (CTA) and indications (CTP) that do not match for different segments of the middle cerebral artery. On the left, time-to-peak perfusion maps are shown. On the right, the hypoperfused regions and the downstream regions (according to Figure 1) are shown. For each example, we only regarded the M3 downstream region with the highest intersection-over-union. These M3 downstream regions are the superior temporal region, the supramarginal region, the supramarginal region, the supramarginal region, and the middle temporal region (from top to bottom). The second-best indications were M1p, M1d, M1p, M2, and M1d (from top to bottom).

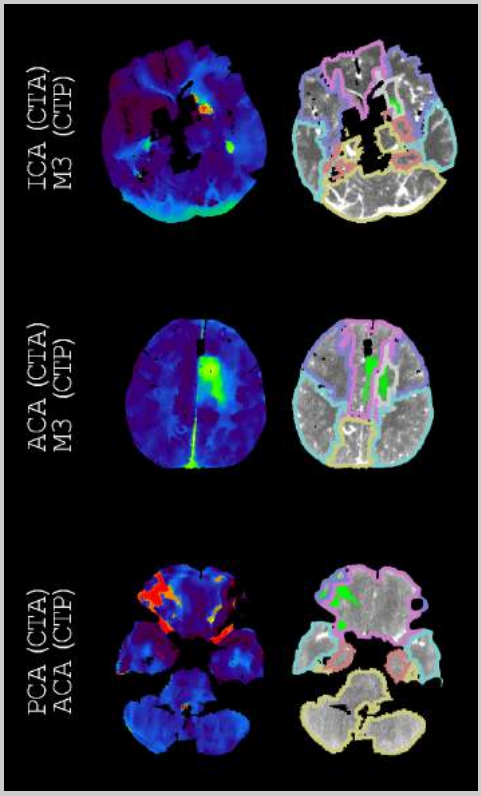

Figure 5

Examples of annotations (CTA) and indications (CTP) that do not match for arteries other than the middle cerebral artery. On the left, time-to-peak perfusion maps are shown. On the right, the hypoperfused regions and the downstream regions (according to Figure 1) are shown. For each example, we only regarded the M3 downstream region with the highest intersection-over-union. If displayed, these M3 downstream regions are the frontal white matter and the frontal white matter (from top to bottom). The second-best indications were M2, ACA, and M2 (from top to bottom).

Table 4

The confusion matrix for the annotated vessel occlusion locations from CT angiography (CTA) and the indicated vessel occlusion locations from CT perfusion (CTP) if we allow the second-best indication to also count as correct. We considered the annotations from CTA as the reference class and the indications from CTP as the predicted class. The percentages in square brackets are over the columns. The overall accuracy was 66% (410/620).

	ICA (CTA)	M1p (CTA)	M1d (CTA)	M2 (CTA)	M3 (CTA)	ACA (CTA)	PC (CTA)
ICA (CTP)	25 [24%]	3 [4%]	7 [5%]	4 [2%]	1 [3%]	1 [7%]	0 [0%]
M1p (CTP)	21 [20%]	61 [84%]	3 [2%]	5 [3%]	1 [3%]	0 [0%]	2 [2%]
M1d (CTP)	23 [22%]	3 [4%]	114 [84%]	27 [17%]	0 [0%]	0 [0%]	0 [0%]
M2 (CTP)	22 [21%]	2 [3%]	3 [2%]	110 [67%]	5 [14%]	3 [21%]	0 [0%]
M3 (CTP)	8 [8%]	1 [1%]	4 [3%]	3 [2%]	24 [67%]	1 [7%]	7 [8%]
ACA (CTP)	0 [0%]	0 [0%]	1 [1%]	1 [1%]	1 [3%]	7 [50%]	5 [5%]
PC (CTP)	2 [2%]	1 [1%]	4 [3%]	9 [6%]	1 [3%]	2 [14%]	69 [74%]
None (CTP)	4 [4%]	2 [3%]	0 [0%]	4 [2%]	3 [8%]	0 [0%]	10 [11%]

Table 5

The confusion matrix for the annotated vessel occlusion locations from CT angiography (CTA) and the indicated vessel occlusion locations from CT perfusion (CTP) if we dichotomize the vessel occlusion locations into anterior large vessel occlusions and other vessel occlusions. We considered the annotations from CTA as the reference class and the indications from CTP as the predicted class. The percentages in square brackets are over the columns. The overall accuracy was 80% (479/597).

	Anterior large vessel occlusion (CTA)	Other vessel occlusion (CTA)
Anterior large vessel occlusion (CTP)	238 [77%]	48 [17%]
Other vessel occlusion (CTP)	70 [23%]	241 [83%]

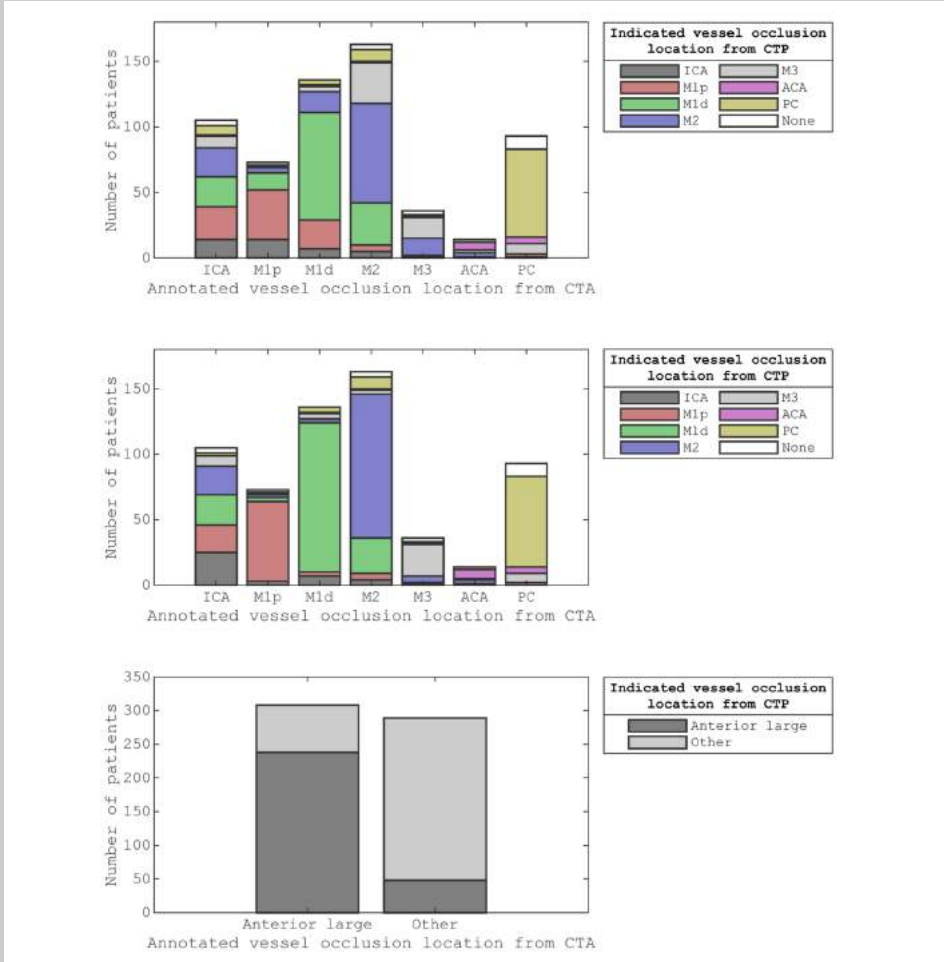

Figure 6

The stacked bar graphs for the confusion matrices from Table 2 (top), Table 4 (middle), and Table 5 (bottom). We considered the annotated vessel occlusion locations from CT angiography as the reference class and the indicated vessel occlusion locations from CT perfusion as the predicted class. For the middle stacked bar graph, we allowed the second best indication to also count as correct. For the bottom stacked bar graph, we dichotomized the vessel occlusion locations into anterior large vessel occlusions and other vessel occlusions.

Discussion

We presented an atlas-based method in which CTP data were used to automatically indicate the vessel occlusion location in acute ischemic stroke patients. We evaluated the performance of these indications by comparing them with the vessel occlusion locations acquired from expert visual assessments of CTA. The inter-rater agreement between the annotations from CTA and the indications from CTP was fair to substantial.

We focused on locating vessel occlusions instead of detecting vessel occlusions. Studies that automatically detected vessel occlusions on CTA did not evaluate their performance in locating vessel occlusions [19–24]. Instead, these studies were designed to distinguish a group of patients with a large vessel occlusion from a group of patients without a detectable vessel occlusion. Similarly, experienced readers of CTP images could distinguish a group of patients with distal vessel occlusion from a group of patients without detectable vessel occlusion [5]. Although these readers did not report the vessel occlusion location, their sensitivity for detecting vessel occlusions with CTP imaging agrees with the percentage of patients that did not show hypoperfusion in our study. Furthermore, expert readers of multiphase CTA images could distinguish a group of patients with a medium vessel occlusion from a group of patients without a detectable vessel occlusion, with a large vessel occlusion, or with the occlusion of the vertebrobasilar circulation [25]. This last study reported that 70% (81/116) of vessel occlusions were located correctly, whereas we indicated 48% (299/620) of vessel occlusion locations correctly.

Our atlas-based method varied in performance by the vessel occlusion location (Table 3). In particular, ICA annotations had the lowest recall (14%) and ICA indications had the second lowest precision (33%). This relative underperformance may be explained by the larger potential for blood supply via conduit collaterals for ICA annotated occlusions than for other vessel occlusions. Conduit collaterals such as the circle of Willis can redirect blood flow based on the patient-specific angioarchitecture, resulting in hypoperfused regions that may be highly variable between patients (compare Figure 3 and Figure 5) [26–28].

Considering both the best and second-best downstream region improved our overall performance. Although the performance for occlusions of the different segments of the middle cerebral artery improved, the performance stayed roughly equal for middle cerebral artery occlusions as a whole as well as for ICA occlusions, ACA occlusions, and PC occlusions (Figure 6). This partial improvement may be due to the variation in vessel architecture of the middle cerebral artery, resulting in a considerable number of consequential boundary

cases [3]. For the different segments of the middle cerebral artery, only M2 annotations with an M1d indication were not resolved by considering both the best and second-best downstream region. For these M2 annotations, the second-best downstream region often was M1p because of the relatively small difference between the M1p downstream region and the M1d downstream region (Figure 4). Thus, the performance of our atlas-based method likely suffered from variation in vessel architecture, emphasizing the need for an approach that incorporates patient-specific vessel data to locate vessel occlusions.

Our atlas-based method was limited by its design. It was unfeasible to differentiate between all possible vessel occlusion locations. To illustrate, consider an occlusion of the recurrent artery of Heubner, which is the largest perforating branch from the proximal anterior cerebral artery. Occlusion of this artery may result in a perfusion deficit that is restricted to the basal ganglia. Although this perfusion deficit is distinctly different from an M1p occlusion, our atlas-based method would indicate M1p. For the sake of clarity, we decided to have no overlapping downstream regions for arteries that are not in ordinal relation.

Several shortcomings should be noted. Although the defined downstream regions appear reasonable (Figure 2 and Figure 4), the performance of our atlas-based method seemed to suffer from physiological variation, for example, in collateral circulation or in M2 angioarchitecture. Furthermore, in contrast with the middle cerebral artery, we did not consider occlusions of different vessels in the posterior circulation because of a limited number of patients with occlusions in the posterior circulation. Moreover, there might be a number of patients with a missed vessel occlusion on the CTA images, especially for the smaller vessel occlusions. Unfortunately, the majority of the patients included in the DUST study did not have digital subtraction angiography (DSA) imaging, so we could not compare CTA and DSA imaging for this group. Finally, technical limitations (e.g. artifacts, the registration, or the perfusion analysis) may have resulted in an inaccurate hypoperfused region, an inaccurate downstream region, an inaccurate alignment of the hypoperfused region and the downstream region, or an unfortunate scoring by the intersection-over-union (Figure 3 and Figure 5).

Conclusion

Spatial CTP data can help to automatically locate vessel occlusions for acute ischemic stroke patients. However, variations in vessel architecture between patients seemed to limit the capacity of CTP data to distinguish between vessel occlusion locations more accurately. Nevertheless, the spatial layout of the hypoperfused region might be employed in combination with patient-specific vessel data to locate vessel occlusions more effectively.

References

1 Wannamaker R, Buck B, Butcher K (2019) Multimodal CT in Acute Stroke. Current Neurology and Neuroscience Reports 19:. https://doi.org/10.1007/s11910-019-0978-z

2 Campbell BCV, Donnan GA, Lees KR, et al (2015) Endovascular stent thrombectomy: The new standard of care for large vessel ischaemic stroke. The Lancet Neurology 14:846–854. https://doi.org/10.1016/S1474-4422(15)00140-4

3 Saver JL, Chapot R, Agid R, et al (2020) Thrombectomy for Distal, Medium Vessel Occlusions: A Consensus Statement on Present Knowledge and Promising Directions. Stroke 2872–2884. https://doi.org/10.1161/STROKEAHA.120.028956

4 Byrne D, Sugrue G, Stanley E, et al (2017) Improved detection of anterior circulation occlusions: The delayed vessel sign on multiphase CT angiography. American Journal of Neuroradiology 38:1911–1916. https://doi.org/10.3174/ajnr.A5317

5 Amukotuwa SA, Wu A, Zhou K, et al (2021) Distal Medium Vessel Occlusions Can Be Accurately and Rapidly Detected Using Tmax Maps. Stroke 3308–3317. https://doi.org/10.1161/STROKEAHA.120.032941

6 Volny O, Cimflova P, Kadlecova P, et al (2017) Single-Phase Versus Multiphase CT Angiography in Middle Cerebral Artery Clot Detection—Benefits for Less Experienced Radiologists and Neurologists. Journal of Stroke and Cerebrovascular Diseases 26:19–24. https://doi.org/10.1016/j.jstrokecerebrovasdis.2016.08.023

7 Fasen BACM, Heijboer RJJ, Hulsmans FJH, Kwee RM (2020) CT Angiography in evaluating large-vessel occlusion in acute anterior circulation ischemic stroke: Factors associated with diagnostic error in clinical practice. American Journal of Neuroradiology 41:607–611. https://doi.org/10.3174/AJNR.A6469

8 Duvekot MHC, van Es ACGM, Venema E, et al (2021) Accuracy of CTA evaluations in daily clinical practice for large and medium vessel occlusion detection in suspected stroke patients. European Stroke Journal 6:357–366. https://doi.org/10.1177/23969873211058576

9 Becks MJ, Manniesing R, Vister J, et al (2019) Brain CT perfusion improves intracranial vessel occlusion detection on CT angiography. Journal of Neuroradiology 46:124–129. https://doi.org/10.1016/j.neurad.2018.03.003

10 Bathla G, Pillenahalli Maheshwarappa R, Soni N, et al (2022) Do CT Perfusion Maps Increase Accuracy for Detection of M2-MCA Occlusions in Acute Ischemic Stroke? Journal of Stroke and Cerebrovascular Diseases 31:106473. https://doi.org/10.1016/j.jstrokecerebrovasdis.2022.106473

11 van Seeters T, Biessels GJ, van der Schaaf IC, et al (2014) Prediction of outcome in patients with suspected acute ischaemic stroke with CT perfusion and CT angiography: the Dutch acute stroke trial (DUST) study protocol. BMC Neurol 14:37. https://doi.org/10.1186/1471-2377-14-37

12 Kaffenberger T, Venkatraman V, Steward C, et al (2022) Stroke population–specific neuroanatomical CT-MRI brain atlas. Neuroradiology. https://doi.org/10.1007/s00234-021-02875-9

13 Klein S, Staring M, Murphy K, et al (2010) elastix: A Toolbox for Intensity-Based Medical Image Registration. IEEE Trans Med Imaging 29:196–205. https://doi.org/10.1109/TMI.2009.2035616

14 Peerlings D, Bennink E, Dankbaar JW, et al (2021) Variation in arterial input function in a large multicenter computed tomography perfusion study. Eur Radiol 31:8317–8325. https://doi.org/10.1007/s00330-021-08067-6

15 Bennink E, Oosterbroek J, Kudo K, et al (2016) Fast nonlinear regression method for CT brain perfusion analysis. Journal of Medical Imaging 3:026003. https://doi.org/10.1117/1.jmi.3.2.026003

16 Peerlings D, van Ommen F, Bennink E, et al (2022) Probability maps classify ischemic stroke regions more accurately than CT perfusion summary maps. Eur Radiol 32:6367-6375. https://doi.org/10.1007/s00330-022-08700-y

17 Zadeh LA (1978) Fuzzy sets as a basis for a theory of possibility. Fuzzy Sets and Systems 1:3–28

18 Landis JR, Koch GG (1977) The Measurement of Observer Agreement for Categorical Data. Biometrics 33:159. https://doi.org/10.2307/2529310

19 Seker F, Pfaff JAR, Mokli Y, et al (2022) Diagnostic accuracy of automated occlusion detection in CT angiography using e-CTA. International Journal of Stroke 17:77–82. https://doi.org/10.1177/1747493021992592

20 Amukotuwa SA, Straka M, Smith H, et al (2019) Automated detection of intracranial large vessel occlusions on computed tomography angiography a single center experience. Stroke 50:2790–2798. https://doi.org/10.1161/STROKEAHA.119.026259

21 Czap AL, Bahr-Hosseini M, Singh N, et al (2021) Machine Learning Automated Detection of Large Vessel Occlusion From Mobile Stroke Unit Computed Tomography Angiography. Stroke 1–6. https://doi.org/10.1161/strokeaha.121.036091

22 Dehkharghani S, Lansberg M, Venkatsubramanian C, et al (2021) High-performance automated anterior circulation CT angiographic clot detection in acute stroke: A multireader comparison. Radiology 298:665–670. https://doi.org/10.1148/radiol.2021202734

23 Dovrat AY, Saban M, Merhav G, et al (2021) Evaluation of artificial intelligence-powered identification of large-vessel occlusions in a comprehensive stroke center. American Journal of Neuroradiology 42:247–254. https://doi.org/10.3174/ajnr.A6923

24 Luijten SPR, Wolff L, Duvekot MHC, et al (2021) Diagnostic performance of an algorithm for automated large vessel occlusion detection on CT angiography. Journal of NeuroInterventional Surgery neurintsurg-2021-017842. https://doi.org/10.1136/neurintsurg-2021-017842

25 McDonough R V., Qiu W, Ospel JM, et al (2021) Multiphase CTA-derived tissue maps aid in detection of medium vessel occlusions. Neuroradiology 887–896. https://doi.org/10.1007/s00234-021-02830-8

26 Van der Grond J (2001) Collateral Ability of the Circle of Willis in Patients With. Stroke 2768–2773

27 Romero JR, Pikula A, Nguyen TN, et al (2010) Cerebral Collateral Circulation in Carotid Artery Disease. Current Cardiology Reviews 5:279–288. https://doi.org/10.2174/157340309789317887

28 Zarrinkoob L, Wåhlin A, Ambarki K, et al (2019) Blood Flow Lateralization and Collateral Compensatory Mechanisms in Patients With Carotid Artery Stenosis. Stroke 50:1081–1088. https://doi.org/10.1161/STROKEAHA.119.024757

Supplementary Table 1

The precision and the recall for each vessel occlusion location if we allow the second-best indication to also count as correct. We considered the annotated vessel occlusion locations from CT angiography as the reference class and the indicated vessel occlusion locations from CT perfusion as the predicted class. The mean accuracy was 91%, the mean precision was 64%, and the mean recall was 64%.

	ICA	M1p	M1d	M2	M3	ACA	PC
Accuracy	85%	93%	88%	86%	94%	98%	93%
Kappa	0.27	0.69	0.67	0.62	0.54	0.47	0.72
Precision	61%	66%	68%	76%	50%	47%	78%
Recall	24%	84%	84%	67%	67%	50%	74%

Supplementary Table 2

The precision and the recall for each vessel occlusion location if we dichotomize the vessel occlusion locations into anterior large vessel occlusions and other vessel occlusions. We considered the annotated vessel occlusion locations from CT angiography as the reference class and the indicated vessel occlusion locations from CT perfusion as the predicted class. The mean precision was 80% and the mean recall was 80%.

	Anterior large vessel occlusion	Other vessel occlusion
Precision	83%	77%
Recall	77%	83%

Chapter 8

General discussion

With a summary of the previous chapters, a general discussion, future perspectives, and a conclusion.

This thesis considered technical CTP imaging protocols in ischemic stroke. The lack of consensus on the CTP imaging acquisition and processing protocol has hindered the widespread adoption of image-based criteria for stroke diagnosis and treatment planning. Accordingly, the CLEOPATRA healthcare evaluation was launched to investigate the cost-effectiveness of selecting ischemic stroke patients for thrombectomy with CTP imaging. We focused on harmonizing and optimizing the CTP imaging acquisition and processing protocol.

Summary

Chapter 2 considered the injection protocol. We took the arterial input function as a direct measure to characterize the injection protocol. The arterial input function varied between centers participating in a multicenter study. Using an anthropomorphic digital CTP phantom, we argued that these differences may impact clinical decision making in stroke diagnosis.

Chapter 3 considered the scan and processing protocol. We requested the scan and processing protocols from the stroke centers participating in the CLEOPATRA healthcare evaluation and compared these protocols using an anthropomorphic digital CTP phantom. We found that the estimated ischemia varied greatly between centers. The primary source of this variation was the perfusion software rather than the scan protocol. The biases in CTP imaging results had a clear relation to the vendor software. Standardizing the estimation of ischemic regions, as described in chapter 5, harmonized CTP imaging results to a degree.

Chapter 4 described our efforts to construct an anthropomorphic physical CTP phantom. Such a phantom could contribute to CTP image quality control and harmonization. The physical phantom was based on the digital phantom used in chapters 2 and 3. By scanning contrast agent printed sheets, we produced CTP imaging results that were visually similar to those of the digital phantom. However, the physical phantom required separate processing before the actual processing protocol and showed suboptimal contrast enhancement in the brain tissue. Nonetheless, we demonstrated the feasibility of mimicking anthropomorphic brain tissue perfusion with a physical phantom. An anthropomorphic physical CTP image quality phantom could help to harmonize and optimize the CTP imaging acquisition and processing protocol.

Chapter 5 introduced a method to standardize the estimation of ischemic regions. Instead of thresholding a selected perfusion map, which results in segregated ischemic regions, we combined perfusion maps into probability maps, which show the likelihood for ischemia. In chapters 3, 5, and 6 together, we showed that this standardized method could harmonize and optimize CTP imaging results to a degree.

Chapter 6 compared the segmentations from four methods to estimate ischemic regions: we considered the segmentations from acute MR diffusion imaging as the ground truth and segmented the perfusion maps from CTP imaging by the clinical vendor default, by hand, and by the standardized method described in chapter 5. The clinical vendor default segmentations underperformed compared to both the manual segmentations and the segmentations from the standardized method. Additionally, the manual segmentations and the segmentations from the standardized method agreed well with each other. Although the segmentations from the four methods differed, CTP imaging still resembled MR diffusion imaging in the acute phase of ischemic stroke overall.

Chapter 7 provided insights into a novel application of CTP imaging results to locate the vessel occlusion. Recent advancements in stent retriever technology could widen the eligibility criteria for thrombectomy by considering occlusions in smaller and more distal vessels. These occlusions are increasingly difficult to locate with CTA imaging. We showed that the spatial layout of the total ischemic region, determined from CTP imaging, can help to locate the vessel occlusion.

Discussion

This thesis concerns the harmonization and optimization of CTP imaging. To simplify, CTP imaging involves three critical stages: acquiring the CTP imaging source data, processing this data into perfusion maps, and translating these maps into clinically relevant information. The existent scientific literature highlights the variability of CTP imaging, leading us to investigate and discuss which of those three stages contributes to this variability.

In chapters 2 and 3, we looked at the acquisition protocols. Despite a wide variation between these protocols in clinical practice, the impact of this variation was small [1]. Therefore, only minimal requirements need to be set to further improve the uniformity of acquisition protocols. Regarding this, we suggest that the interval between CTP frames is at most two seconds around maximal contrast enhancement to ensure that no critical information about the contrast enhancement is missed. We also suggest having at least two frames, or a single frame at double the radiation dose, before the first contrast enhancement to establish a proper baseline needed for an accurate perfusion analysis. Tube settings should be 80 kVp at most and 100 mAs at least. Most of the centers participating in the CLEOPATRA healthcare evaluation already met these criteria. For the injection protocol, it is important to inject enough iodine [2]. New guidelines, which specify that 15 g iodine is injected at 1.8 g iodine per second, have been issued already to centers in the CONTRAST consortium [3–5].

In chapters 3, 5, and 6, we looked at the perfusion maps from different clinical vendor software and examined the estimation of ischemic regions from these perfusion maps. Our findings indicate that this estimation of ischemic regions causes most of the variation in the clinically relevant information derived from CTP imaging [1]. It is interesting to discuss why such variation exists when clinical experts seem to assess the perfusion maps as useful and reliable, and agree on the ischemic information contained within these maps. We argue that these inconsistencies arise from an incorrect interpretation of the perfusion maps by the perfusion software and we identify two key reasons for the suboptimal estimation of ischemic regions.

First, simply thresholding the perfusion maps to estimate the infarct core and penumbra does not work satisfactorily [1, 6–8]. The quantitative differences in the perfusion parameters between different software have led to the use of various threshold values to different perfusion maps, which is very impractical. Additionally, because the perfusion parameters vary naturally throughout the brain, thresholding inevitably leads to false positive and false negative estimations. Each software seems to mitigate these false estimations differently, for example by additional filtering of the source data, by calculating relative values of the perfusion parameters, or by additional processing of the summary maps. In our view, by combining all the available perfusion maps, we were able to standardize the estimation of ischemic regions and we found that false negative estimations were substantially reduced. Still, additional processing turned out to be necessary to reduce false positive estimations also. Experts can easily discard these false positive estimations based on anatomical knowledge or by comparing hemispheres to each other, but both thresholding and our standardized method make predictions for individual voxels. Not knowing whether such an individual voxel belongs to white or gray matter, for example, elevates the risk of a false prediction. Hence, to estimate ischemic regions, we should leverage all perfusion data, while also accounting for spatial information, including anatomical information.

Second, the habit of calibrating CTP imaging based on follow-up imaging appears to be unproductive [7]. Visual assessments of perfusion maps and follow-up imaging should make this clear. But in scientific literature as well, the comparison between CTP imaging and follow-up imaging has consistently yielded limited results [8–10]. In chapter 6, we took an alternative approach to calibrate CTP imaging. Our findings reveal that clinical experts can confidently delineate CTP imaging without an external ground truth reference, emphasizing the intrinsic value of CTP imaging. We should aim to automate this process, as there is no time to manually delineate CTP imaging in clinical practice.

In conclusion, to reduce inconsistencies in the clinically relevant information derived from CTP imaging, we recommend establishing a standardized framework to estimate ischemic regions. This framework should leverage all perfusion data, take into account spatial information, and rely on manual segmentations as a ground truth reference.

The CLEOPATRA healthcare evaluation was launched to investigate whether CTP imaging is cost-effective in selecting patients for thrombectomy. Recent scientific literature suggests that CTP imaging is of limited additional value to NCCT and CTA imaging in patient selection [11–13]. Despite this, we believe that CTP imaging still holds clinical value, though an interpretation other than patient selection may be required. Experts agree that perfusion maps provide a quick and informative snapshot of the patient's condition. Chapter 6 demonstrated that the perfusion maps resemble acute MR diffusion imaging, implying that CTP imaging is of diagnostic value. Additionally, chapter 7 illustrated that CTP imaging can help interpret CTA imaging, which could be important for the treatment of smaller and more distal vessel occlusions. CTA and CTP imaging can thus complement each other, and neither renders the other redundant.

In summary, CTP imaging remains an interesting modality in managing ischemic stroke patients. Harmonization of the acquisition protocol should prioritize guidelines for the timing of CTP frames. We argue against the calibration of CTP imaging to follow-up imaging and we speak out for the intrinsic value of the perfusion maps. The clinical value of CTP imaging in ischemic stroke deserves attention, but adjusting the current unrealistic expectation of patient selection based on the infarct core and penumbra may yield meaningful results.

Future perspectives

For the future, a number of improvements can be implemented to optimize CTP image quality and to advance harmonization.

Regarding the injection protocol, the easiest enhancement of CTP imaging can be achieved by increasing the concentration of the contrast agent, as this increases both the amount and the rate of the iodine [14]. While some centers have already adopted contrast concentrations beyond the typical 300 mg I/mL, other centers could follow suit in the future. Another, more advanced, optimization of the injection protocol could involve personalized contrast injection, considering that personal factors such as weight and cardiac output have been shown to affect the contrast enhancement in large arteries [14, 15].

Regarding the scan protocol, scanning at 70 kVp could reduce the radiation dose while maintaining diagnostic image quality [16, 17]. Alternatively, some centers that already scan at 70 kVp in clinical practice decided to increase the mAs to improve image quality at a maintained radiation dose. More centers might choose to scan at 70 kVp in the future.

Another interesting avenue for optimization is to work towards a single contrast-enhanced scan. Currently, the CTP and CTA scan are two separate scans, necessitating additional iodine and radiation. However, CTP and CTA imaging are converging both in acquisition and in application. For example, the CTA imaging acquisition protocol can be extended to accommodate perfusion imaging, while CTP imaging can help to detect and locate vessel occlusions [18–23]. Integrating the CTP and CTA imaging acquisition protocols offers the potential to decrease the amount of iodine and radiation for the patient and to increase image quality.

Modern techniques could advance the clinical impact of CTP imaging. Photon counting CT systems and, to a lesser extent, spectral CT imaging have a higher resolution and a higher sensitivity to contrast material [24–26]. This could ensure the detection of small lacunar infarcts that remain unnoticed on CTA imaging. Detecting these subtle infarcts holds significance for future patient treatment, as they indicate an increased risk of recurrent strokes, thereby facilitating timely preventive measures [27, 28].

Regarding the processing protocol, we pursued decentral harmonization through anthropomorphic phantoms and a method to harmonize the estimated ischemic regions between clinical vendor software. However, central harmonization may also be a viable option. The Dutch stroke technology software StrokeViewer (Nicolab, Amsterdam) offers a cloud-based stroke portfolio that is already in clinical use across various Dutch stroke centers. This portfolio covers the multiple facets of stroke diagnosis, such as detecting hemorrhage, locating the vessel occlusion, and estimating ischemic regions. For CTP imaging, such a platform presents an opportunity to implement desired improvements in the production of perfusion maps and in the estimation of ischemic regions.

Conclusion

This thesis addresses the harmonization and optimization of the CTP imaging acquisition and processing protocol. We argue that the inconsistencies in clinically relevant information from CTP imaging arise from the conversion of perfusion maps to ischemic regions. We suggest a shift in perspective, urging to assess CTP imaging on its own merits. This involves recognizing the intrinsic value of the perfusion maps and considering diverse clinical applications of CTP imaging. Only then can the full diagnostic potential of CTP imaging be unveiled.

References

1 Peerlings D, Bennink E, Dankbaar JW, et al (2023) Standardizing the estimation of ischemic regions can harmonize CT perfusion stroke imaging. Eur Radiol. https://doi.org/10.1007/s00330-023-10035-1

2 Peerlings D, Bennink E, Dankbaar JW, et al (2021) Variation in arterial input function in a large multicenter computed tomography perfusion study. Eur Radiol 31:8317–8325. https://doi.org/10.1007/s00330-021-08067-6

3 Chalos V, Van De Graaf RA, Roozenbeek B, et al (2020) Multicenter randomized clinical trial of endovascular treatment for acute ischemic stroke. The effect of periprocedural medication: Acetylsalicylic acid, unfractionated heparin, both, or neither (MR CLEAN-MED). Rationale and study design. Trials 21:1–17. https://doi.org/10.1186/s13063-020-04514-9

4 Treurniet KM, LeCouffe NE, Kappelhof M, et al (2021) MR CLEAN-NO IV: intravenous treatment followed by endovascular treatment versus direct endovascular treatment for acute ischemic stroke caused by a proximal intracranial occlusion—study protocol for a randomized clinical trial. Trials 22:1–15. https://doi.org/10.1186/s13063-021-05063-5

5 Pirson FAV (Anne), Hinsenveld WH, Goldhoorn R-JB, et al (2021) MR CLEAN Late study protocol. Trials 15:1–13

6 Flottmann F, Broocks G, Faizy TD, et al (2017) CT-perfusion stroke imaging: a threshold free probabilistic approach to predict infarct volume compared to traditional ischemic thresholds. Sci Rep 7:6679. https://doi.org/10.1038/s41598-017-06882-w

7 Goyal M, Ospel JM, Menon B, et al (2020) Challenging the Ischemic Core Concept in Acute Ischemic Stroke Imaging. Stroke 3147–3155. https://doi.org/10.1161/STROKEAHA.120.030620

8 Peerlings D, van Ommen F, Bennink E, et al (2022) Probability maps classify ischemic stroke regions more accurately than CT perfusion summary maps. Eur Radiol 32:6367–6375. https://doi.org/10.1007/s00330-022-08700-y

9 Hoving JW, Koopman MS, Tolhuisen ML, et al (2022) Accuracy of CT perfusion ischemic core volume and location estimation: A comparison between four ischemic core estimation approaches using syngo.via. PLoS One 17:. https://doi.org/10.1371/journal.pone.0272276

10 Koopman MS, Hoving JW, Tolhuisen ML, et al (2023) Accuracy of Four Different CT Perfusion Thresholds for Ischemic Core Volume and Location Estimation Using IntelliSpace Portal. J Cardiovasc Dev Dis 10:. https://doi.org/10.3390/jcdd10060239

11 Nogueira RG, Haussen DC, Liebeskind D, et al (2021) Stroke Imaging Selection Modality and Endovascular Therapy Outcomes in the Early and Extended Time Windows. Stroke 491–497. https://doi.org/10.1161/STROKEAHA.120.031685

12 Pinckaers FM, Evers SM, Olthuis SG, et al (2023) Cost-effectiveness of endovascular treatment after 6–24 h in ischaemic stroke patients with collateral flow on CT-angiography: A model-based economic evaluation of the MR CLEAN-LATE trial. Eur Stroke J. https://doi.org/10.1177/23969873231220464

13 Van Voorst H, Hoving JW, Koopman MS, et al (2023) Costs and health effects of CT perfusion-based selection for endovascular thrombectomy within 6 hours of stroke onset: A model-based health economic evaluatin. J Neurol Neurosurg Psychiatry. https://doi.org/10.1136/jnnp-2023-331862

14 Bae KT (2010) Intravenous contrast medium administration and scan timing at CT: Considerations and approaches. Radiology 256:32–61. https://doi.org/10.1148/radiol.10090908

15 Awai K, Hiraishi K, Hori S (2004) Effect of Contrast Material Injection Duration and Rate on Aortic Peak Time and Peak Enhancement at Dynamic CT Involving Injection Protocol with Dose Tailored to Patient Weight. Radiology 230:142–150. https://doi.org/10.1148/radiol.2301021008

16 Wintermark M, Maeder P, Verdun FR, et al (2000) Using 80 kVp versus 120 kVp in perfusion CT measurement of regional cerebral blood flow. American Journal of Neuroradiology 21:1881–1884

17 Fang XK, Ni QQ, Schoepf UJ, et al (2016) Image quality, radiation dose and diagnostic accuracy of 70 kVp whole brain volumetric CT perfusion imaging: a preliminary study. Eur Radiol 26:4184–4193. https://doi.org/10.1007/s00330-016-4225-6

18 Menon BK, D'Esterre CD, Qazi EM, et al (2015) Multiphase CT angiography: A new tool for the imaging triage of patients with acute ischemic stroke. Radiology 275:510–520. https://doi.org/10.1148/radiol.15142256

19 Reid M, Famuyide AO, Forkert ND, et al (2019) Accuracy and Reliability of Multiphase CTA Perfusion for Identifying Ischemic Core. Clin Neuroradiol 29:543–552. https://doi.org/10.1007/s00062-018-0717-x

20 Dundamadappa S, Iyer K, Agrawal A, Choi DJ (2021) Multiphase ct angiography: A useful technique in acute stroke imaging-collaterals and beyond. American Journal of Neuroradiology 42:221–227

21 Sousa JA, Sondermann A, Bernardo-Castro S, et al (2024) CTA and CTP for Detecting Distal Medium Vessel Occlusions: A Systematic Review and Meta-analysis. American Journal of Neuroradiology 45:51–56. https://doi.org/10.3174/ajnr.a8080

22 Peerlings D, De Jong HWAM, Bennink E, et al Spatial CT perfusion data helpful in automatically locating vessel occlusions for acute ischemic stroke patients

23 Amukotuwa SA, Wu A, Zhou K, et al (2021) Distal Medium Vessel Occlusions Can Be Accurately and Rapidly Detected Using Tmax Maps. Stroke 3308–3317. https://doi.org/10.1161/STROKEAHA.120.032941

24 Hardie AD, Picard MM, Camp ER, et al (2015) Application of an advanced image-based virtual monoenergetic reconstruction of dual source dual-energy CT data at low keV increases image quality for routine pancreas imaging. J Comput Assist Tomogr 39:716–720. https://doi.org/10.1097/RCT.0000000000000276

25 Willemink MJ, Persson M, Pourmorteza A, et al (2018) Photon-counting CT: Technical principles and clinical prospects. Radiology 289:293–312

26 Kikano EG, Rajdev M, Salem KZ, et al (2020) Utility of iodine density perfusion maps from dual-energy spectral detector CT in evaluating cardiothoracic conditions: A primer for the radiologist. American Journal of Roentgenology 214:775–785. https://doi.org/10.2214/AJR.19.21818

27 Staaf G, Lindgren A, Norrving B (2001) Pure Motor Stroke From Presumed Lacunar Infarct Long-Term Prognosis for Survival and Risk of Recurrent Stroke

28 Jackson C, Sudlow C (2005) Comparing risks of death and recurrent vascular events between lacunar and non-lacunar infarction. Brain 128:2507–2517

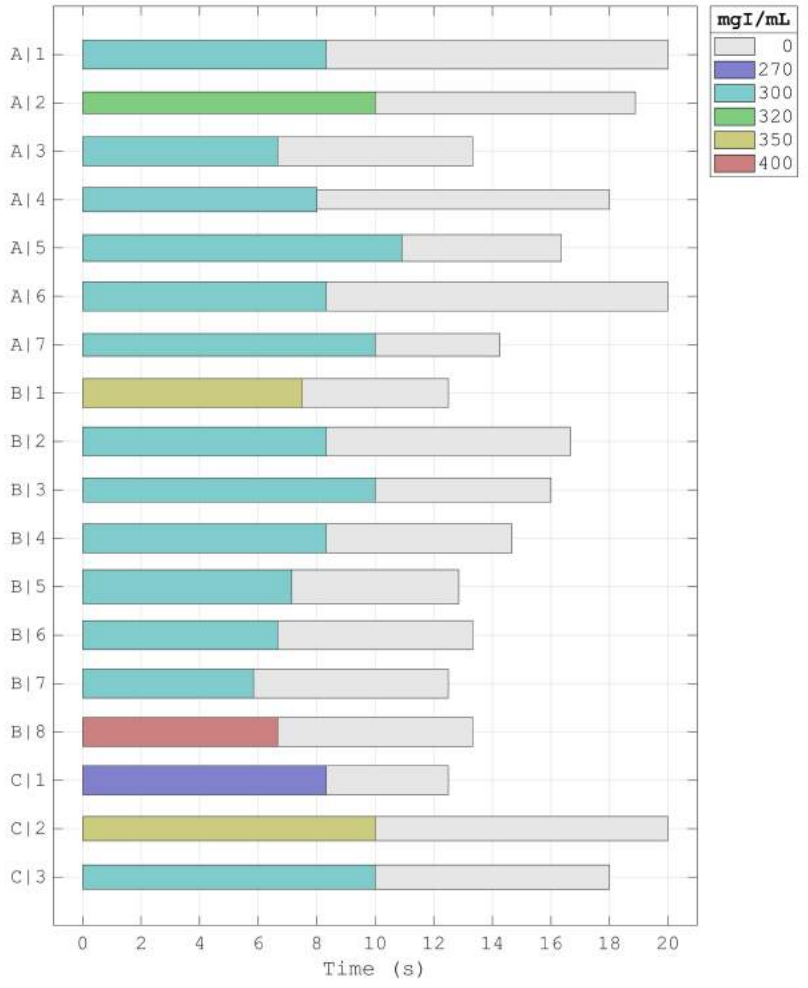

Supplementary Figure 1

The injection protocols shared by the centers participating in the CLEOPATRA healthcare evaluation. The nomenclature is the same as in chapter 3. The width of each bar represents the injection rate. From top to bottom, the contrast bolus injection volumes are 50, 45, 40, 40, 60, 50, 47, 45, 50, 50, 50, 50, 40, 35, 40, 50, 50, and 50 mL.

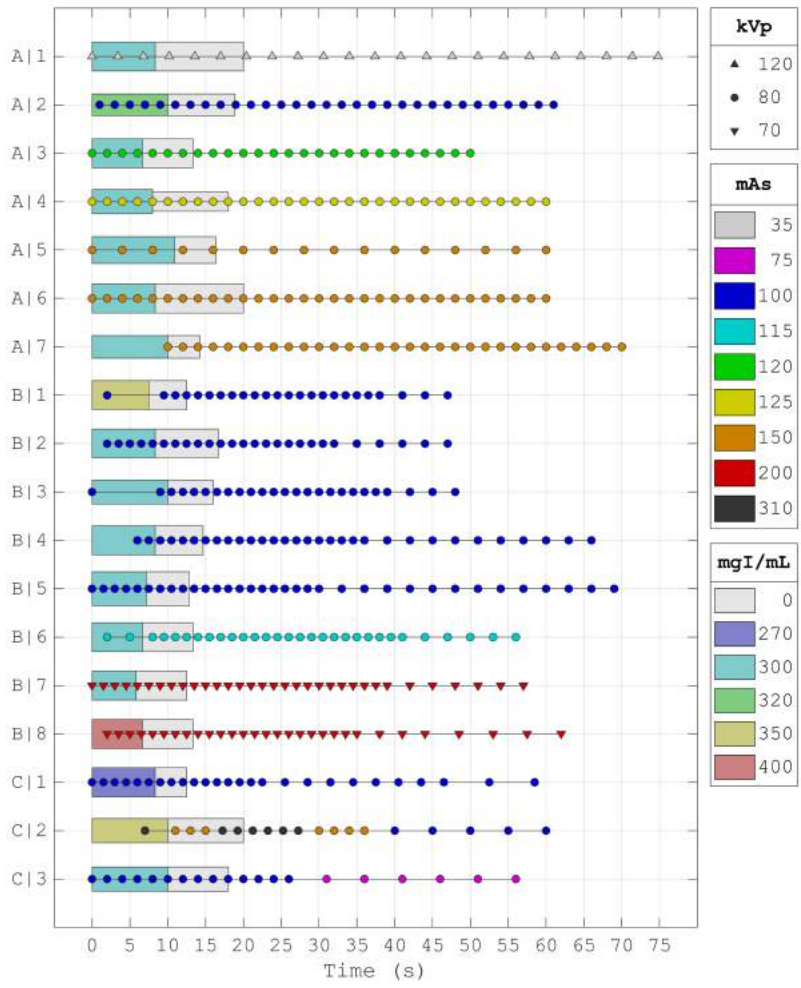

Supplementary Figure 2

The scan protocols on top of the injection protocols for the acquisition protocols shared by the centers participating in the CLEOPATRA healthcare evaluation. The nomenclature is the same as in chapter 3.

Appendices

A Nederlandse samenvatting

Dit proefschrift gaat over het harmoniseren en optimaliseren van CT perfusie (CTP) beroertebeeldvorming. CTP beeldvorming kan helpen bij het selecteren van patiënten met een herseninfarct voor trombectomie. Echter, omdat consensus over het CTP acquisitie- en verwerkingsprotocol ontbreekt, is een brede acceptatie van op beeld gebaseerde behandelingscriteria uitgebleven. De CLEOPATRA zorgbeoordeling is opgezet om te bepalen of het kosteneffectief is om patiënten met een herseninfarct te selecteren voor trombectomie op basis van beroertebeeldvorming. Wij richtten ons daarbij op het harmoniseren en optimaliseren van de protocollen voor CTP beroertebeeldvorming.

Hoofdstuk 1 introduceert enkele concepten van CTP beeldvorming. Bij CTP beeldvorming wordt contrastmiddel in de bloedbaan geïnjecteerd. Door veranderingen in contrastverlichting door de tijd heen te meten, kunnen perfusieafbeeldingen worden gemaakt. Deze perfusieafbeeldingen tonen de doorbloeding van het hersenweefsel en worden gebruikt om ischemische (minder doorbloede) gebieden af te schatten. De afgeschatte ischemische gebieden helpen de klinische besluitvorming rond een herseninfarct.

Hoofdstuk 2 behandelt het injectieprotocol van CTP beeldvorming. We beschouwden de contrastverlichting in een grote ader als een directe maat om het injectieprotocol te karakteriseren. Deze contrastverlichting varieerde tussen centra die deel hadden genomen aan een geharmoniseerde multicenterstudie. Met behulp van een antropomorf digitaal CTP fantoom beargumenteerden we dat deze variatie van invloed kan zijn op de klinische besluitvorming bij de diagnose van een herseninfarct.

Hoofdstuk 3 behandelt het scanprotocol en verwerkingsprotocol van CTP beeldvorming. We hebben de scanprotocollen en verwerkingsprotocollen opgevraagd bij de beroertecentra die deelnamen aan de CLEOPATRA zorgbeoordeling en hebben deze protocollen vergeleken met behulp van een antropomorf digitaal CTP fantoom. De scanprotocollen varieerden allen in instellingen. De CTP beeldresultaten waren relatief weinig beïnvloed door deze instellingen. Voor de verwerking van de CTP scans hebben we drie leverancierssoftware gebruikt. De CTP beeldresultaten waren duidelijk gegroepeerd op basis van de leverancierssoftware. Door de afschatting van ischemische gebieden te standaardiseren zoals beschreven in hoofdstuk 5, konden de CTP beeldresultaten tot op zekere hoogte geharmoniseerd worden.

Hoofdstuk 4 beschrijft onze inspanningen om een antropomorf fysiek CTP fantoom te vervaardigen. Dit fysieke fantoom was gebaseerd op het digitale fantoom gebruikt in hoofdstukken 2 en 3. Door het scannen van papieren vellen bedrukt met contrastmiddel, verkregen we CTP beeldresultaten die vergelijkbaar waren met die van het digitale fantoom. Het fysieke fantoom vereiste echter aparte verwerking vóór het daadwerkelijke verwerkingsprotocol en vertoonde suboptimale contrastverlichting. Desondanks hebben we aangetoond dat het nabootsen van antropomorf hersenweefselperfusie met een fysiek fantoom haalbaar is.

Hoofdstuk 5 introduceert een methode om het afschatten van ischemische gebieden te standaardiseren. In plaats van een drempelwaarde te stellen op een specifieke perfusieafbeelding, combineerden we perfusieafbeeldingen tot een enkele kansafbeelding voor ischemie. In hoofdstukken 3, 5 en 6 tezamen, toonden we aan dat deze gestandaardiseerde methode de CTP beeldresultaten tot op zekere hoogte kon harmoniseren en optimaliseren.

Hoofdstuk 6 vergelijkt de segmentaties van vier methoden om ischemische gebieden af te schatten: we beschouwden de segmentaties van acute MR-diffusiebeelden als de referentiestandaard en segmenteerden de perfusieafbeeldingen van de CTP beeldvorming volgens de klinische standaard, handmatig, en volgens de gestandaardiseerde methode beschreven in hoofdstuk 5. De segmentaties van de klinische standaard presteerden minder goed ten opzichte van zowel de handmatige segmentaties als de segmentaties van de gestandaardiseerde methode. Bovendien kwamen de handmatige segmentaties en de segmentaties van de gestandaardiseerde methode goed met elkaar overeen. Hoewel de segmentaties van de vier methoden verschilden, kwamen de CTP beeldresultaten over het algemeen goed overeen met de MR-diffusiebeelden in de acute fase van een herseninfarct.

Hoofdstuk 7 geeft een kijk op een nieuw gebruik van CTP beeldvorming als hulpmiddel om de vaatafsluiting te lokaliseren. Recente verbeteringen aan stent retrievers zouden de criteria voor trombectomie kunnen verruimen door afsluitingen van kleinere en meer distale vaten mee te nemen. Dit soort afsluitingen is echter steeds moeilijker te lokaliseren met CT angiografie beeldvorming. We toonden aan dat de ligging van het totale ischemische gebied, bepaald uit CTP beeldvorming, kan helpen bij het lokaliseren van de vaatafsluiting.

Hoofdstuk 8 beveelt aan een gestandaardiseerd kader op te stellen voor het afschatten van ischemische gebieden, om zo de onsamenhangendheden in de klinisch relevante informatie verkregen uit CTP beeldvorming te verminderen. Gebaseerd op ons onderzoek, zou dit kader alle informatie over de perfusie moeten benutten, ruimtelijke informatie in overweging moeten nemen, en moeten steunen op handmatige segmentaties als referentiepunt.

Kortom, volgens ons is en blijft CTP beeldvorming belangrijk om patiënten met een herseninfarct te helpen. Dit proefschrift beargumenteert dat huidige onsamenhangendheden voortkomen uit een verkeerde interpretatie van de perfusieafbeeldingen. We pleiten voor een verschoven perspectief waarin CTP beeldvorming op intrinsieke waarde wordt beoordeeld en waarbij breder wordt gekeken naar klinische toepassingen. Alleen zo kan het volledige potentieel van CTP beeldvorming gedaante krijgen.

B Dankwoord

Hugo, bedankt voor de kans om een promotietraject in de medische beeldvorming te doorlopen, zeker omdat mijn academische achtergrond daarbuiten lag. In dit nieuwe onderzoeksgebied was er veel te leren en ontdekken, en ik kreeg de ruimte om dit te doen. Jouw begeleiding op vorm en inhoud heeft me door de jaren heen op het wetenschappelijke rechte pad gehouden.

Henk, bedankt voor het ontvangen van een Utrechter in het Amsterdamse. Op deze nieuwe plek zat ik dichter bij de onderzoekers van mijn eigen project, maar ook die van aanverwante projecten. Bovendien heeft jouw vermogen om de verschillende kanten van de beroertebeeldvorming tevens inhoudelijk met elkaar te verbinden zijn waarde bewezen, zowel binnen als buiten dit proefschrift.

Edwin, bedankt voor je altijd welkome houding, door me mee te nemen in de wereld van perfusie alsook een plek op je kantoor aan te bieden. Jouw scherpe analytische blik en oog voor detail leiden tot steekhoudende resultaten die in waarde worden onderschat. Zonder de door jou ontwikkelde software had dit proefschrift er simpelweg niet gelegen.

Jan Willem, bedankt voor de benodigde klinische kijk op de zaak. Enerzijds was het van bijkomstig belang om knopen door te hakken. Anderzijds was het van aldoor belang om het onderzoek klinisch relevant te houden. Het bewustzijn dat theorie moet worden gekoppeld aan praktijk zal ik altijd met me meedragen.

Betrokkenen bij het CLEOPATRA-project, bedankt voor de prettige samenwerkingen en de mogelijkheid om deel uit te maken van een nationaal samenwerkingsverband. Het streven naar standaardisatie is moedig, gezien de vele belangen en het weinig aantrekkelijke imago, maar het tegelijkertijd grote belang voor de samenleving.

Utrechtse collega's, bedankt voor alle goede gesprekken en verhalen over het reilen en zeilen van het UMC Utrecht. Een zekere pandemie heeft ons samenzijn bemoeilijkt, maar mettertijd heb ik toch velen van jullie mogen leren kennen. Jullie ervaringen hebben een onschatbare rol gespeeld in de totstandkoming van dit proefschrift.

Amsterdamse collega's, bedankt voor alle leerzame en bovenal leuke tijden die ik met jullie heb mogen delen. De gedeelde smart van het promoveren, is toch de halve smart. Jullie aanwezigheid heeft mijn promotietijd ontegenzeggelijk verrijkt.

Alle ph'tjes bedank ik graag bij naam: Arnoud, Daniël, Dianne, Femke, Hans, Jordi, Karlijn, Liesbeth, Marissa, Stella, Stijn, Tim, en Tonya. Zonder jullie had ik waarschijnlijk zelf een beroerte aan dit proefschrift overgehouden.

Mam, pap, en Lotte, bedankt dat jullie er altijd zijn en bedankt voor de doorlopende ruggensteun die uiteindelijk ook in dit proefschrift verweven zit.

C CLEOPATRA investigators and coordinators

Principal investigators

Bart Emmer (MD, PhD)[1], Charles Majoie (MD, PhD)[1], Henk Marquering (PhD)[1], Hugo de Jong (PhD)[2], Hester Lingsma (PhD)[3], Diederik Dippel (MD, PhD)[3]

Study coordinators

Arnolt-Jan Hoving (MD, PhD)[1], Henk van Voorst (MD)[1], Daan Peerlings (MSc)[2], Jasper Daems (MD)[3], Miou Koopman (MD)[1]

Executive and writing committee

Bart Emmer (MD, PhD)[1], Charles Majoie (MD, PhD)[1], Erik Buskens (MD, PhD)[5], Hester Lingsma (PhD)[3], Henk Marquering (PhD)[1], Hugo de Jong (PhD)[2], Olvert Berkhemer (MD, PhD)[1], Wim van Zwam (MD, PhD)[8], Marianne van Walderveen (MD, PhD)[6], Ido van den Wijngaard (MD, PhD)[10], Aad van der Lugt (MD, PhD)[3], Diederik Dippel (MD, PhD)[3], Arnolt-Jan Hoving (MD, PhD)[1], Henk van Voorst (MD)[1], Daan Peerlings (MSc)[2], Jasper Daems (MD)[3]

Local principal investigators

Jonathan Coutinho (MD, PhD)[1], Bart van der Worp (MD, PhD)[2], Rob Lo (MD, PhD)[2], Jan Willem Dankbaar (MD, PhD)[2], Bob Roozenbeek (MD, PhD)[3], Adriaan van Es (MD, PhD)[3], Pieter-Jan van Doormaal (MD)[3], Jasper Martens (MD)[4], Jeanette Hofmeijer (MD, PhD)[4], Maarten Uyttenboogaart (MD, PhD)[5], Reinoud Bokkers (MD, PhD)[5], Marianne van Walderveen (MD, PhD)[6], Marieke Wermer (MD, PhD)[6], Lonneke Yo (MD, PhD)[7], Koos Keizer (MD, PhD)[7], Rob Gons (MD)[7], Aad van der Lugt (MD, PhD)[3], Julie Staals (MD, PhD)[8], Wim van Zwam (MD, PhD)[8], Inger de Ridder (MD, PhD)[8], Karlijn de Laat (MD, PhD)[9], Lukas van Dijk (MD, PhD)[9], Jelis Boiten (MD, PhD)[10], Sebastiaan de Bruijn (MD, PhD)[9], Geert Lycklama à Nijeholt (MD, PhD)[10], Ido van den Wijngaard (MD, PhD)[10], Paul de Kort (MD, PhD)[11], Michel Remmers (MD)[11], Anouk van Norden (MD)[11], Issam Boukrab (MD)[11], Julia van Tuijl (MD)[11], Hans Kortman (MD)[11], Anton Meijer (MD, PhD)[12], Floris Schreuder (MD, PhD)[12], Ewoud van Dijk (MD, PhD)[12], Hieronymus Boogaarts (MD, PhD)[12], Heleen den Hertog (MD, PhD)[13], Zwenneke Flach (MD)[13], Jan van den Berg (MD)[13], Boudewijn van Hasselt (MD)[13], Michel Remmers (MD)[14], Anouk van Norden (MD)[14], Farshad Imani (MD)[14], Otto Elgersma (MD, PhD)[15], Anouk Rozeman (MD)[15], Paul Brouwers (MD, PhD)[16], Dick Gerrits (MD)[16], Thomas Bulut (MD)[16], Paul Brouwers (MD)[16], Jan Albert Vos (MD, PhD)[17], Wouter Schonewille (MD, PhD)[17]

Local collaborators

Arnolt-Jan Hoving (MD, PhD)[1], Henk van Voorst (MD)[1], Daan Peerlings (MSc)[2], Jasper Daems (MD)[3], Agnetha Bruggeman (MD)[1], Miou Koopman (MD)[1], Anke Wouters (MD, PhD)[1], Floor Pinckaers (MD)[8], Susan Olthuis (MD)[8], Lucas de Vries (MSc)[1]

Data management group

Bart Emmer (MD, PhD)[1], Charles Majoie (MD, PhD)[1], Henk van Voorst (MD)[1], Arnolt-Jan Hoving (MD, PhD)[1]

CLEOPATRA advisory board

Albert Yoo (MD, PhD)[18], Wolfgang Kunz (MD, PhD)[19], Bruce Campbell (MD, PhD)[20]

Trial coordinator

Nienke Pannekoek (PhD)[21]

Trial statistician

Hester Lingsma (PhD)[3]

Affiliations

1 Amsterdam University Medical Centers, Amsterdam, the Netherlands

2 University Medical Center Utrecht, Utrecht, the Netherlands

3 Erasmus MC University Medical Center, Rotterdam, the Netherlands

4 Rijnstate Hospital, Arnhem, the Netherlands

5 University Medical Center Groningen, Groningen, the Netherlands

6 Leiden University Medical Center, Leiden, the Netherlands

7 Catharina Hospital, Eindhoven, the Netherlands

8 Maastricht University Medical Center, Maastricht, The Netherlands

9 HagaZiekenhuis, the Hague, the Netherlands

10 Haaglanden Medical Center, the Hague, the Netherlands

11 Elisabeth-TweeSteden Hospital, Tilburg, the Netherlands

12 Radboud University Medical Center, Nijmegen, the Netherlands

13 Isala Klinieken, Zwolle, the Netherlands

14 Amphia Hospital, Breda, the Netherlands

15 Albert Schweitzer Hospital, Dordrecht, the Netherlands

16 Medisch Spectrum Twente, Enschede, the Netherlands

17 St. Antonius Hospital, Nieuwegein, the Netherlands

18 Texas Stroke Institute, Plano, Texas, United States of America

19 University Hospital, Ludwig Maximilian University of Munich, Munich, Germany

20 Royal Melbourne Hospital, Parkville, Victoria, Australia

21 Trialbureau Zorgevaluatie Nederland, Diemen, the Netherlands

D Publications

In this thesis

Daan Peerlings, Edwin Bennink, Jan W Dankbaar, Birgitta K Velthuis, Hugo WAM de Jong. Variation in arterial input function in a large multicenter computed tomography perfusion study. *European Radiology* 31.11 (2021): 8317-8325.

Daan Peerlings, Fasco van Ommen, Edwin Bennink, Jan W Dankbaar, Birgitta K Velthuis, Bart J Emmer, Jan W Hoving, Charles BLM Majoie, Henk A Marquering, Hugo WAM de Jong. Probability maps classify ischemic stroke regions more accurately than CT perfusion summary maps. *European Radiology* 32.9 (2022): 6367-6375.

Daan Peerlings, Hugo WAM de Jong, Edwin Bennink, Jan W Dankbaar, Birgitta K Velthuis, Bart J Emmer, Charles BLM Majoie, Henk A Marquering. Spatial CT perfusion data helpful in automatically locating vessel occlusions for acute ischemic stroke patients. *Frontiers in Neurology* 14 (2023): 1136232.

Daan Peerlings, Edwin Bennink, Jan W Dankbaar, Birgitta K Velthuis, Bart J Emmer, Jan W Hoving, Charles BLM Majoie, Henk A Marquering, Henk van Voorst, Hugo WAM de Jong. Standardizing the estimation of ischemic regions can harmonize CT perfusion stroke imaging. *European Radiology* (2023): 1-11.

Daan Peerlings, Hugo WAM de Jong, Edwin Bennink, Jan W Dankbaar, Henk A Marquering, Bart J Emmer, Lucas de Vries, Charles BLM Majoie. CT perfusion imaging resembles MR diffusion imaging in the acute phase of ischemic stroke. *Submitted*.

Other publications

Miou S Koopman, Jan W Hoving, Henk van Voorst, Jasper D Daems, Daan Peerlings, Erik Buskens, Hester F Lingsma, Henk A Marquering, Hugo WAM de Jong, Olvert A Berkhemer, Wim H van Zwam, Marianne AA van Walderveen, Ido van den Wijngaard, Aad van der Lugt, Diederik WJ Dippel, Albert J Yoo, Bruce CV Campbell, Wolfgang G Kunz, Charles BLM Majoie, Bart J Emmer. Cost-effectiveness of CT perfusion for patients with acute ischemic stroke (CLEOPATRA)-Study protocol for a healthcare evaluation study. *European Stroke Journal* 7.2 (2022): 188-197.

Jan W Hoving, Henk van Voorst, Daan Peerlings, Jasper D Daems, Miou S Koopman, Anke Wouters, Manon Kappelhof, Natalie E LeCouffe, Kilian M Treurniet, Agnetha AE Bruggeman, Leon A Rinkel, Ido R van den Wijngaard, Jonathan M Coutinho, Aad van der Lugt, Henk A Marquering, Yvo BWEM Roos, Charles BLM Majoie, Bart J Emmer. Association between computed tomography perfusion and the effect of intravenous alteplase prior to endovascular treatment in acute ischemic stroke. *Neuroradiology* 65 (2023): 1053-1061.

Henk van Voorst, Jan W Hoving, Miou S Koopman, Jasper D Daems, Daan Peerlings, Erik Buskens, Hester F Lingsma, Ludo FM Beenen, Hugo WAM de Jong, Olvert A Berkhemer, Wim H van Zwam, Yvo BWEM Roos, Marianne AA van Walderveen, Ido van den Wijngaard, Diederik WJ Dippel, Albert J Yoo, Bruce CV Campbell, Wolfgang G Kunz, Bart J Emmer, Charles BLM Majoie. Cost-effectiveness of CT perfusion for the detection of large vessel occlusion acute ischemic stroke followed by endovascular treatment: a model-based health economic evaluation study. *European Radiology* (2023): 1-16.

Henk van Voorst, Jan W Hoving, Miou S Koopman, Jasper D Daems, Daan Peerlings, Erik Buskens, Hester Lingsma, Henk A Marquering, Hugo WAM de Jong, Olvert A Berkhemer, Wim H van Zwam, Marianne AA van Walderveen, Ido R van den Wijngaard, Diederik WJ Dippel, Albert J Yoo, Bruce Campbell, Wolfgang G Kunz, Charles B Majoie, Bart J Emmer. Costs and health effects of CT perfusion-based selection for endovascular treatment of patients with a large vessel occlusion presenting within six hours after symptom onset: a model-based health economic evaluation. *Journal of Neurology, Neurosurgery & Psychiatry* (2023).

E About the author

Daan Peerlings (Middelburg, 1995) finished his pre-university education in 2013 at Nehalennia Stedelijke Scholengemeenschap in Middelburg. He received his bachelor degrees in Mathematics and Physics & Astronomy in 2017 at Utrecht University and he received his master degree in Theoretical Physics in 2019 at Utrecht University. In 2019, he started his doctoral degree at the University Medical Center Utrecht under the supervision of prof. dr. ir. Hugo de Jong, prof. dr. Henk Marquering, dr. ir. Edwin Bennink, and dr. Jan Willem Dankbaar, resulting in this PhD thesis on harmonizing and optimizing CT perfusion stroke imaging. As of 2024, he started working as a data scientist at the Goede Doelen Loterijen.